

Investigation and Analysis of the New Walterdale Bridge to Develop a Structural Health  
Monitoring System

by

Aimee De Laurentiis

A thesis submitted in partial fulfillment of the requirements for the degree of

Master of Science

in

Structural Engineering

Department of Civil and Environmental Engineering

University of Alberta

## **Abstract**

Structural Health Monitoring (SHM), a technique of applying sensors to a structure to monitor for damage, is becoming a good preventative and management application to use on new and existing infrastructure, such as bridges, in order to effectively monitor and evaluate their performance under various loading scenarios. The application of SHM can be a cost-effective solution, as it can decrease the cost of maintenance by allowing engineers to confirm their design assumptions and make well informed decisions on the extent of damage present. In order to do so, however, it is necessary to understand the actual behaviour of the structure and how the behaviour can best be measured.

In Edmonton, Alberta, Canada, the century-old Walterdale Bridge has reached the end of its service life and is being replaced by a new bridge. The new Walterdale Bridge is a thrust-arch bridge that has been designed to meet the functional and aesthetic needs of users. It will be the first of its kind in Edmonton. In this project, a preliminary finite element (FE) model of the new bridge was modified and analyzed under design and predicted loading. A sensor layout was then developed that incorporates 199 sensors. Preliminary investigation into the accelerometer layout plan was conducted using the Complex Mode Indicator Function (CMIF) modal identification algorithm. This investigation found that global damage, such as a change in boundary conditions, can be detected more easily than local damage simulations, which would be expected using global measurement techniques. The ability to detect local damage was dependent on the severity of damage present and the locations of the sensors on the structure. As this damage detection analysis is preliminary, the ability to detect damage may change in further studies that incorporate other algorithms and measurement types.

“Believe in your flyness, conquer your shyness.”

-Kanye West

## **Acknowledgements**

I would like to express my gratitude to my supervisors, Dr. Mustafa Gül and Dr. J.J. Roger Cheng, for their guidance and mentorship throughout this project. I would also like to thank the committee members of my MSc. defense, Dr. Robert Driver and Dr. Lijun Deng for their time and feedback.

I am deeply grateful for the structural engineering students on the fifth floor and all of the members of the SHM research team, especially: Saeideh Fallah Nafari, Pouya Salem, Safa Masajedian, Amir Jamshidi, Ngoan Do Tien, Jianfeng Gu, Branislav Kostic, Lihua Zhang, Haiyang Zhang and Mahdi Okasha. My experience would not have been as enjoyable without their collaboration and friendship.

Thank you to DIALOG for providing information and knowledge into the project. I would also like to thank the Natural Sciences and Engineering Research Council of Canada.

Finally, I am extremely thankful to my beloved friends and family for their continuous encouragement, love and support. This would not have been possible without them.

# Table of Contents

<b>Chapter 1: Introduction.....</b>	<b>1</b>
1.1 Introduction to Structural Health Monitoring .....	1
1.2 Introduction to the New Walterdale Bridge .....	2
1.3 Objectives and Scope.....	3
1.4 Organization of the Thesis.....	4
<b>Chapter 2: Literature Review .....</b>	<b>5</b>
2.1 Literature Review of Structural Health Monitoring of Bridges.....	5
2.2 Literature Review of Methods for Structural Health Monitoring .....	7
2.3 Literature Review of the History and Importance of the Walterdale Bridge in Edmonton .....	15
<b>Chapter 3: Bridge Description and Modeling .....</b>	<b>18</b>
3.1 Material Properties .....	19
3.1.1 Concrete .....	19
3.1.2 Structural Steel .....	20
3.1.3 Freyssinet® Cables .....	20
3.1.4 Reinforcing Steel.....	21
3.1.5 Wearing Surface .....	21
3.2 Bridge Deck .....	22
3.2.1 Edge Girders .....	24
3.2.2 Floor Beams .....	25
3.2.3 Stringers.....	25

3.2.4	Composite Deck.....	26
3.2.5	Connection Beams.....	26
3.2.6	Bearings.....	27
3.2.7	Traffic Lanes.....	28
3.3	<i>Arches</i> .....	29
3.3.1	Freyssinet Cables.....	29
3.3.2	Arch Ribs.....	30
3.3.3	Struts.....	31
3.3.4	Thrust Blocks.....	32
3.4	<i>Shared-Use Pathway (SUP)</i> .....	33
3.4.1	Girders.....	33
3.4.2	Floor Beam Extensions.....	34
3.4.3	Bearings.....	34
3.4.4	Delta Piers.....	35
3.5	<i>General Behaviour of a Thrust-Arch Bridge</i> .....	35
<b>Chapter 4: Structural Analysis.....</b>		<b>38</b>
4.1	<i>Modal Analysis</i> .....	38
4.1.1	Natural Frequencies and Mode Shapes.....	38
4.2	<i>Design Load Analysis</i> .....	40
4.2.1	Dead Load Analysis.....	40
4.2.2	Temperature Load Analysis.....	40

4.2.3	Vehicle Load Analysis.....	44
4.2.4	Pedestrian Load Analysis .....	46
4.2.5	Wind Load Analysis.....	47
4.2.6	Serviceability Limit State Analysis.....	48
4.3	<i>Predicted Vehicle Load Analysis</i> .....	54
4.3.1	Displacements .....	56
4.3.2	Stresses.....	58
4.3.3	Vibrations .....	61
4.4	<i>Conclusion</i> .....	64
<b>Chapter 5: Proposed Sensor Layout Plan .....</b>		<b>65</b>
5.1	<i>Proposed Sensor Layout Plan</i> .....	65
5.1.1	Strain Monitoring.....	65
5.1.2	Vibration Monitoring .....	67
5.1.3	Displacement Monitoring.....	68
5.1.4	Layout .....	68
5.1.5	Other Monitoring Considerations.....	73
5.1.6	Data-Acquisition System.....	75
5.2	<i>Limited Budget Sensor Layout Plan</i> .....	76
5.3	<i>Conclusion</i> .....	77
<b>Chapter 6: Damage Simulations Using The Finite Element Model.....</b>		<b>79</b>
6.1	<i>CMIF Modal Identification Analysis</i> .....	79

6.2	<i>Full Accelerometer Layout with No Damage</i> .....	85
6.3	<i>Damage Simulations</i> .....	86
6.4	<i>Bearing Damage</i> .....	86
6.4.1	Complete Longitudinal Stiffness Fixity.....	87
6.4.2	2X Bearing Longitudinal Stiffness Increase .....	89
6.5	<i>Cable Damage</i> .....	91
6.5.1	Removal of Cable Member .....	91
6.5.2	20% Stiffness Reduction of Cable .....	94
6.6	<i>Arch Strut Damage</i> .....	96
6.6.1	80% Stiffness Reduction to Full Arch Member .....	96
6.6.2	20% Stiffness Reduction to Half Arch Member .....	99
6.7	<i>Connection Damage</i> .....	101
6.8	<i>Conclusion</i> .....	104
	<b>Chapter 7: Conclusions and Recommendations</b> .....	<b>105</b>
7.1	<i>Conclusions</i> .....	105
7.2	<i>Recommendations</i> .....	106
	<b>References</b> .....	<b>108</b>
	<b>APPENDIX A</b> .....	<b>113</b>
	<b>APPENDIX B</b> .....	<b>116</b>
	<b>APPENDIX C</b> .....	<b>127</b>
	<b>APPENDIX D</b> .....	<b>135</b>

**APPENDIX E ..... 141**

## List of Figures

Figure 1-1: A Typical SHM System .....	2
Figure 3-1: General Layout of The Walterdale Bridge.....	19
Figure 3-2: Bridge Deck Cross-Section in Meters.....	22
Figure 3-3: Bridge Deck Top View in Meters .....	23
Figure 3-4: Edge Girder Cross-Section in Millimeters.....	24
Figure 3-5: Floor Beam Geometry in Millimeters .....	25
Figure 3-6: Stringer Cross-Section in Millimeters.....	26
Figure 3-7: Connection Beam Layout in Millimeters.....	27
Figure 3-8: Connection Beam Cross-Section in Millimeters.....	27
Figure 3-9: Deck Bearing Layout .....	28
Figure 3-10: Traffic Lane and West Walkway Layout.....	28
Figure 3-11: Bridge Arch Side View .....	29
Figure 3-12: Bridge Arch Top View in Millimeters.....	29
Figure 3-13: Arch Rib Cross-Section in Millimeters.....	31
Figure 3-14: Arch Strut Layout.....	31
Figure 3-15 Arch Strut Cross-Section in Millimeters.....	32
Figure 3-16: Thrust Block Layout in Millimeters.....	33
Figure 3-17: Floor Beam Extension Cross-Section in Millimeters .....	34
Figure 3-18: SUP Bearing Layout .....	35
Figure 3-19: Delta Pier Side View in Millimeters .....	35
Figure 3-20: General Behaviour of a Thrust-Arch Bridge.....	37
Figure 4-1: Natural Frequencies and Mode Shapes of the Walterdale Bridge .....	39
Figure 4-2: Modification for Effective Temperatures (CAN/CSA-S6 2006).....	41

Figure 4-3: Modifications to Effective Temperatures (CAN/CSA-S6 2006).....	42
Figure 4-4: Temperature Differentials for Type A and C Superstructures (CAN/CSA-S6 2006).....	43
Figure 4-5: CL-W800 Truck Load (CAN/CSA-S6 2006).....	45
Figure 4-6: CL-W800 Lane Load (CAN/CSA-S6 2006).....	46
Figure 4-7: Load Patterns of SUP Pedestrian Load.....	47
Figure 4-8: Vibration Limits of SLS (CAN/CSA-S6 2006).....	50
Figure 4-9: Deflected Shape Envelope under SLS2 Load.....	51
Figure 4-10: SLS2 SUP Displacement Envelope.....	51
Figure 4-11: SLS2 West Walkway Displacement Envelope.....	52
Figure 4-12: Normal Stress Envelope of Edge Girders under SLS1 Load.....	53
Figure 4-13: Normal Stress Envelope of Arches under SLS1 Load.....	53
Figure 4-14: Normal Stress Envelope of SUP under SLS1 Load.....	54
Figure 4-15: Normal Stress of Hangers under SLS1 Load.....	54
Figure 4-16: Predicted Truck Top View.....	55
Figure 4-17: Predicted Truck Side View.....	55
Figure 4-18: Deflected Shape Envelope under Predicted Traffic Load.....	56
Figure 4-19: Vertical Displacement Envelope of the Bridge Deck under Predicted Traffic Load.....	57
Figure 4-20: Transverse Displacement Envelope of Bridge Deck under Predicted Traffic Load.....	57
Figure 4-21: Longitudinal Displacement Envelope of the Bridge Deck under Predicted Traffic Load.....	58
Figure 4-22: Vertical Displacement Envelope of SUP under Predicted Traffic Load.....	58
Figure 4-23: Normal Stress Envelope of the Edge Girders under Predicted Traffic Load.....	59

Figure 4-24: Normal Stress Envelope of Inner Girders under Predicted Traffic Load ....	60
Figure 4-25: Normal Stress Envelope of Arches under Predicted Traffic Load.....	60
Figure 4-26: Normal Stress of Hangers under Predicted Traffic Load.....	61
Figure 4-27: Vertical Acceleration of Bridge Deck at South End due to Predicted Traffic Load .....	62
Figure 4-28: Vertical Acceleration of Bridge Deck at Mid-span due to Predicted Traffic Load .....	62
Figure 4-29: Accelerations at 30 m, mid-span and 170 m along the Walterdale Bridge under Predicted Vehicle Loading.....	63
Figure 5-1: Bridge Deck Sensor Layout (Plan View).....	70
Figure 5-2: Arch Sensor Layout .....	71
Figure 5-3: SUP Sensor Layout .....	72
Figure 6-1: Top View of Bridge Deck Accelerometer Layout and Impact Locations .....	82
Figure 6-2: Top View of Steel Arches Accelerometer Layout and Impact Locations .....	83
Figure 6-3: SUP Accelerometer Layout .....	84
Figure 6-4: Full Bearing Stiffness Mode Shape 2 Comparison.....	88
Figure 6-5: 2X Bearing Stiffness Mode Shape 1 Comparison .....	90
Figure 6-6: Full E12 Hanger Removal Mode Shape 4 Comparison.....	93
Figure 6-7: 20% Reduction in Stiffness of E12 Hanger Mode Shape 4 Comparison.....	95
Figure 6-8: 80% Stiffness Reduction of Full Arch Strut 4 Member Mode Shape 5 Comparison.....	98
Figure 6-9: 20% Stiffness Reduction of Half Arch Strut 4 Member Mode Shape 5 Comparison.....	100
Figure 6-10: Connection Damage at East Edge Girder Mode 1 Comparison.....	103
Figure A-1: South-West Thrust Block Construction (August 20 <sup>th</sup> , 2015).....	114

Figure A-2: South Abutment Construction (August 20 <sup>th</sup> , 2015) .....	114
Figure A-3: Temporary Modular Barge (August 20 <sup>th</sup> , 2015) .....	115
Figure A-4: Mid-arch Section Construction (August 20 <sup>th</sup> , 2015).....	115
Figure B-1: Edge Girder Normal Stress under Negative Effective Temperature .....	116
Figure B-2: Arch Normal Stresses under Negative Effective Temperature .....	116
Figure B-3: SUP Normal Stresses under Negative Effective Temperature .....	117
Figure B-4: Hanger Normal Stresses under Negative Effective Temperature .....	117
Figure B-5: Edge Girder Normal Stresses under Negative Thermal Gradient .....	118
Figure B-6: Arch Normal Stresses under Negative Thermal Gradient.....	118
Figure B-7: SUP Normal Stresses under Negative Thermal Gradient .....	119
Figure B-8: Hanger Normal Stresses under Negative Thermal Gradient .....	119
Figure B-9: Edge Girder Normal Stresses under CL-W800 Truck .....	120
Figure B-10: Arch Normal Stresses under CL-W800 Truck .....	120
Figure B-11: SUP Normal Stress under CL-W800 Truck .....	121
Figure B-12: Hanger Normal Stress under CL-W800 Truck.....	121
Figure B-13: Edge Girder Normal Stress under SUP Pedestrian Load .....	122
Figure B-14: Arch Normal Stress under SUP Pedestrian Load.....	122
Figure B-15: SUP Normal Stress under SUP Pedestrian Load .....	123
Figure B-16: Hanger Normal Stress under SUP Pedestrian Load .....	123
Figure B-17: Edge Girder Normal Stress under Wind Load Envelope .....	124
Figure B-18: Arch Normal Stress under Wind Load Envelope .....	124
Figure B-19: SUP Normal Stresses under Wind Load Envelope .....	125
Figure B-20: Hanger Normal Stresses under Wind Load Envelope.....	125
Figure B-21: Floor Beam Extension Normal Stress under SLS1 Load Combination ....	126

Figure B-22: Arch Strut Normal Stress under SLS1 Load Combination .....	126
Figure C-1: Cross-Section at Hanger 6 Location.....	127
Figure C-2: Nonlinear Dead Load Analysis Results of 200 GPa Member.....	128
Figure C-3: Nonlinear Dead Load + Live Load Analysis Results of 200 GPa Member	129
Figure C-4: Nonlinear Dead Load Analysis Results of Fully Rigid Member .....	130
Figure C-5: Nonlinear Dead Load + Live Load Analysis Results of Fully Rigid Member .....	131
Figure C-6: Linear Dead Load Analysis Results of 200 GPa Member .....	132
Figure C-7: Linear Live Load Analysis Results of 200 GPa Member .....	132
Figure C-8: Linear Dead Load Analysis Results of Fully Rigid Member .....	133
Figure C-9: Linear Live Load Analysis Results of Fully Rigid Member .....	134
Figure D-1: Bridge Deck Top View of Layout Plan 1.....	137
Figure D-2: Bridge Deck Top View of Layout Plan 2.....	139
Figure D-3: Steel Arch Top View of Layout Plan 2.....	140
Figure E-1: Impact 1 Channel 6 - Vertical Acceleration .....	141
Figure E-2: Impact 1 Channel 56 - Horizontal Acceleration.....	141
Figure E-3: Impact 1 Channel 88 - Longitudinal Acceleration .....	142
Figure E-4: Impact 2 Channel 28 - Vertical Acceleration .....	142
Figure E-5: Impact 3 Channel 20 - Vertical Acceleration .....	143
Figure E-6: Impact 4 Channel 65 - Horizontal Acceleration.....	143

## **List of Tables**

Table 3-1: Specified Concrete Material Properties.....	19
Table 3-2: Concrete Strength Properties.....	20
Table 3-3: Specified Steel Material Properties.....	20
Table 3-4: Grades of Steel.....	20
Table 3-5: Specified Cable Material Properties.....	21
Table 3-6: Specified Cable Strength Properties.....	21
Table 3-7: Reinforcing Steel Specified Strength Properties.....	21
Table 3-8: Edge Girder Dimensions.....	24
Table 3-9: Floor Beam Dimensions.....	25
Table 3-10: Lane Dimensions.....	28
Table 3-11: Cable Areas.....	30
Table 3-12: Strut End Dimensions.....	32
Table 3-13: Thrust Block Dimensions.....	33
Table 3-14: Delta Pier Dimensions.....	35
Table 4-1: Mean Daily Temperatures from CSA-S6-06.....	41
Table 4-2: Temperature Based on Structure Type from CSA-S6-06.....	42
Table 5-1: Sensor Legend.....	69
Table 5-2: Comparison of Unlimited and Limited Sensor Layout Plan.....	78
Table 6-1: Summary of Channel Direction Measurements.....	85
Table 6-2: No Damage CMIF Natural Frequencies.....	86
Table 6-3: Fully Fixed South-East Deck Bearing Natural Frequency Comparison.....	87
Table 6-4: 2X Bearing Stiffness Natural Frequency Comparison.....	89
Table 6-5: Removal of East Hanger 12 Natural Frequency Comparison.....	92

Table 6-6: 20% Stiffness Reduction to East Hanger 12 Natural Frequency Comparison .....	94
Table 6-7: 80% Stiffness Reduction to Full Arch Strut 4 Natural Frequency Comparison .....	97
Table 6-8: 20% Stiffness Reduction to Half of Arch Strut 4 Natural Frequency Comparison .....	99
Table 6-9: Connection Damage Natural Frequency Comparison .....	102
Table D-1: Layout Plan 1 Natural Frequencies .....	136
Table D-2: Layout Plan 2 Natural Frequencies .....	138

## List of Nomenclature

$p$	Design static pedestrian load
$s$	Total loaded length of walkway
$C_g$	Gust coefficient
$C_e$	Wind exposure coefficient
$C_H$	Horizontal drag coefficient
$C_v$	Vertical drag coefficient
$F_H$	Horizontal drag load
$F_v$	Vertical drag load
$q$	Wind pressure
$N_o$	Number of measurement locations
$N_i$	Number of impact locations
$N$	Degrees of freedom
$j\omega$	Frequency variable
$[H(j\omega)]$	FRF matrix
$[S(j\omega)]$	Singular value matrix
$[U(j\omega)]$	Left singular matrix
$[V(j\omega)]$	Right singular matrix
$[\Psi]$	Mode shape matrix
$Q$	Scaling factor
$\lambda$	System pole
$[L]$	Modal participation factor matrix
$e\hat{H}(j\omega)$	Enhanced FRF
$\{U(j\omega)\}$	Unscaled mode shape vector
$\{V(j\omega)\}$	Equivalent mode participation factor vector

# CHAPTER 1: INTRODUCTION

## 1.1 Introduction to Structural Health Monitoring

The structural condition of infrastructure in North America is increasingly deteriorating due to age and neglect. In 2013, the bridges in the United States were given a grade of C+ for their condition by the American Society of Civil Engineers, requiring an estimated annual investment of \$20.5 billion to eliminate the deficiency backlog by 2028. Approximately 1 in 9 bridges in the United States are rated as structurally deficient, meaning that areas of the bridge are in need of repair (Infrastructurereportcard.org 2015). In 2003, the Canadian Society for Civil Engineering reported that only 41% of the infrastructure in Canada is less than 40 years old, 31% between the age of 40 to 80 years old, and the remaining 28% over the age of 80 years old (Mirza 2009). The cost to rehabilitate the aging municipal infrastructure is estimated at \$57 billion, and if left unchecked, could rise to \$110 billion by 2027 (*Civil Infrastructure Systems Technology Road Map* 2013). With the current state of the aging infrastructure in both the United States and Canada, a method to prioritize funds and repairs should be applied in order to efficiently resolve the issues faced. Not only is the health of existing infrastructure declining, but in recent years, the design of new structures is becoming more unique. As information in design codes is based on research conducted on small-scale specimens, it is impossible to completely model the behaviour of full-scale structures (Bisby and Briglio 2004). Since the full-scale behaviour is not completely understood, educated assumptions on the in-situ behaviour have to be made.

The application of a structural health monitoring (SHM) system on current and new bridges can solve many of these problems and provide several benefits, including: (1) improved understanding of in-situ structural behaviour, (2) early damage detection, (3) assurances of a structure's strength and serviceability, (4) improved strategies for the allocation of resources, and (5) the encouragement to use innovative design and materials (Bisby and Briglio 2004). Damage in this context refers to a change in structural behaviour over time that can affect its future performance.

SHM is commonly defined as a method that uses three main components to collect, store and process data, as shown in Figure 1-1. The first is a sensory system that is applied to the structure. The sensors are capable of measuring different signals regarding structural response such as vibration, stress and displacement. The second component is a data acquisition system that temporarily stores the information collected by the sensors, converts the signals to digital measurements that can be transmitted to the central control system, which is the final component of the system. The data goes through many procedures in the control system, including processing and control, management and evaluation in order to assess the data for potential damage to the structure. This complete system is capable of both measuring the ongoing, real time performance of structures, as well as conducting off-line data analysis. In real-time measurement, data can be compared with design values, analysis results and pre-determined thresholds. Using off-line measurements, data is managed through data management and damage detection algorithms (Xu and Xia 2011). Connection between the sensory system, data acquisition system and the control office can be either completely wired, wireless or a combination of the two (Figure 1-1).



Figure 1-1: A Typical SHM System

## 1.2 Introduction to the New Walterdale Bridge

The new Walterdale Bridge is a thrust-arch bridge currently under construction in Edmonton, Alberta, Canada. A thrust-arch bridge uses thrust blocks beneath the foundations to carry the loads applied to the main structure. This unique type of bridge will be the first of its kind to be designed and constructed in Edmonton. The bridge will span the North Saskatchewan River, connecting Queen Elizabeth Park Road and

Walterdale Hill on the south side of the river to River Valley Road/Rossdale Road/105 Street intersection on the river's north side. It is a main corridor to access Edmonton's downtown and is expected to carry a high volume of daily traffic. The purpose of constructing the new Walterdale Bridge is to replace the current two-lane Walterdale Bridge, a century old structure that has reached the end of its service life.

The span length of the bridge is 230 m and contains three northbound traffic lanes and a shared-use pathway (SUP) on the east side of the structure that is partially separated from the main bridge deck to accommodate pedestrians and cyclists. Along with the thrust blocks and SUP, other main features include two 56 m high steel arches on either side of the bridge deck connected by steel struts, 8 floor beam extensions that connect the east side of the main bridge deck to the SUP, and 46 Freyssinet cables that hang from the arches to support the bridge deck and the SUP. Construction started in the summer of 2013 and the bridge expected to open in the fall of 2016. Once construction is completed, the current Walterdale Bridge will be demolished. The use of a SHM system on the new Walterdale Bridge can aid in understanding the in-situ behaviour of the structure and verifying the design assumptions made. SHM can also help to ensure the design strength and serviceability of the bridge and help detect future damage at an earlier stage, thereby minimizing the severity of damage occurring, reducing maintenance costs and increasing safety.

### **1.3 Objectives and Scope**

The main objective of this research is to develop a sensor layout plan for the new Walterdale Bridge. In order to accomplish this, a finite element (FE) model of the bridge was modified base on a preliminary model given by the designers. The model was analyzed under both design and predicted loading conditions in order to better understand the behaviour of the structure and the best locations to place the sensors. Once the behaviour and sensor locations were established, damage was simulated using the model by changing the stiffness of certain members at specific locations. The structure was excited using impact loads and the response data of the damaged model was extracted, analyzed and compared to the original model in order to conduct a preliminary investigation on the effectiveness of the accelerometer layout and how the accelerometers

might interpret global and local changes of the structure using modal identification measurements. Further investigation into damage detection algorithms and measurement types will be needed, as the results obtained in this study are preliminary and useful for global measurements only.

#### **1.4 Organization of the Thesis**

This thesis consists of seven chapters with the following order:

- Chapter 2 is a literature review on works related to this research, which include various methods and common sensors used for structural health monitoring of bridges, the history of the Walterdale Bridge and the general behaviour of this type of structure under loading.
- Chapter 3 describes the Walterdale Bridge material properties and geometry in detail and discusses how the bridge was modeled using CSiBridge<sup>®</sup> (Computers & Structures Inc. 2014).
- In Chapter 4, the loads used to analyze the bridge model are described and the results of serviceability limit state and predicted vehicle loading are presented.
- Chapter 5 presents two sensor layout plans. The first layout plan uses the analysed results to create a complete sensor layout plan under no budgetary restriction. The second plan describes a layout plan under a budgetary constraint and investigates the best sensor options available under this limitation.
- Chapter 6 uses the Complex Mode Indicator Function (CMIF) modal identification algorithm developed in MATLAB<sup>®</sup> (The MathWorks, Inc. 2015) to investigate the proposed sensor layout plan proposed in Chapter 5 by simulating damage to the model created and comparing the modal measurements of the healthy and damaged model. The analysis conducted in this chapter is a preliminary investigation into the effects of damage on the overall global behaviour of the structure.
- Chapter 7 concludes the work presented in this thesis and provides recommendations for future work on the SHM system development of the new Walterdale Bridge.

# CHAPTER 2:LITERATURE REVIEW

## 2.1 Literature Review of Structural Health Monitoring of Bridges

Bridge monitoring has been used since the construction of the Golden Gate and Bay Bridges in San Francisco in the 1930s. In 1940, the wind-induced collapse of the Tacoma Narrows Bridge in Washington, United States led to the development of more extensive bridge monitoring programs in North America (Xu and Xia 2011). Today, more than 600,000 bridges in the USA are inspected at least once every two years (Pines and Aktan 2002). In order to understand the behaviour and reliability of structures in various types of loading and environmental situations, two types of testing systems can be employed: destructive and non-destructive. Destructive testing involves analyzing a structure or element until it reaches failure. This type of testing can produce a lot of useful information regarding the behaviour of a structure. However, since this can be costly and cannot be repeated on the same specimen, the application of destructive testing is usually only performed in a laboratory setting and on a small scale. Non-destructive testing (NDT) is a term used to define tests that do not interfere with the integrity of the structure. This type of testing is preferred when studying the integrity of large-scale structures such as bridges and buildings.

The most commonly used NDT is visual inspection. Although visual inspection is normally acceptable by engineers, it must be performed routinely and is prone to human error. An intensive study was conducted by the U.S. Department of Transportation on the reliability of visual inspections for highway bridges. It was found that visual inspection is conducted with significant variability, especially when assigning condition ratings (Moore et al. 2001). If visual inspection cannot be completely reliable, further deterioration of current bridge structures could lead to major failure. Wardhana and Hadipriono (2003) studied the cause of bridge failure on 500 bridges in the US from 1989 – 2000. Deterioration of bridge components was an essential cause of failure, with 43 cases observed. From the 43 cases, 18 bridge failures were caused from maintenance deficiencies that may have been prevented with proper inspections in bridges under 50

years old, while the remaining failures were linked to old age. Overloading and impacts contributed to 20% of bridge failures.

Other types of NDT, which are implemented to compliment visual inspection, include but are not limited to ultrasonic testing, infrared and thermal testing, as well as radiographic testing. Infrared testing is a commonly used NDT technique used for measuring the temperature differences of an object. If a disruption of heat distribution is shown, it can be an indication of damage. Clark et al. (2003) used infrared testing to study the health of a concrete bridge in the UK. The testing did indicate damage, but was limited by many factors that changed the temperature of the surface including: sunlight, wind, as well as rocks and trees that cover the surface being tested. These limitations led to more bridge spans being tested than originally planned, causing inefficiency and higher cost.

In recent years, it has become more common to aid visual inspection with the use of a structural health monitoring (SHM) system, a technique used to help understand the behaviour and performance of structures under real loadings and environmental conditions to ensure their safety, serviceability, durability, and sustainability (Li and Ou 2015). Chang et al. (2003) compared SHM to medical health monitoring of human beings. In medical health monitoring, health is assessed by first testing the pulse and blood pressure for a patient. If there are signs of health risks, more testing can be done. This is the same with structural health monitoring, where damage can be identified by measuring certain characteristics of the structure, such as vibrations, strains, and deflections. If an anomaly is detected by the SHM system, visual inspection or other NDT methods can be performed in the location identified to further assess the damage. This can lead to a more efficient monitoring and maintenance program, which could decrease or mitigate the extent of damage on the structure.

The most common definition of SHM involves the use of a sensory system and a data acquisition system on a structure that captures continuous information on its behaviour in real-time. The data gathered from the sensor and data acquisition system is then sent to a central control location where it is processed, managed and assessed for any signs of damage. The sensory system involves the use of various types of sensors capable of collecting different signals of interest. These signals are transmitted to the data

acquisition system where they are temporarily stored and eventually sent to the control location (Xu and Xia 2011). The SHM systems are commonly connected via cables; however, a wireless connection can be utilized and is rapidly becoming more popular.

Wireless sensor monitoring involves the use of a wireless sensor network (WSN) and is built of nodes. The node consists of several parts, including: a sensing device, a processor, a communication channel, and a power unit. The information collected from nodes is then wirelessly transferred to other nodes or a computer network where it can be evaluated (Potdar et al. 2009).

Although a wired system is the most widely used, there is an effort to increase the use and reliability of a WSN. Chintalapudi et al. (2006) lists the benefits and drawbacks of using a WSN. One main advantage of a wireless network is the reduction in cost of installation of cables. These sensors are battery-powered, making them easy to install. The fact that they run on batteries is also a drawback, as during early development the battery life was not extensive. Battery-powered sensor nodes could only operate for a few hours in working state, reducing the time of monitoring and the amount of data collected. Also, the network connection between the nodes and gateway could be unreliable due to the range, bandwidth, noisy environment or loss of connection. In recent years, these drawbacks have been significantly improved. Wireless SHM systems are now being designed specifically for low power consumption and long-range communication. It is due to the latest developments of WSN and the cost reduction achieved by these systems that SHM now has the potential to expand its application to a larger number of existing and new infrastructures (Harms et al. 2010).

## **2.2 Literature Review of Methods for Structural Health Monitoring**

By the early 1980s, research on SHM began to develop rapidly (Doebeling et al. 1996). It is now being applied to many civil engineering applications, especially bridges. Bridge SHM is typically employed to validate and improve design assumptions, detect anomalies at an early stage, provide real-time information for safety assessment, and to provide data when planning bridge inspections and repairs (Ko and Ni 2005). The ideal continuous SHM system typically employs sensors to monitor three main aspects: environmental conditions, loading sources and bridge response. It is also beneficial to complement the

system with a numerical or analytical model to efficiently assess bridge response and performance. Many bridges are equipped with a full long-term SHM system that is capable of measuring various aspects (Ni et al. 2005). One to note is the Wind and Structural Health Monitoring System (WASHMS) of the Tsing Ma Bridge in Hong Kong, the world's longest suspension bridge with a middle span of 1377 m that carries both highway and railway transportation. Xu and Xia (2011) discussed the extensive sensor plan installed on this bridge. It is equipped with a total of 297 wired sensors. To measure environmental conditions, the bridge was equipped with 6 thermometers to measure the ambient temperature. Loading sources are measured using 7 weigh-in-motion stations for highway traffic measurement, 6 anemometers to measure wind speed and direction and 109 temperature sensors to measure bridge temperature. Bridge response is measured using 13 accelerometers for vibration measurements, 110 strain gauges for strain measurements, 2 displacement transducers, 14 GPS stations, and 9 level sensing stations for displacement measurements. The sensors were installed in 1997 when the structure was completed, and provides the owners with useful information of the loading and response of the structure.

Other long-span bridges with similar fully equipped SHM systems include the Zhijiang Bridge in China (Chen et al. 2014), the Bill Emerson Memorial Bridge in the US (Çelebi et al. 2004), and the Confederation Bridge in Canada (Cheung and Naumoski 2002).

Fully equipped continuous SHM systems can become costly, and when limited funds are available or if only specific aspects are of interest to be monitored, a SHM system using a few types of sensors can be used to track specific behaviour or detect damage. Such monitoring techniques include vibration monitoring and damage detection using accelerometers, as well as stress and fatigue monitoring using strain gauges. While vibration and strain measurements are useful to SHM, it should be noted that the use of deflection measurement alone to detect damage may be impractical in the application of large-scale SHM systems, since it is difficult to measure absolute displacement of long-span bridges. Common displacement transducers can only measure relative displacement, while other displacement measurement devices, such as laser transducers, total stations and global positioning systems (GPS) may not produce the precise measurements needed

(Ni et al. 2005). Vibration-based and strain monitoring is more reliable and more commonly utilized than displacement measurements in SHM.

Doebeling et al. (1998) wrote an extensive summary on vibration-based damage identification methods. Vibration-based damage detection is capable of measuring the modal parameters of a structure, such as natural frequencies, damping ratios and mode shapes of the structure over time. Since modal parameters are dependent on mass, stiffness and damping, a change in these properties can be an indicator of damage. An issue found with vibration-based damage detection is that the localization of damage can be difficult to detect due to the dependence on the location and number of accelerometers, the environmental conditions, and the loading conditions experienced. Also, only global behaviour can be captured since global response is normally measured at lower frequency modes, whereas local response is measured at higher frequency modes, which are difficult to excite. From this study, it was concluded that vibrational data can be useful for damage detection, although more research should be applied to real-life structures.

In order to carry out vibration-based damage detection, the vibration response of a structure due to transient or ambient loading is measured using accelerometers. Ambient vibration testing, also known as output-only testing is preferred over forced vibration, input-output, tests on large structures. Forced vibration tests can be more costly because they require purchasing excitation equipment such as shakers or drop weights. Also, the normal use of the structure must be shut down when tests are conducted. Ambient testing, however, can be performed under normal loading events, such as traffic or wind, and do not require the use of excitation equipment. A drawback of ambient vibration testing is not having a complete knowledge of the noise levels and load on the structure, resulting in an approximate scaling of identified mode shapes (Ren et al. 2004).

Since vibration-based damage detection is dependent on loading and environmental conditions, such as traffic loads, wind loads and temperature, their effects on dynamic parameters should be well understood. Galvin and Daminguez (2007) conducted dynamic analysis of a 168 m span cable-stayed deck steel arch bridge using nine accelerometers and two set-up plans. Two accelerometers were used at reference measurement locations, while the other seven were placed at fourteen selected measurement locations based on

the FE model created. Acceleration measurements were taken under ambient traffic loading. The flexural modal frequencies and mode shapes were measured and compared against a FE model. This measured information on dynamic parameters was intended to be compared against future measurements, where damage can be detected if a change in parameters is observed. Vehicle-structure interaction was also measured, and an increase in damping ratios was discovered when a traffic jam was present on the structure. A small decrease in natural frequency was also measured in the traffic jam scenario. Zhang et al. (2002) studied the variability of dynamic properties of a cable-stayed bridge due to traffic loads. The study was performed on the Xupu Bridge in Shanghai, China under normal traffic conditions and a steady wind and temperature environment for a 24 hour period. Acceleration data was recorded. Due to a limited number of sensors, measurement points were limited to only 16 points, 14 vertical and 2 lateral, on the 590 m mid-deck span. Air temperature varied from 4 to 11°C and wind speed reached a maximum of 3 m/s. A total of 17 vibration modes were obtained, ranging from 0 to 2 Hz. The results showed that traffic-induced vibration accounts for a 1.11% change in natural frequencies of the bridge. Changes were dependent on the time of day, due to a change in the number of vehicles present and lower night temperatures. It was noted that changing traffic loads could have a significant effect on the vibration of the cables, although these vibrations were not measured. Unknown environmental variations, such as temperature changes can also become an issue.

Zhou and Yi (2014) wrote a summary review on research of the correlation between temperatures and vibration properties of long-span bridges. Temperature variation may cause larger changes to the natural behaviour of a structure than damage, some reasons being that temperature distribution may be non-uniform across the entire structure, temperature can cause a change in the stiffness of members or boundary conditions, and temperature can also create stresses, which would change the properties of the members. This change may cause a false alarm in damage detection, or conceal the effects caused by structural damage. Ni et al. (2005) measured the relationship between temperature and the modal properties of the Ting Kau Bridge, a cable-stayed bridge in Hong Kong. 45 accelerometers and 83 temperature sensors were permanently installed on the structure, and modal properties were measured over a one year period. It was concluded that a

temperature variation of 2.8 to 53.5<sup>0</sup>C accounts for a 0.2% to 1.5% change in modal frequencies for the first ten modes. Liu and DeWolf (2007) studied the effects of temperature on the dynamic behaviour of a concrete bridge under ambient loads. This 20 year old bridge is located in Connecticut and is 235 m in length. 12 temperature sensors, 6 tilt meters, and 16 accelerometers - 14 vertical and 2 lateral, were permanently installed on the structure. A database of response was created over a 5 year period of monitoring, and a baseline was then created. Results showed that the natural frequencies varied by a maximum of 6% for a temperature range of 20<sup>0</sup>C, with the first and second modes being the most influenced. With the data collected, linear regression models that predict the natural frequencies under temperature changes were created, which proved to show satisfactory and consistent results. While higher modes do not experience a large change in dynamic properties due to temperature change, their linear behaviour is less predictable. It was established that when detecting damage, dynamic properties should be compared at the same temperatures so as not to measure false-positives.

Efforts have been made in recent research to reduce the chance of detecting a false-positive due to environmental effects. Many numerical methods have been proposed to eliminate environmental effects in vibration-based structural damage detection. Some methods, such as back-propagation neural network (BPNN) proposed by Zhou et al. (2011), have been proven to eliminate temperature effects and detect damage when the frequency change due to damage is approximately 1%.

In addition to vibration-based damage identification, accelerometers can be applied to measure local vibration response and human comfort in structures. The Canadian Highway Bridge Design Code (CAN/CSA-S6 2006) limits the amount of vertical deflection, which is converted from vertical accelerations, experienced on a bridge based on the amount of pedestrian usage predicted and natural frequency. The conversion of acceleration to static deflection was made based on field observations of vehicle induced vibrations and deflections, since dynamic behaviour increases the amount of deflection experienced. Sway vibration is another concern to designers, which is generated by a crowd of people walking in step on a pedestrian bridge. Sadeghi et al. (2013) studied the vibration characteristics of a slender composite footbridge under simulated human running loads in order to ensure that the more sophisticated footbridges being built today

still meet the current design code criteria for vibration. The study was also done in order to ensure the bridge would not be affected by resonance. Pedestrian loads were simulated as harmonic time-history load functions for running slowly, running at a normal pace and sprinting scenarios. A footbridge model was created with dimensions of 22.5 m in length and 2.3 m in width. From the analysis, it was determined that the acceleration values obtained satisfied all practical guide limitations for all three loading scenarios. MacKenzie et al. (2005) carried out an intensive study on four different footbridges under ambient and forced vibrations to determine the pedestrian tolerance to dynamic loading and to assess the sensitivity of different bridge types, in order to have more insight into designing modern lightweight structures. Fourteen users were asked specific questions regarding their comfort under the loading conditions. After testing, a proposal for a more user friendly design was presented. Acceleration was found to be dependent on four factors: site usage, route redundancy, height of structure, and exposure of structure. It was concluded that subjective aspects need to be measured, and thought on what the design is intended for must be considered.

The measurement of strain has also been proven to detect damage in structures. Two types of strain measurements exist: static and dynamic strain. Static strain refers to the slow-rate strain that occurs over a long period of time, typically caused by temperature. Dynamic strain changes more rapidly due to dynamic loads, such as vehicles. Strain gauges have been applied to countless SHM layouts.

Many studies on the application of strain gauges for vibration-based damage identification methods have been conducted. Dos Santos et al. (2014) mentioned advantages to using strain gages for dynamic measurements. One main advantage noted is that when applications of static and dynamic tests are needed, the same sensors can be used, depending on their type. Wang and Chan (2009) summarized various vibration-based damage detection methods and concluded that methods involving strains were better at localizing damage than typical acceleration based measurements, such as mode shapes and natural frequency. Another benefit of strain gauges is the fact that they are less costly. Drawbacks include more time required for installation, larger number of sensors required to accurately measure strains, high background noise levels in

measurement, permanent installation of gauges is typically required, and they have a shorter life-span.

Strain gauges can also be used for more local applications. Lee et al. (2007) developed a SHM system used to monitor a highway bridge's steel girder stress that can track usage and help owners identify overload, collision, damage, structure change and deterioration by the installation of quarter-bridge strain gauges. A threshold load was established in software that could alert owners to potential damage risks measured. Strain data was captured for 30 days and during that time, a histogram of maximum hourly and daily strain was established. It was concluded that the designed system was acceptable to allow owners to monitor and control overloads, as well as develop insight into traffic and structural information that can be used for future need, all for a relatively low cost. Cardini and DeWolf (2008) used a total of 20 uniaxial strain gauges in a long-term monitoring application of a multi-girder steel composite bridge. Strain data was collected from normal truck traffic to determine live load stresses, load distribution factors and the location of the neutral axis in each girder of the bridge deck to verify if any major changes in structural integrity are present on the bridge over time. Distribution factors were measured to determine where damage was situated; peak strains are measured to check for fatigue damage and changes in girder strength, while the neutral axis location is used to check the condition of the concrete deck and cracking in the composite steel girders. A FE model was developed to verify the results. From the study, strain data alone proved to be a useful tool in the long-term application of SHM, and was able to capture all three parameters.

Catbas et al. (2008) used vibrating wire strain gauges to conduct a one year analysis on temperature-induced stress on a fracture-critical hanger element of a long span truss bridge. The study was performed in order to understand the reliability of the bridge due to changes in temperature. The temperature-induced stress measured showed that the response of the structure may be difficult to conceptualize. It was also noted that stress from temperature was roughly ten times higher than stress due to traffic loads. This temperature-induced stress reduced the reliability of the local hanger, as well as the overall structure, and should be monitored for long-term effects.

To increase service life of a structure, monitoring of existing local damage can be performed. This can aid in understanding the extent of damage, and deciding on a proper method of repair. DeWolf (2009) used strain gauges to evaluate the cause of fatigue cracks occurring in tie plate connections on the transverse floor beam in a multi-span steel plate-girder bridge built in 1964. After a short-term monitoring application, it was concluded that repairs were only needed on certain tie plates, instead of all tie plates as originally planned, reducing the cost needed for repair. Roeder et al. (2000) monitored the cause of excess vibration and fatigue cracking on the Toutle River Bridge, a 92.66 m long tied-arch bridge located in Washington, US. The bridge was built in 1969. High vibrations were felt by pedestrians as the bracing members visibly sagged under their own weight and horizontal floor beam web cracking had occurred. An SHM plan consisting of strain gauges, linear potentiometers, and accelerometers were placed on the structure to understand the cause of damage. A FE model of the structure was used to predict behaviour and establish the instrumentation testing and layout plan. After free and forced vibration tests were performed, a load spectrum was established and a fatigue life of critical components was predicted. It was determined that fatigue occurred due to large deformations. Stiffening of the bridge was suggested in order to reduce the amount of deformation.

In summary, visual inspection and other NDT applications alone are found to be unreliable tools in maintenance and damage detection of structures. The use of a SHM system, consisting of sensors, a data acquisition system and a processing system, is developing into a successful way of aiding visual and NDT techniques. SHM assists in understanding the behaviour of structures under different loading conditions and in detecting anomalies earlier than commonly used visual inspections alone. Environmental conditions, loading sources and bridge response are the ideal parameters to be measured when applying a continuous monitoring system to large structures. When funds are limited, a partial SHM system can be used to monitor specific factors, such as vibrations and strains, for long-term or short-term applications in order to understand the behaviour of the structure, detect damage or to help increase the service life of a damaged structure. WSN are also proving to become a less costly and viable option in SHM systems.

Although these applications can be limited by environmental and loading properties that may mask damage, research is developing rapidly in how to mitigate these effects.

### **2.3 Literature Review of the History and Importance of the Walterdale Bridge in Edmonton**

The name Walterdale has historic significance to the City of Edmonton. John Walter immigrated to Canada in 1870 to find work with the Hudson's Bay Company at Fort Edmonton. After moving to Edmonton, he was one of the first to build his home on the south bank of the North Saskatchewan River and to start his own business. A neighbourhood on the south end of the river started to evolve due to his entrepreneurship, and was given the name Walterdale in his honor. One of his businesses included running a ferry service across the North Saskatchewan River before any bridges had been built (Edmonton.ca 2015).

The current Walterdale Bridge, located in the Walterdale area, opened in 1913. At the time of its completion, it was named the Fifth Street Bridge and was Edmonton's fourth river crossing for vehicles. The bridge has a length of 214 m, with three steel Pratt Truss spans. It was originally designed with two sidewalks, and a single track for streetcars (YEGisHome.ca 2015)

More than one-hundred years later, the current Walterdale Bridge serves two lanes of Northbound traffic across the North Saskatchewan River and has reached the end of its service life. A condition assessment of the Walterdale Bridge was completed in 2001. *Walterdale Bridge Rehabilitation Assessment Summary* (2001) outlined the strength and fatigue problems that the bridge faces. The steel grating deck was overstressed by 40% due to overloading of traffic that caused reduction in the depth of the bearing bars. The transverse stringers, longitudinal stringers, floor beams, expansion bearings and various members making up the trusses experienced significant corrosion leading to fatigue. The piers and abutments also experienced cracks and surface delamination.

A rehabilitation plan was proposed in the assessment that would allow the bridge to run safely for at least 10 more years. The rehabilitation included repainting, deck grating and traverse stringer replacement, replacement of expansion joint components, and

delamination repairs. Ongoing visual inspection was proposed, along with ultrasonic testing to detect cracks behind gusset plates. To carry out visual inspection, access platforms hanging below truss spans had been recommended. From the assessment, it was concluded that the Walterdale Bridge was nearing the end of its economic and service life.

Due to the decline in health of the current Walterdale Bridge, a new bridge was proposed. From 2010 to 2011, a new Walterdale Bridge plan was in the concept phase. The Transportation Department and the project team held their first open house in November 2010 to obtain public input on options for road alignment and new bridge style options for the proposed replacement. By July 2011, the project moved into the preliminary design phase. Three designs meeting the following criteria were presented to a public open house in 2012:

1. Approximate \$132 million project cost
2. Aesthetics should be pleasing, have a light appearance and compliment the natural environment
3. Comfortable and safe pedestrian and cyclist experience
4. Ease of constructability
5. Good schedule
6. Positive driving experience
7. 75-year service life
8. Existing bridge should be able to remain open during construction
9. Minimal disturbance to the environment

A final design meeting the above criteria was presented to the public in February 2013. The final design, a \$155 million steel-arch bridge with an attached shared-use pathway, is proposed and is the first of its kind in Edmonton.

Construction of the new Walterdale Bridge started in January 2013. Construction involves a complex staged construction process, presented in Appendix A along with photos of the construction process, which was originally scheduled to be completed in the fall of 2015. Due to delays involving the delivery of the steel members from South Korea, the new expected completion date of the Walterdale Bridge has been pushed back by one

year, to fall 2016 (Cbc.ca 2015). Once construction is complete, the current Walterdale Bridge will be removed (Edmonton.ca 2015).

The application of a SHM system to the new Walterdale Bridge would be a great benefit to the city. Given that the Walterdale Bridge name is an important part of the history and community of Edmonton, and the bridge is a main route for residents to cross the North Saskatchewan River, the health and longevity of the structure is vital. Further, as this new design is the first of its kind in Edmonton, a SHM system would help engineers in understanding the behaviour of the unfamiliar structure and confirm their design assumptions. Installation of a SHM system would also benefit in its future maintenance and repair, with the potential to minimize the amount of damage experienced and extending its life span. Furthermore, a continuous SHM system would contribute to the history of the Walterdale Bridge, as it would become the first bridge in Edmonton to have applied a complete SHM system, i.e., a smart bridge.

## **CHAPTER 3: BRIDGE DESCRIPTION AND MODELING**

The Walterdale Bridge was modeled using CSiBridge 2014 Version 16.1.0 Advanced with Rating. A preliminary model was provided by the designers, although it was not up-to-date with the final structural drawings. As such, many of the bridge elements were changed to properly reflect the drawings.

The bridge can be split into three main structural components: the bridge deck, the arches and the shared-use pathway (SUP). The material properties and structural members of each component are summarized below.

The structural components of the Walterdale Bridge are laid out in Figure 3-1. The bridge deck is made up of 26 W-shaped floor beams running the transverse width of the deck, 5 lines of W-shaped stringers, rectangular hollow edge girders that are 1.6 m in depth at both the east and west ends of the bridge deck, two rectangular hollow connection beams that connect the two arches and bridge deck, a 230 m composite deck with a 225 mm thick concrete deck and 8 elastomeric bearings at the end spans and connection beam locations. The arches consist of box hollow arch ribs at the east and west sides of the structure, struts that connect the two arches, Freyssinet cables and four thrust blocks. The SUP contains polygonal shaped girders with a maximum depth of 1.4 m, W-shape floor beam extensions, concrete delta piers, 4 elastomeric bearings and 4 pot bearings.

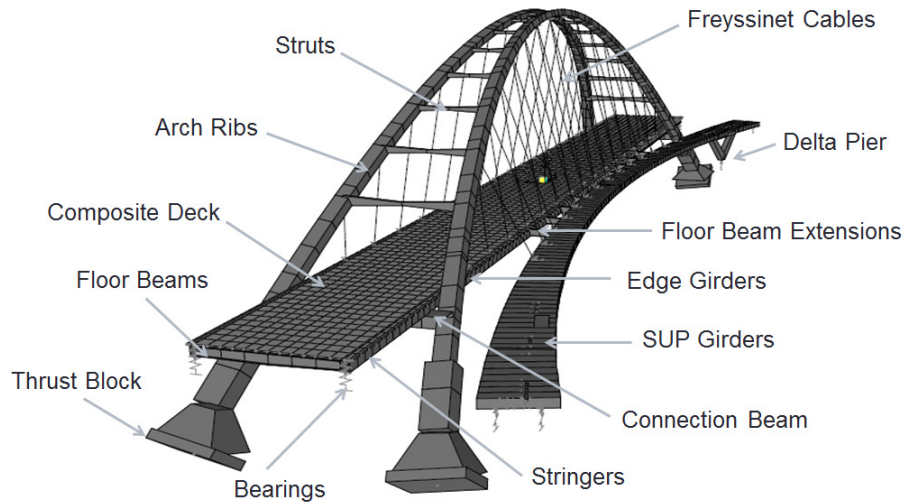


Figure 3-1: General Layout of The Walterdale Bridge

### 3.1 Material Properties

#### 3.1.1 Concrete

The type of concrete used was dependent upon the structural components. The specified concrete material and strength properties used for specific structural components in the model are listed in Table 3-1 and Table 3-2, respectively.

Table 3-1: Specified Concrete Material Properties

Property	Value	Unit
<b>Modulus of Elasticity, E</b>	29.00	GPa
<b>Poisson's Ratio, <math>\nu</math></b>	0.20	
<b>Coefficient of Thermal Expansion, <math>\alpha</math></b>	$9.90 \times 10^{-6}$	$^{\circ}\text{C}^{-1}$
<b>Shear Modulus, G</b>	12.08	GPa
<b>Weight per Unit Volume</b>	24.00	$\text{kN/m}^3$

Table 3-2: Concrete Strength Properties

<b>Component</b>	<b>Strength (MPa)</b>	<b>Age (Days)</b>
<b>Thrust blocks</b>	35 Class C	28
<b>Deck, delta piers, arch pedestal</b>	45 Class HPC	28

### 3.1.2 Structural Steel

Different grades of steel were specified based on the structural component. The specified structural steel material and strength properties are listed in Table 3-3 and Table 3-4, respectively.

Table 3-3: Specified Steel Material Properties

<b>Property</b>	<b>Value</b>	<b>Unit</b>
<b>Modulus of Elasticity, E</b>	200	GPa
<b>Poisson's Ratio, <math>\nu</math></b>	0.30	
<b>Coefficient of Thermal Expansion, <math>\alpha</math></b>	$1.20 \times 10^{-5}$	$^{\circ}\text{C}^{-1}$
<b>Shear Modulus, G</b>	76.90	GPa
<b>Weight per Unit Volume</b>	96.22	$\text{kN/m}^3$

Table 3-4: Grades of Steel

<b>Component</b>	<b>Specification</b>	<b>Grade</b>
<b>Arch ribs, connection beam, arch top struts, edge girders, floor beams, stringers, SUP girders, all steel welded to these components</b>	CSA G40.21M	350WT
<b>Floor beam extensions</b>	CSA G40.21M	480WT

### 3.1.3 Freyssinet® Cables

The hanger cables are Freyssinet parallel strand cables, with a H1000 and H2000 stay cable system. The H1000 system is used for all pedestrian cables, while the H2000

system is used in the main bridge structure. The specified hanger material and strength properties are listed below in Table 3-5 and Table 3-6, respectively.

Table 3-5: Specified Cable Material Properties

<b>Property</b>	<b>Value</b>	<b>Units</b>
<b>Modulus of Elasticity, E</b>	195	GPa
<b>Poisson's Ratio, <math>\nu</math></b>	0.30	
<b>Coefficient of Thermal Expansion, <math>\alpha</math></b>	$1.20 \times 10^{-5}$	$^{\circ}\text{C}^{-1}$
<b>Shear Modulus, G</b>	75.00	GPa
<b>Weight per Unit Volume</b>	76.97	kN/m <sup>3</sup>

Table 3-6: Specified Cable Strength Properties

<b>Strength</b>	<b>Value (MPa)</b>
<b>Min. Yield Strength, <math>F_y</math></b>	1050
<b>Min. Tensile Strength, <math>F_u</math></b>	1860

### 3.1.4 Reinforcing Steel

Two types of reinforcing steel, plain steel and stainless steel, are used depending on the locations. Plain steel is only used in areas where concrete is not exposed to a high level of chlorides. Table 3-7 lists the specified strength properties of plain and stainless steel bars.

Table 3-7: Reinforcing Steel Specified Strength Properties

<b>Reinforcement Type</b>	<b>Specification</b>	<b>Min. Yield Strength (MPa)</b>
<b>Plain Steel</b>	CSA G30.18M	400
<b>Stainless Steel</b>	ASTM A276 ASTM A955/A955M	420

### 3.1.5 Wearing Surface

The wearing surface of the bridge deck is 90 mm thick; 10 mm of the wearing surface consists of a hot-applied asphalt membrane and the remaining 80 mm thickness is

asphaltic concrete pavement (ACP). The wearing surface of the SUP is 50 mm thick, made of polymer modified asphalt (PMA). The weight per unit volume of the wearing surface is specified as 23.5 kN/m<sup>3</sup>.

### 3.2 Bridge Deck

The main bridge deck consists of 21 different edge girder sections on both the east and west edge of the bridge, 26 floor beams, 5 lines of interior stringers, a composite deck system, 2 deck support beams and 8 bearings. The layout of all members is shown in Figure 3-2 and Figure 3-3. The arch elements, bearings and SUP are not shown in both figures for clarity.

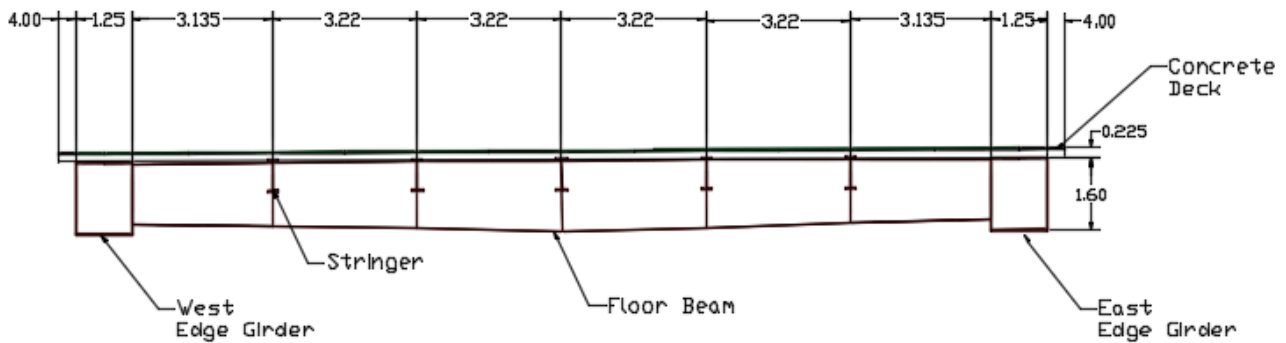


Figure 3-2: Bridge Deck Cross-Section in Meters



### 3.2.1 Edge Girders

The 21 different edge girder segments were modeled as frame elements with the appropriate dimensions. Figure 3-4 shows the edge girder cross-section and Table 3-8 gives dimensions. Girder 2 and girder 20 segments, both sharing the same properties, vary in flange and web thickness across their lengths.

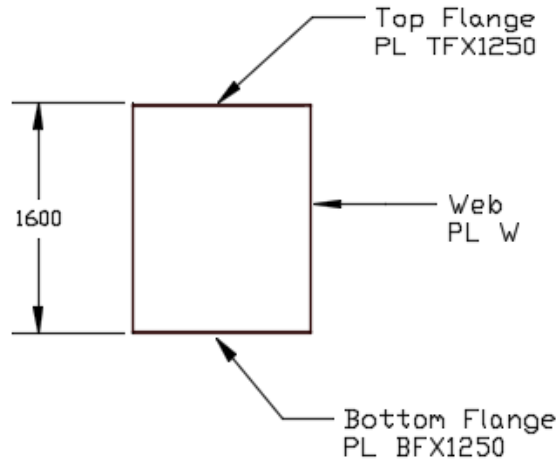


Figure 3-4: Edge Girder Cross-Section in Millimeters

Table 3-8: Edge Girder Dimensions

<b>Girder Section</b>	<b>TF (mm)</b>	<b>BF (mm)</b>	<b>W (mm)</b>	<b>Girder Section</b>	<b>TF (mm)</b>	<b>BF (mm)</b>	<b>W (mm)</b>
<b>G1</b>	25	28	18	<b>G11</b>	28	30	16
<b>G2 &amp; G20</b>	28 - 35	30-40	18-20	<b>G12</b>	28	30	16
<b>G3</b>	25	28	18	<b>G13</b>	28	30	18
<b>G4</b>	25	28	18	<b>G14</b>	28	30	18
<b>G5</b>	25	28	16	<b>G15</b>	28	30	18
<b>G6</b>	28	30	18	<b>G16</b>	28	30	18
<b>G7</b>	28	30	18	<b>G17</b>	25	28	16
<b>G8</b>	28	30	18	<b>G18</b>	25	28	18
<b>G9</b>	28	30	18	<b>G19</b>	25	28	18
<b>G10</b>	28	30	16	<b>G21</b>	25	28	18

### 3.2.2 Floor Beams

There are a total of 26 floor beams that span the width of the bridge deck. Four different types of floor beam sections were specified in the bridge drawings, varying in height, flange thickness and web thickness. The floor beams are modeled as frame elements, following the dimensions provided in the drawings. Figure 3-5 and Table 3-9 provide the floor beam geometry and dimensions.

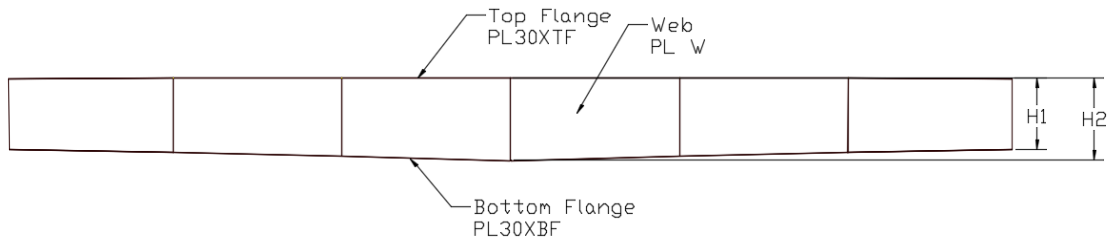


Figure 3-5: Floor Beam Geometry in Millimeters

Table 3-9: Floor Beam Dimensions

Flange Section	TF (mm)	BF (mm)	W (mm)	H1 (mm)	H2 (mm)
F1	400	425	16	1340	1576
F2	500	500	16	1400	1636
F3	400	425	16	1340	1576
F4	400	600	20	1345	1581

### 3.2.3 Stringers

W690X140 stringers were specified in the drawings, and are modeled as frame elements with the appropriate dimensions. The cross-sectional properties are shown in Figure 3-6.

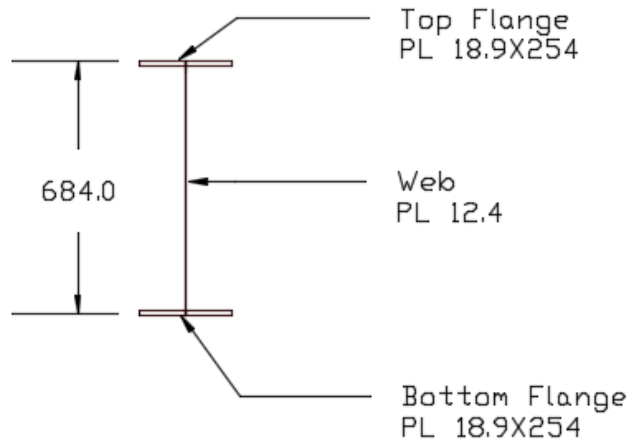


Figure 3-6: Stringer Cross-Section in Millimeters

### 3.2.4 Composite Deck

The 225 mm concrete deck is attached to the steel deck sections with the use of shear studs, making for a composite decking system. In the model, the bridge deck is modeled as shell elements. To deliver a composite deck system, constraints were assigned to both the steel and deck elements at the joint locations.

### 3.2.5 Connection Beams

Two connection beams are located 24 m from the north and south ends of the bridge deck. The two deck connection beams span between the arches, each carrying two elastomeric bearings. Figure 3-7 shows their layout and their cross-section dimensions are shown in Figure 3-8.

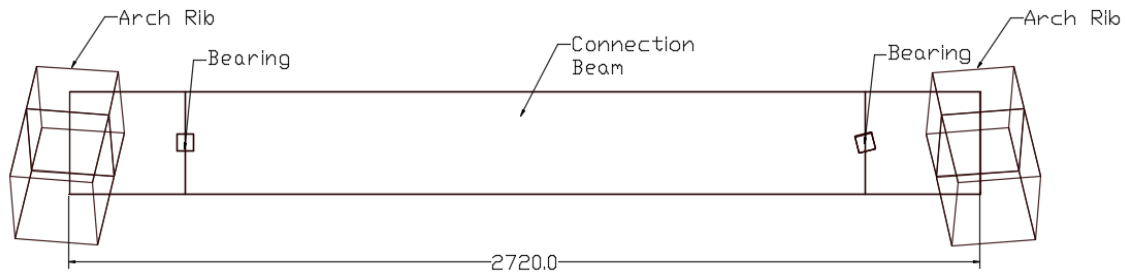


Figure 3-7: Connection Beam Layout in Millimeters

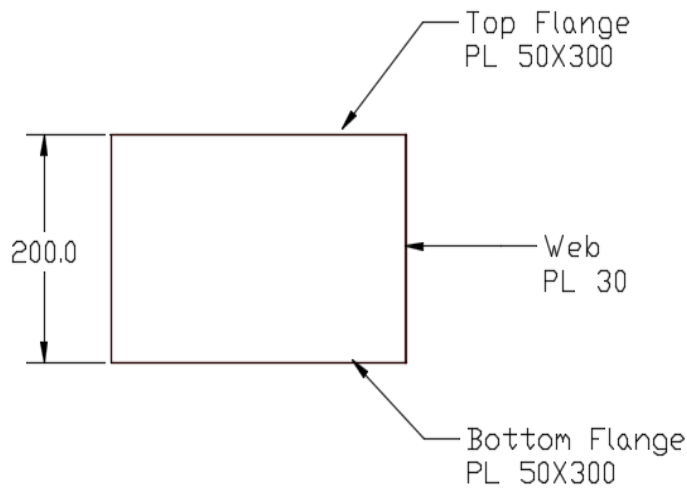


Figure 3-8: Connection Beam Cross-Section in Millimeters

### 3.2.6 Bearings

The bridge deck is seated on a total of eight elastomeric bearings, 4 on the outer corners of the deck that can move in the longitudinal direction with a stiffness of 2420 kN/m. A concrete block on the abutments prevents movement in the transverse direction. The four remaining bearings resting on the connection beams are free to move in both the longitudinal and transverse direction, with a stiffness of 2780 kN/m. In the model, the outer bearings are represented as links, while the inner bearings are modeled as frame elements with zero weight, all assigned with the proper restraints (Figure 3-9).

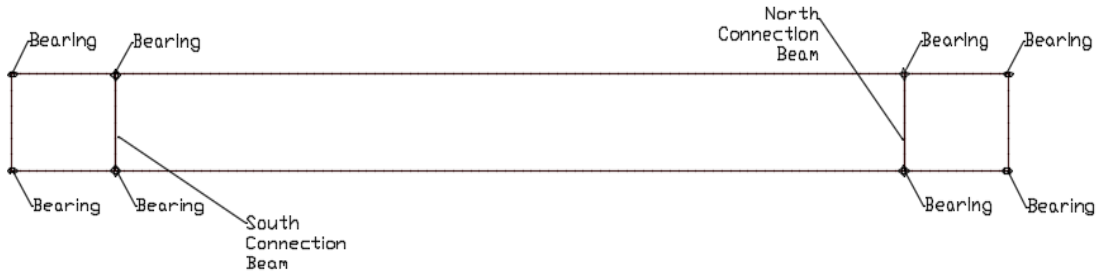


Figure 3-9: Deck Bearing Layout

### 3.2.7 Traffic Lanes

The bridge has been designed with 3 northbound bridge lanes as illustrated in Figure 3-10. Table 3-10 summarizes the lane geometry. In the model, the traffic lanes were specified by adding lanes with the appropriate placement and width to the bridge layout.

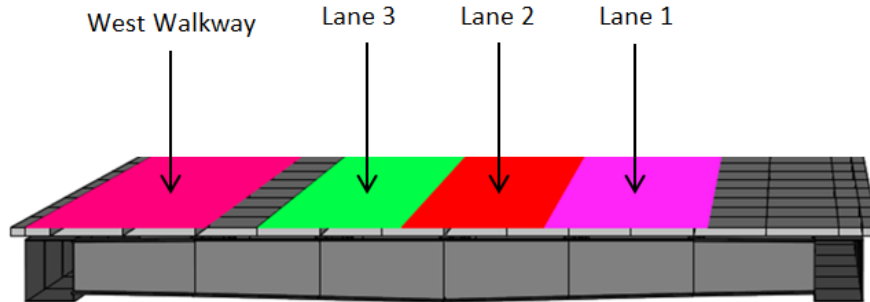


Figure 3-10: Traffic Lane and West Walkway Layout

Table 3-10: Lane Dimensions

Lane	Width (mm)
1	4200
2	3700
3	3700
<b>West Walkway</b>	3200

### 3.3 Arches

The arches are composed of 21 arch rib segments and 16 hangers on the east and west side of the structure. Sixteen arch struts are used to brace the arch ribs. The 4 thrust blocks are the main support elements, located at the ends of the arches. A side view is shown below (Figure 3-11). The SUP elements are not shown for clarity. A top view, showing the strut layout, is given in Figure 3-12. The maximum height measured from the bridge deck to the top of the archway is 56 m.

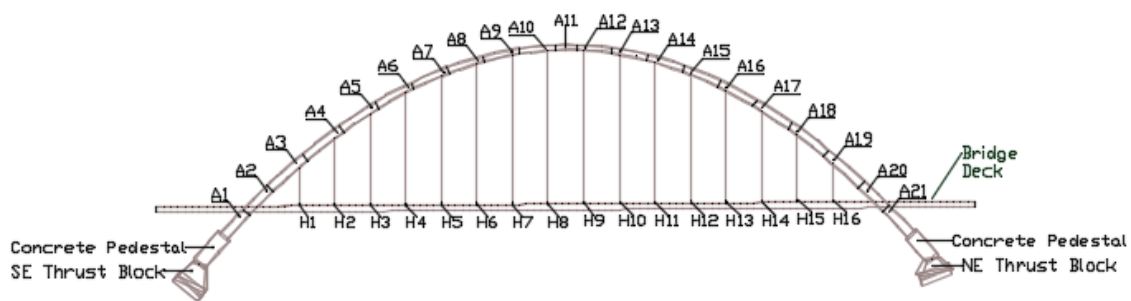


Figure 3-11: Bridge Arch Side View

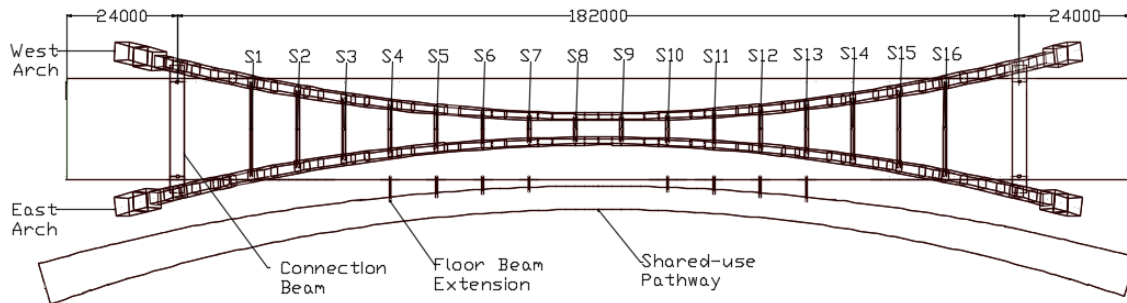


Figure 3-12: Bridge Arch Top View in Millimeters

#### 3.3.1 Freyssinet Cables

A total of 46 Freyssinet cables are used on the Walterdale Bridge. There are 16 Freyssinet cables on both the east and west edges of the bridge deck, vertically connecting the edge

girders to the arch. Another 14 cables are connected diagonally from the east arch to the SUP girders. The cables are modeled as cable elements, with the appropriate areas specified in the drawings (Table 3-11). From Table 3-11, the east cables may have a smaller area than the west cables due to the fact that both the east and SUP cables are attached to the east arch and are capable of supporting the east loads.

Table 3-11: Cable Areas

<b>Cable Section</b>	<b>West Area (mm<sup>2</sup>)</b>	<b>East Area (mm<sup>2</sup>)</b>	<b>SUP Area (mm<sup>2</sup>)</b>	<b>Cable Section</b>	<b>West Area (mm<sup>2</sup>)</b>	<b>East Area (mm<sup>2</sup>)</b>	<b>SUP Area (mm<sup>2</sup>)</b>
<b>H1</b>	4050	3750	N/A	<b>H9</b>	3300	2400	750
<b>H2</b>	3150	2400	1800	<b>H10</b>	3300	2100	1350
<b>H3</b>	3300	2250	1050	<b>H11</b>	3300	2400	1200
<b>H4</b>	3300	2100	1500	<b>H12</b>	3300	2250	1200
<b>H5</b>	3300	2250	1350	<b>H13</b>	3300	2250	1650
<b>H6</b>	3300	2400	1200	<b>H14</b>	3300	2250	1050
<b>H7</b>	3300	2100	1350	<b>H15</b>	3150	2250	1800
<b>H8</b>	3300	2550	750	<b>H16</b>	4050	3900	N/A

### 3.3.2 Arch Ribs

21 arch rib segments with 20 splice locations make up the archway on both the east and west edges of the bridge. The box arch ribs are of variable dimensions. They were modeled as non-prismatic frame elements to account for the parabolic change in dimensions along the length of the bridge. The maximum height and width of 2.5 m is achieved at the ends of the arch ribs, while the mid-section height and width at the top of the arches is 1.4 m. The largest flange and web thicknesses are 100 mm and 80 mm, respectively, located at the ends of the arches. The smallest flange and web thicknesses are both 70 mm, located at the mid-section of the arch. Figure 3-13 shows a typical arch rib cross-section.

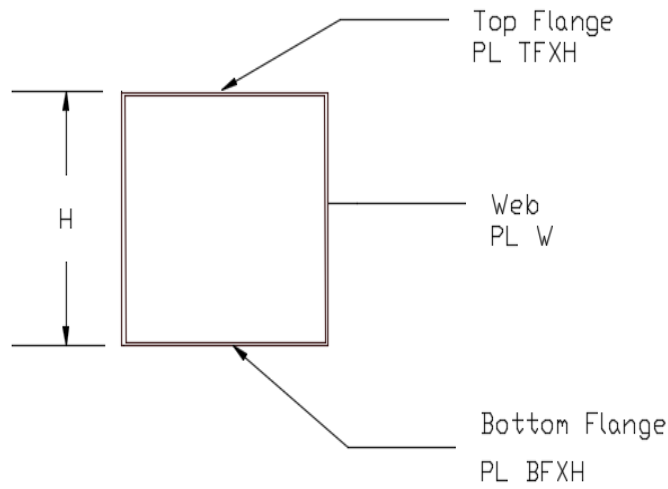


Figure 3-13: Arch Rib Cross-Section in Millimeters

### 3.3.3 Struts

A total of 16 struts span between the east and west arches. The struts are modeled as non-prismatic frame elements to account for their change in dimensions with length. The strut mid-section has a height of 500 mm. The outer strut heights vary with strut number. The general geometry, cross-section, and dimensions are summarized below in Figure 3-14, Figure 3-15 and Table 3-12, respectively.

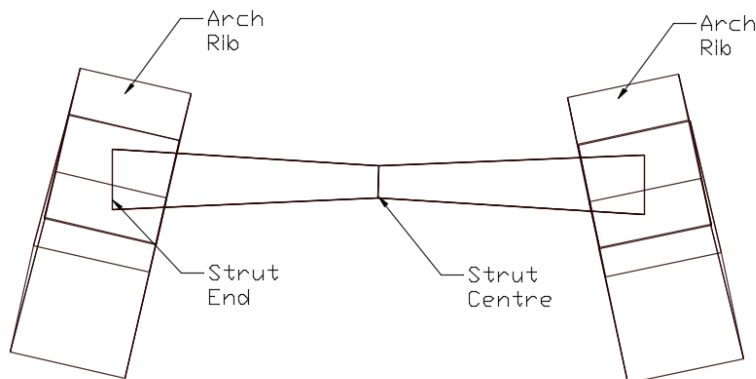


Figure 3-14: Arch Strut Layout

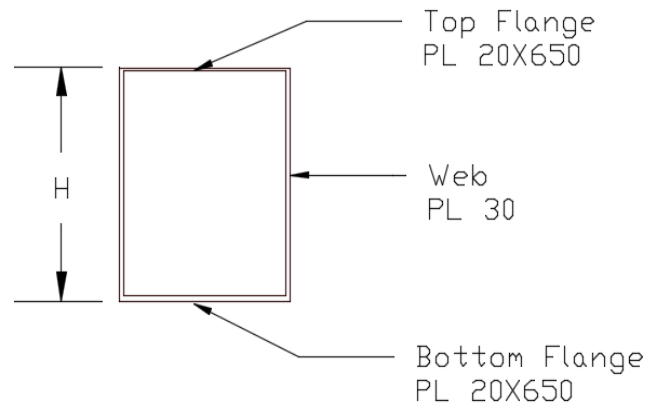


Figure 3-15 Arch Strut Cross-Section in Millimeters

Table 3-12: Strut End Dimensions

<b>Strut Section</b>	<b>End Height (mm)</b>
<b>S1 &amp; S16</b>	1800
<b>S2 &amp; S15</b>	1400
<b>S3 &amp; S14</b>	1200
<b>S4 &amp; S13</b>	1075
<b>S5 &amp; S12</b>	950
<b>S6 &amp; S11</b>	825
<b>S7 &amp; S10</b>	825
<b>S8 &amp; S9</b>	775

### 3.3.4 Thrust Blocks

Four thrust-blocks at the ends of both arch ways are responsible for carrying the loads transferred. The thrust blocks are made with concrete, reinforcing steel, and contain micro piles (not modeled). The thrust blocks are modeled as frame elements and are assigned with spring constraints at the ends of the thrust block base. The north and south thrust blocks vary in dimensions (Figure 3-16 and Table 3-13). The thrust block base is 9.00 m x 10.50 m, while the concrete pedestal above the thrust block is 4.00 m x 4.00 m. From Table 3-13, the north and south thrust blocks are not symmetric. This may be due to the soil conditions supporting them.

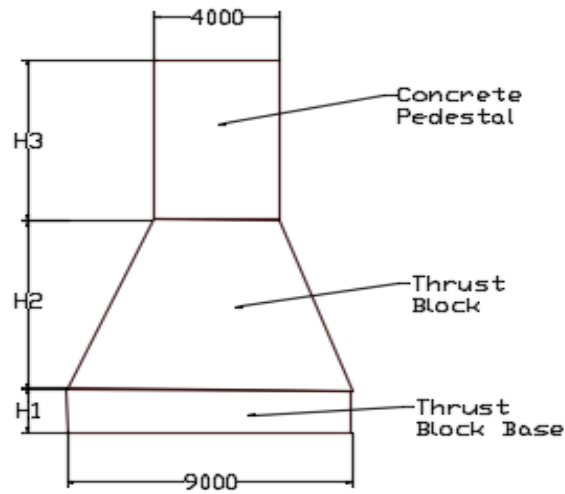


Figure 3-16: Thrust Block Layout in Millimeters

Table 3-13: Thrust Block Dimensions

Thrust Block Segment	H1 (mm)	H2 (mm)	H3 (mm)
North	2500	4000	8940
South	2500	4800	10450

### 3.4 Shared-Use Pathway (SUP)

The SUP consists of 25 SUP girder elements, 8 floor beam extensions, 8 bearings and 2 delta piers. The details of this structural component are explained below.

#### 3.4.1 Girders

The SUP girders are a polygonal geometry with a constant change in width along the length of the bridge. In the drawings, there are 25 splice locations. For ease of modeling, the girders are modeled as general frame sections with the correct properties. The maximum depth of the SUP is a constant 1.40 m, while the maximum width ranges from 9.13 m at the end sections to 5.07 m at the mid-section of the SUP.

### 3.4.2 Floor Beam Extensions

There are a total of 8 floor beam extensions that connect the east edge girder with the SUP girders. They have been modeled as frame sections, with the dimensions shown below in Figure 3-17.

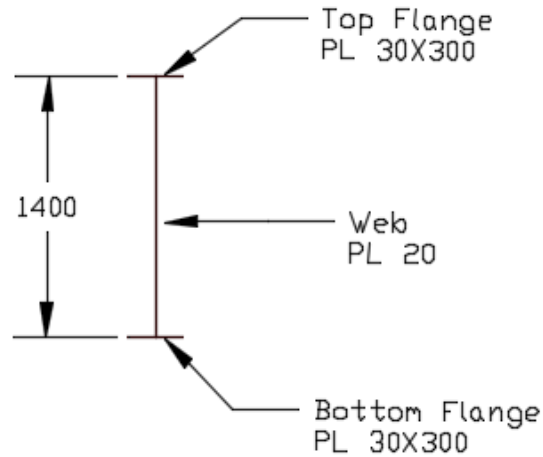


Figure 3-17: Floor Beam Extension Cross-Section in Millimeters

### 3.4.3 Bearings

The SUP rests on 8 bearings. There are 4 edge elastomeric bearings that can move in the longitudinal direction, modeled as restraints and springs, with a stiffness of 1225 kN/m, while the inner 4 are pot bearings that rest on the concrete delta piers free to move in both the longitudinal and transverse direction, and are modeled as frame elements. Figure 3-18 shows the SUP bearing layout.

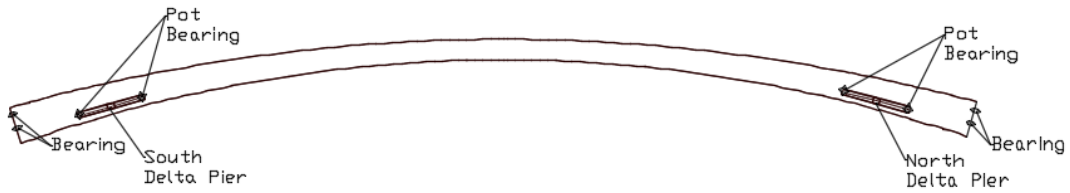


Figure 3-18: SUP Bearing Layout

### 3.4.4 Delta Piers

Two concrete delta piers are situated to support the SUP, varying in dimension at the north and south locations. They are located 26.17 m and 31.00 m inward from the south and north ends of the bridge deck, respectively. The dimensions of the north and south delta piers are summarized in Figure 3-19 and Table 3-14.

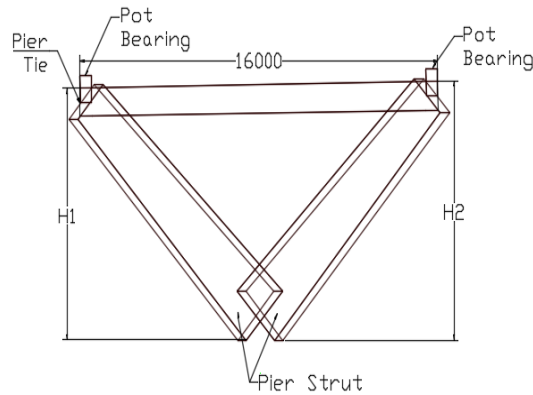


Figure 3-19: Delta Pier Side View in Millimeters

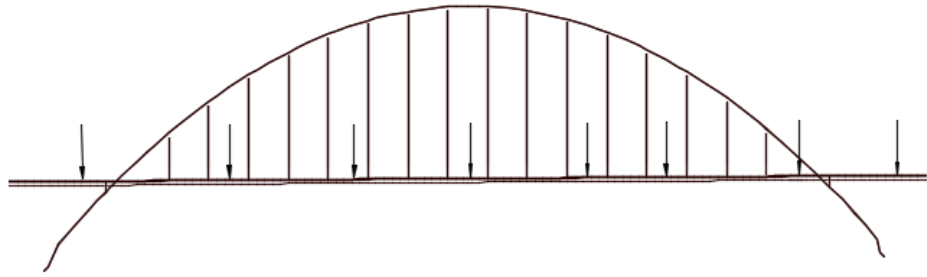
Table 3-14: Delta Pier Dimensions

Pier Segment	H1 (mm)	H2 (mm)
North	9995	9975
South	9975	10120

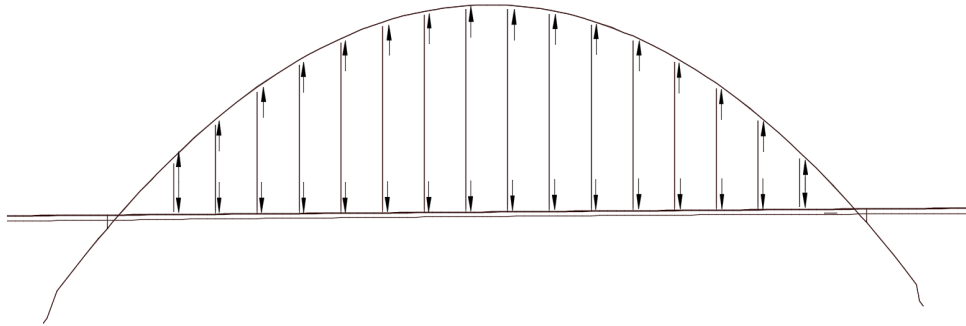
### 3.5 General Behaviour of a Thrust-Arch Bridge

The general behaviour of a thrust-arch structure was investigated and described, as shown in Figure 3-20. As shown in the figure, when a load is applied to the bridge deck (Figure

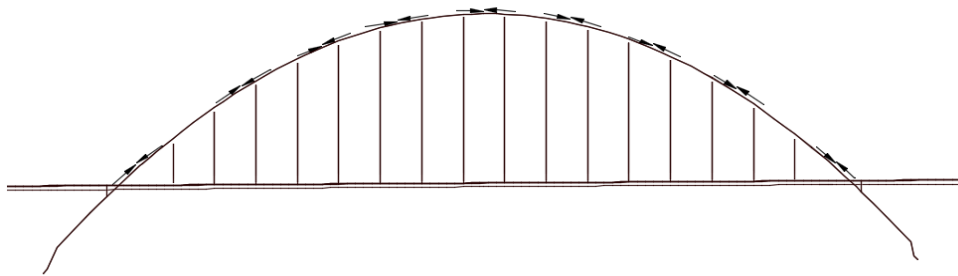
3-20a), the load is transferred from the deck to the cables in tension (Figure 3-20b). The load is then distributed to the arch above in compression (Figure 3-20c), and resolved at the thrust-blocks into horizontal, vertical and moment reactions, as shown in Figure 3-20d (Steelconstruction.info 2015). It should be noted that the cables are tension-only members, and must be analyzed using geometric nonlinearity in order to obtain meaningful results (CSI Analysis Reference Manual 2013). In order to capture the tension experienced in the cables, geometric nonlinear static analysis for static loads and nonlinear time-history analysis for moving loads were the two best options available in the analytical software, CSiBridge, that could generate the most accurate results considering the geometric nonlinearity limitations.



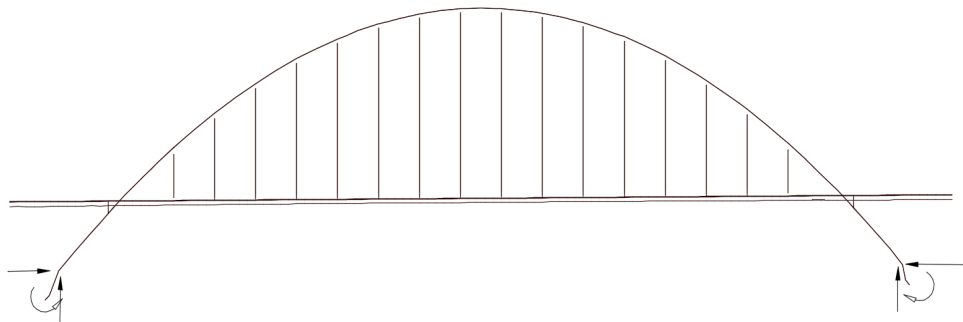
a. A load is applied to the bridge deck



b. The load is transferred to the tension-only cable members



c. The arch transfers the load in compression



d. The load is resolved into horizontal, vertical and moment reactions at the thrust blocks

Figure 3-20: General Behaviour of a Thrust-Arch Bridge

# CHAPTER 4: STRUCTURAL ANALYSIS

In order to develop an effective sensor layout plan, the behaviour of the bridge must first be clearly understood. This chapter presents the response of the bridge structure under different loading scenarios. The analysis results shown in this chapter were then used to determine the sensor locations. Since the Waltherdale Bridge contains tension-only cables, geometric nonlinear analysis was performed on the FE model in order to obtain appropriate results that capture the effects of these tension-only members. The model was analyzed under modal parameters, dead load, design temperature loads, design and predicted vehicle loads, design wind loads, design pedestrian load and a combination of these loadings. Design loads were taken from the Canadian Highway Bridge Design Code, S6 (CAN/CSA-S6 2006) and were analyzed in order to determine the design assumptions and locations which may be more conservatively designed. For design loads, serviceability limit state (SLS) analysis results are presented in this chapter, as it is a combination of loadings. Sample results from individual design loading cases are provided in Appendix B. Predicted vehicle loads were analyzed to understand what type of stresses, displacements, and vibrations should be expected under real loading conditions.

## 4.1 Modal Analysis

The dynamic properties of the Waltherdale Bridge were investigated to determine the natural frequencies,  $f_n$ , and the natural mode of vibration, known as mode shapes, that the structure experiences under free vibration using eigenvalue/eigenvector analysis. These properties are directly related to the mass and stiffness of the structure.

### 4.1.1 Natural Frequencies and Mode Shapes

The natural frequency of the structure, measured in Hz, refers to the frequency at which the system oscillates. The mode shapes of the structure describe the natural pattern of oscillation associated with a mode's natural frequency that the structure experiences. The natural frequency and mode shapes of the first 15 modes are shown in Figure 4-1. The higher modes are combined modes of vibration.

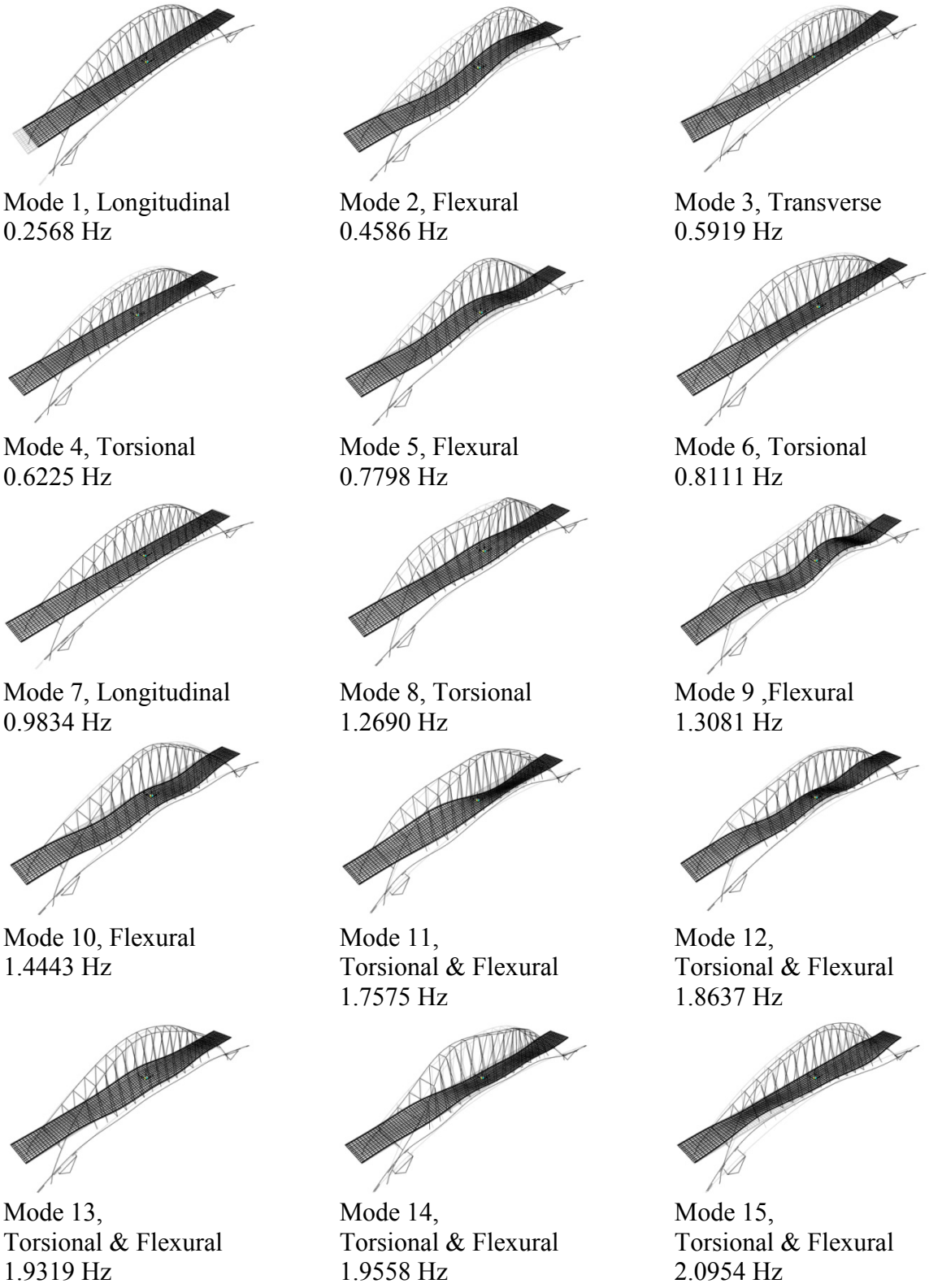


Figure 4-1: Natural Frequencies and Mode Shapes of the Waltherdale Bridge

## **4.2 Design Load Analysis**

The following section examines the bridge response under design dead load, temperature load, vehicle load, pedestrian load and SLS loading. Discussed in this section are the methods of determining the design loads based on CSA-S6-06, as this is the standards used for the design of the Walterdale Bridge. Only the results of SLS are presented.

### **4.2.1 Dead Load Analysis**

Dead load analysis investigates the effects caused by all materials on the structure that are not subject to movement. This includes the self-weight of the structural members, the SUP rails on the east and west edge of the SUP, traffic barriers, the utility loads along the deck, the wearing surface on the deck and SUP, the pre-strain forces and hanger anchorage load.

The weights of the structural members and surfaces used were presented in Chapter 3, provided in the preliminary model. Other dead loads include the pedestrian barriers, which have a uniform gravity load of 1.20 kN/m on both the east and west edge of the SUP, specified in S6. The utility loads are applied at the two utility duct tray locations found on the bridge deck. Utility tray 1 has a total weight of 7.15 kN/m, and utility tray 2 has a total weight of 6.53 kN/m that span throughout the entire bridge deck. The utility dead loads are specified in the Walterdale Bridge drawings.

The pre-strain forces were calculated based on the difference between the stressed and unstressed length of the hangers, as provided in the drawings. The main hanger anchorage loads are based on the size and material weight of the anchors. Both the pre-strain and anchorage loads were provided with the preliminary model.

### **4.2.2 Temperature Load Analysis**

Design temperature load consists of effective temperature ranges for expansion and contraction, as well as summer and winter thermal gradients. The loads described in the following section were provided with the preliminary model, and checked to ensure their correctness based on the following method. For SLS analysis, a temperature load

envelope was created to consider the maximum effects from each loading scenario presented below.

**4.2.2.1 Effective Temperature**

CSA-S6-06 indicates the maximum and minimum mean daily temperatures for the Edmonton region are summarized in Table 4-1 below.

Table 4-1: Mean Daily Temperatures from CSA-S6-06

<b>Maximum Mean Daily Temperature</b>	28 <sup>0</sup> C
<b>Minimum Mean Daily Temperature</b>	-41 <sup>0</sup> C

The maximum and minimum effective temperatures are then modified based on the mean temperatures. Modification is dependent on the superstructure type, given in Table 3.7 of CSA-S6-06 (reproduced in Figure 4-2). The superstructure types are specified in Table 4-2.

**Table 3.7**  
**Maximum and minimum effective temperatures**  
 (See Clause 3.9.4.1.)

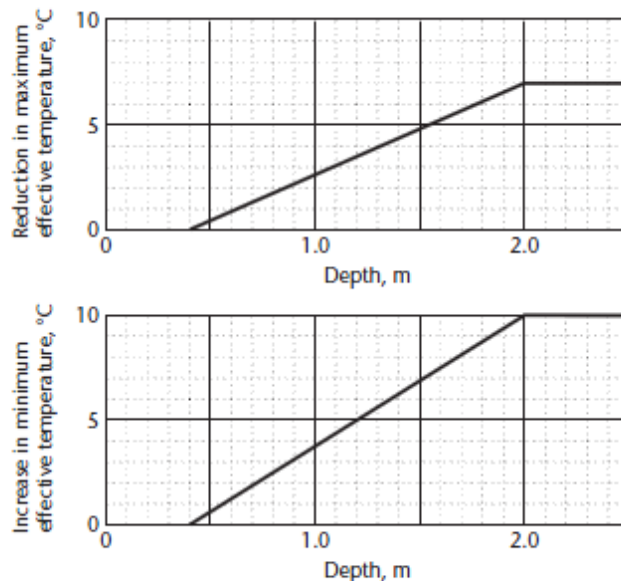
Superstructure type (see Clause 3.9.3.)	Maximum effective temperature	Minimum effective temperature
A	25 °C above maximum mean daily temperature	15 °C below minimum mean daily temperature
B	20 °C above maximum mean daily temperature	5 °C below minimum mean daily temperature
C	10 °C above maximum mean daily temperature	5 °C below minimum mean daily temperature

Figure 4-2: Modification for Effective Temperatures (CAN/CSA-S6 2006)

Table 4-2: Temperature Based on Structure Type from CSA-S6-06

Structure Type	Element	Maximum Effective Temperature	Minimum Effective Temperature
A	Main arch steel and SUP	53 <sup>0</sup> C	-56 <sup>0</sup> C
B	Deck and Floor Beams	48 <sup>0</sup> C	-46 <sup>0</sup> C
C	Delta Piers	38 <sup>0</sup> C	-46 <sup>0</sup> C

After adjustments were made based on superstructure type, changes were made to the maximum and minimum effective temperatures based on their depth, specified in Figure 3.5 of CSA-S6-06 (reproduced in Figure 4-3). The difference between maximum and minimum effective temperatures and effective construction temperature of -5<sup>0</sup>C, specified in the drawings, was then considered to calculate the effective temperature ranges for expansion and contraction.



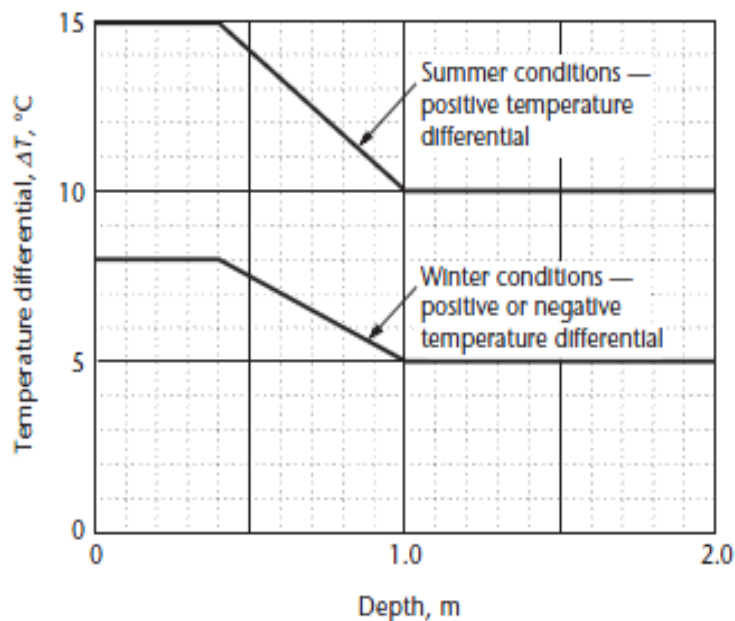
**Figure 3.5**  
**Modifications to maximum and minimum effective temperatures**  
 (See Clause 3.9.4.1.)

Figure 4-3: Modifications to Effective Temperatures (CAN/CSA-S6 2006)

#### 4.2.2.2 Thermal Gradient

The effect of thermal gradients throughout the depth of the structure types was also analyzed. The temperature differential for type A and C structures were provided in Figure 3.6 of CSA-S6-06 (reproduced in Figure 4-4). Both summer and winter conditions are considered. For winter conditions, both positive and negative thermal gradients are analyzed. For summer conditions, only positive gradients are considered, as specified in CSA-S6-06. Positive gradients refer to a top surface being warmer, with a linear decrease until the bottom surface.

For type B structures, a positive temperature differential decreasing linearly by 30°C from top to bottom of the deck slab was considered. The structural elements below the concrete slabs are not considered when analysing thermal gradient effects. Type B structures consider only positive differentials.



**Figure 3.6**  
**Temperature differentials for Type A and C superstructures**  
(See Clause 3.9.4.4.)

Figure 4-4: Temperature Differentials for Type A and C Superstructures (CAN/CSA-S6 2006)

### 4.2.3 Vehicle Load Analysis

The primary live load experienced by a bridge will be due to vehicles. The FE model was analyzed under a vehicle design load of a CL-W800 truck. Although this is unlikely to occur on the structure very often, it is necessary that the bridge be designed for this loading situation.

CSA-S6-06 specifies a CL-W Truck load with dynamic load allowance (DLA) and a CL-W Lane load to be used when designing a bridge. The specific loading required for the Walterdale Bridge is a CL-W800 Truck and CL-W800 Lane load, referring to  $W$ , the gross load of the axle loads, as being 800 kN. A CL-W800 Truck is a five axle truck with the gross load distribution shown below in Figure 4-5 (reproduced from CSA-S6-06). A CL-W800 Lane Load (Figure 4-6), reduces the axle load by 80%, but includes a uniformly distributed load of 9 kN/m across the length of the bridge (reproduced from CSA-S6-06).

In order to perform nonlinear moving load analysis in the CSiBridge software, time-history moving load analysis was used. In this case a constant force with a time step of 0.02 seconds and damping of 2%, with no DLA applied to the truck loading, as the load applied can be considered dynamic. Although a DLA typically incorporates the effects of irregularity of riding surface, bridge static and dynamic deflections, and the interaction between a moving vehicle and the bridge, CSiBridge time-history analysis includes the effects of vibrations only. For SLS1, a loading envelope was created for CL-W800 Truck and Lane loading to produce the maximum effects from either CL-W800 load type.

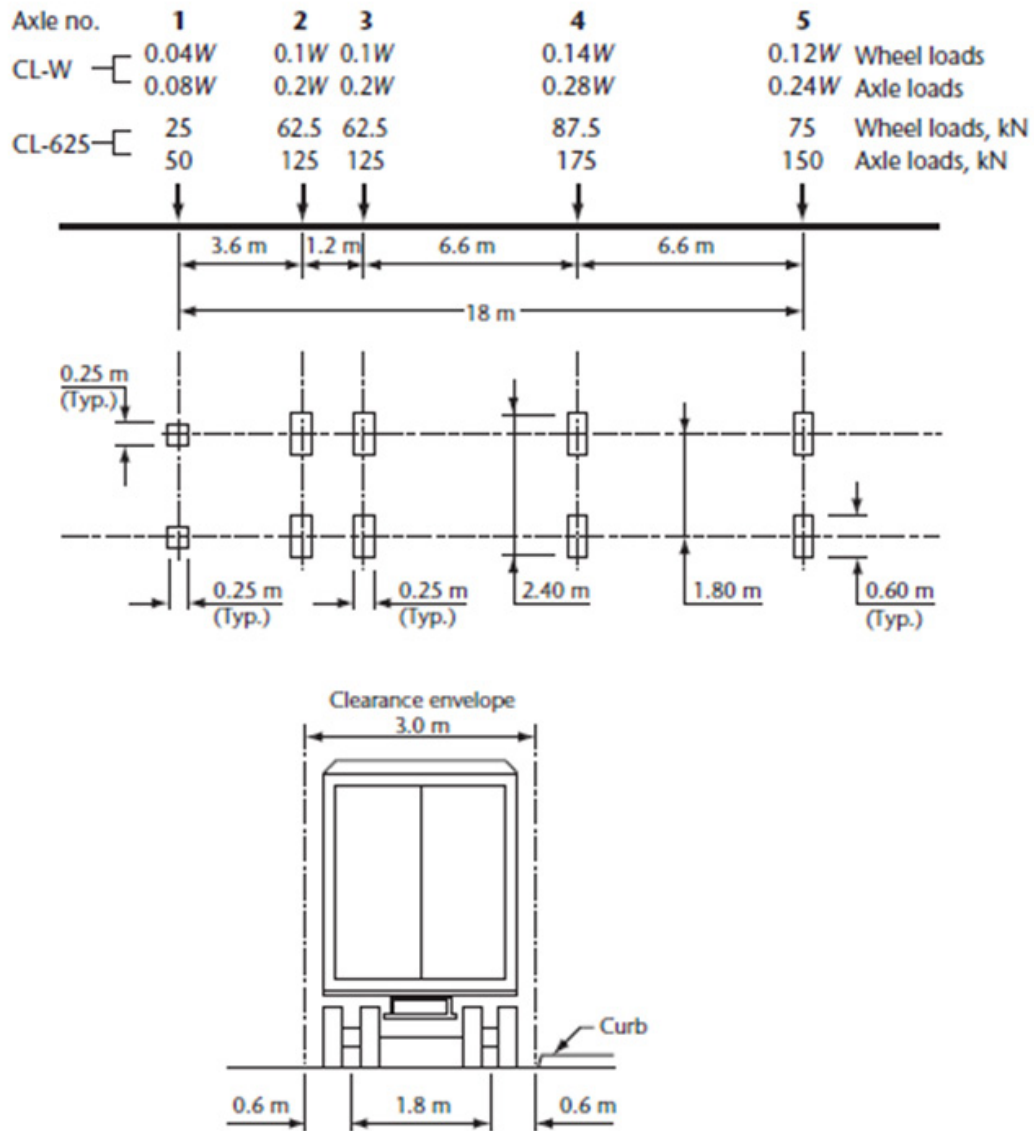


**Figure 3.2**  
**CL-W Truck**  
 (See Clause 3.8.3.2.)

Figure 4-5: CL-W800 Truck Load (CAN/CSA-S6 2006)

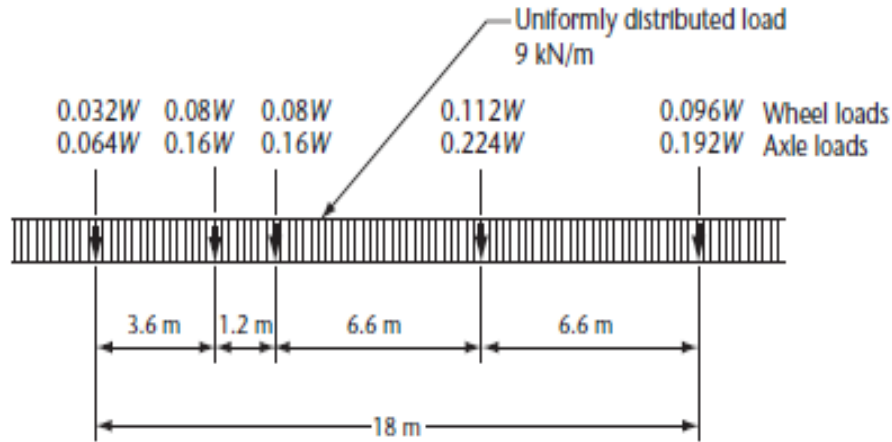


**Figure 3.3**  
**CL-W Lane Load**  
 (See Clause 3.8.3.3.)

Figure 4-6: CL-W800 Lane Load (CAN/CSA-S6 2006)

#### 4.2.4 Pedestrian Load Analysis

The Walterdale Bridge contains two locations for pedestrian use: a west walkway located at the west edge of the bridge deck, and the shared-use pathway, a pedestrian bridge located on the east side of the bridge. Pedestrian loads at both locations were analyzed.

CSA-S6-06 specifies a static pedestrian load of:

$$p = 5.0 - \frac{s}{30} \quad [4-1]$$

where the loading is calculated in kPa and  $s$  is the total loaded length of walkway in Equation 4-1, which is roughly 230 m for both. The resulting load is negative.

##### 4.2.4.1 West Walkway

A uniform negative load of 2.67 kPa was placed on the west walkway lane created and analyzed for critical locations.

##### 4.2.4.2 Shared-use Pathway

The shared-use pathway pedestrian load required analysis under a load envelope using multiple load patterns, since the SUP hangers create additional boundary conditions that

can have a significant effect on the behaviour of the structure. The highest effects of loading may not be captured using a uniformly distributed load only.

With the use of influence lines created at locations of critical bending moment and shear, multiple load patterns were produced, and the SUP was analyzed under a loading envelope of the load patterns in order to determine locations that experience the highest amount of deflection and stress. The influence lines used were extracted from the FE model. In addition to a uniformly distributed load along the SUP, the following load patterns shown in Figure 4-7 were also applied to the structure.

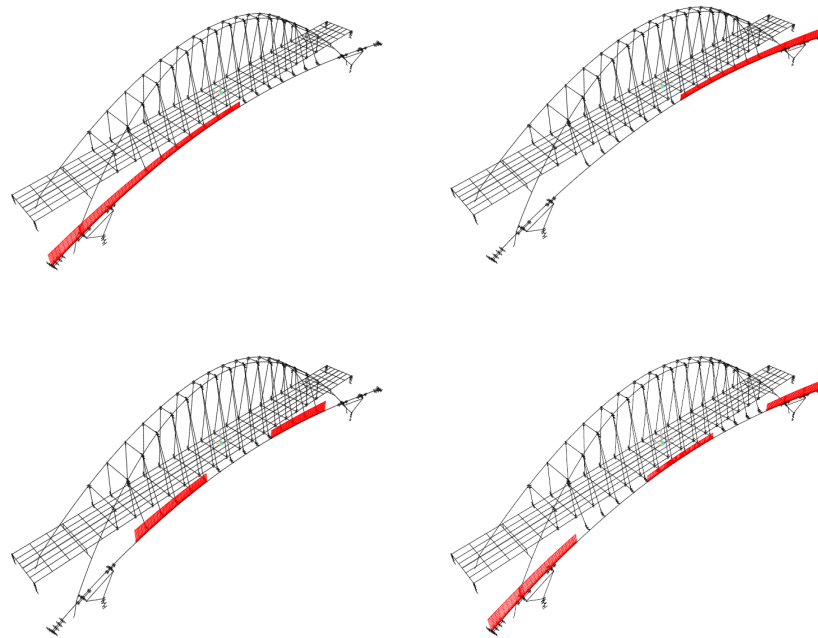


Figure 4-7: Load Patterns of SUP Pedestrian Load

#### 4.2.5 Wind Load Analysis

The design wind loads were provided with the preliminary model and checked to ensure their correctness using the following method. Wind loads were calculated based on an hourly mean reference pressure of 510 Pa for a return period of 100 years in the Edmonton region, as specified in CSA-S6-06. Design wind load is a static load analysis. A gust coefficient, wind exposure coefficient, horizontal drag coefficient and vertical drag coefficient were considered in calculations, according to CSA-S6-06. The hourly mean reference pressure was increased by 20% in calculations for horizontal and vertical

drag loads to account for potential funneling, as specified in Clause 3.10.1.2 of CSA-S6-06.

The gust coefficient,  $C_g$ , was taken as 2.5; a wind exposure coefficient,  $C_e$ , is calculated based on the height,  $H$ , above ground of the superstructure in which wind load is being applied (Equation 4-2).

$$C_e = (0.10H)^{0.2} \quad [4-2]$$

A horizontal drag load, calculated using Equation 4-3, where the horizontal drag coefficient,  $C_H$ , is specified as 2.0.

$$F_H = qC_eC_gC_H \quad [4-3]$$

CSA-S6-06 specifies a vertical drag load, calculated using Equation 4-4, where the vertical drag coefficient,  $C_v$ , is specified as 1.0. The vertical load is applied both upward and downward. Along with the vertical drag load applied uniformly over the entire plan area exposed to wind load, the effect of eccentricity was also considered, as specified in CSA-S6-06. To consider the effects of eccentricity, the same vertical load was applied as an equivalent vertical line load at the windward quarter point of the transverse superstructure width.

$$F_V = qC_eC_gC_V \quad [4-4]$$

Wind load on live load was also considered by taking the horizontal drag coefficient as 1.2, and multiplying by a height of 1.2 m for the SUP live load, and 3.0 m for the roadway surface, as specified in CSA-S6-06.

For analysis, multiple load combinations based on horizontal and vertical directions were created for wind loading. A loading enveloped using all load combinations was then used to analyze the most critical locations.

#### **4.2.6 Serviceability Limit State Analysis**

The design load combination of Serviceability Limit States (SLS) was analyzed using Equation 4-5 and Equation 4-6, taken from CSA-S6-06.

$$SLS1 = 1.00 \times \text{Dead Load} + 0.90 \times \text{Live Load} + 0.80 \times \text{Deformation Load} \quad [4-5]$$

$$SLS2 = 0.90 \times \text{Live Load} \quad [4-6]$$

Equation 4-6 is used to analyse superstructure vibrations due to live load only, and pertains to the deflection and vibration chart in Figure 4-8 (reproduced from CSA-S6-06). Live load refers to both traffic and pedestrian design loads, while deformation load refers to temperature design loads in this analysis, although deformation loads can also be caused from other sources, such as settlement.

SLS is a design criterion concerned with durability, functionality and human comfort levels. Although SLS is not an actual physical situation that the bridge is likely to experience, it is a necessary computational check to ensure that the structure adheres to certain serviceability limits specified in CSA-S6-06, and to identify the locations that are the most critical under this type of load combination. CSA-S6-06 states that the serviceability limit state must consider the deflections, yielding and superstructure vibration limits of the structure. The superstructure vibration limits can be determined using Figure 4-8, where the load used in analysis shall be only one CL-W800 truck load with DLA placed at the centre of one lane multiplied by a factor of 0.9, as computed in Equation 4-6 above, although this figure may not be applicable for a thrust-arch bridge, since CSA-S6-06 is mostly used for typical highway girder-beam bridge structures. However, Figure 4-8 will be used to evaluate the vibration of this bridge since no other information is available for arch type bridges. For yielding, CSA-S6-06 states:

*“Members of all classes of sections shall be proportioned so that general yielding does not occur. Localized limited yielding shall be permitted.”*

For SHM purposes, SLS load combination gives a good indication of areas that may be more prone to high stresses and areas of occupant discomfort. SLS load combination can also be used for areas that are susceptible to fatigue failure. These are areas that can be monitored to ensure the structure fulfills its function under everyday use and continues to meet the SLS limits in CSA-S6-06.

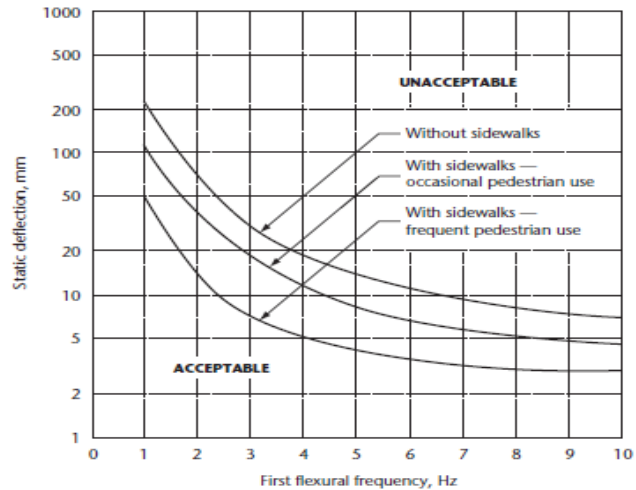


**Figure 3.1**  
**Deflection limits for highway bridge superstructure vibration**  
 (See Clause 3.4.4.)

Figure 4-8: Vibration Limits of SLS (CAN/CSA-S6 2006)

#### 4.2.6.1 Displacements

Since vibration limitations are based on SLS2, the following will present the displacements given by Equation 4-6 only. The first flexural frequency of the structure is 0.4586 Hz, which can be interpreted in Figure 4-8 as a static deflection maximum of 50 mm at both the SUP and west walkway, since it should be expected that both walkways will experience frequent pedestrian usage, considering the location of the bridge. Since the west edge girder is part of the west walkway, the deflections of the west edge girder are shown. The deflection envelope, showing the maximum displacements experienced on the bridge is shown in Figure 4-9. From Figure 4-10 and Figure 4-11, both walkways meet the criteria necessary for deflections. The largest displacements are seen at 91 m and 143 m along the SUP, and at 85 m and 140 m along the west walkway.

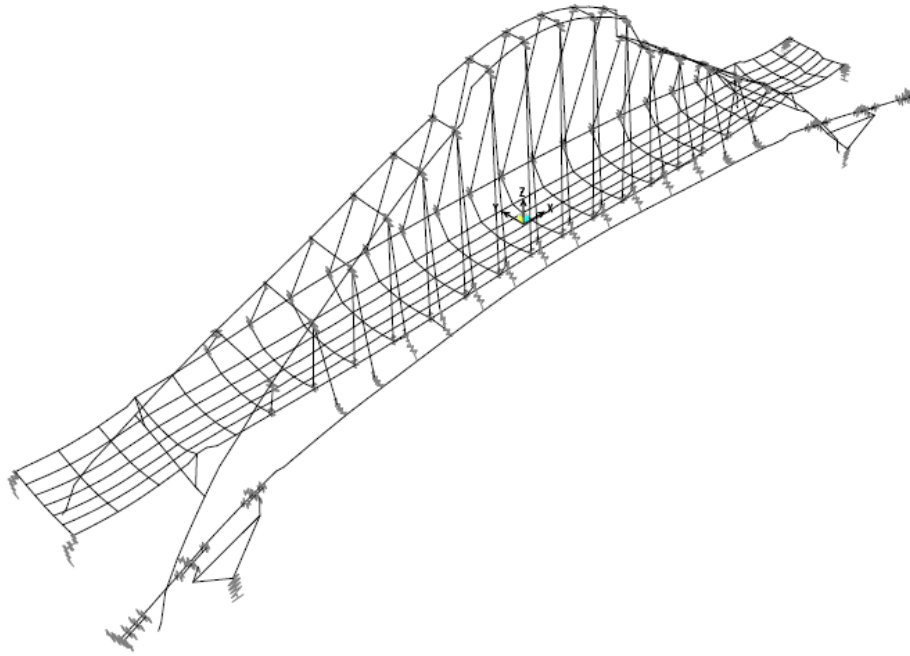


Figure 4-9: Deflected Shape Envelope under SLS2 Load

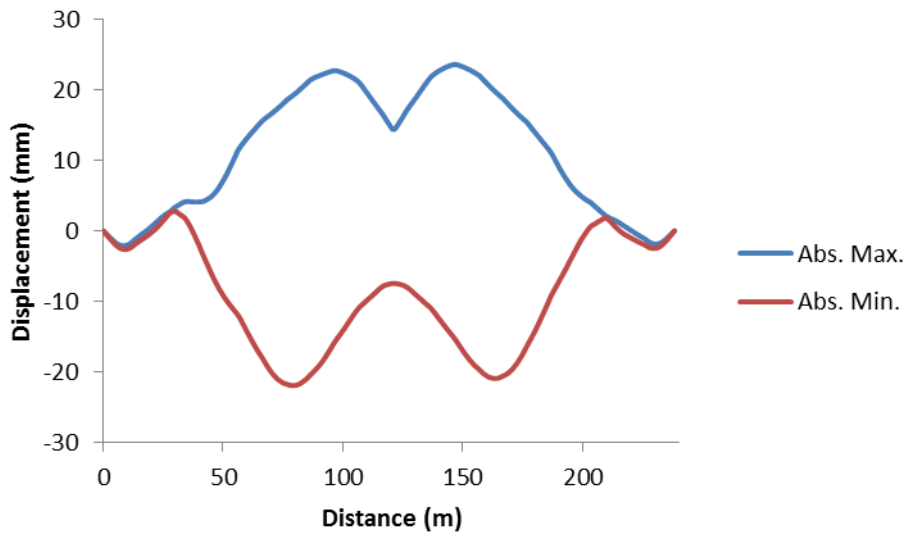


Figure 4-10: SLS2 SUP Displacement Envelope

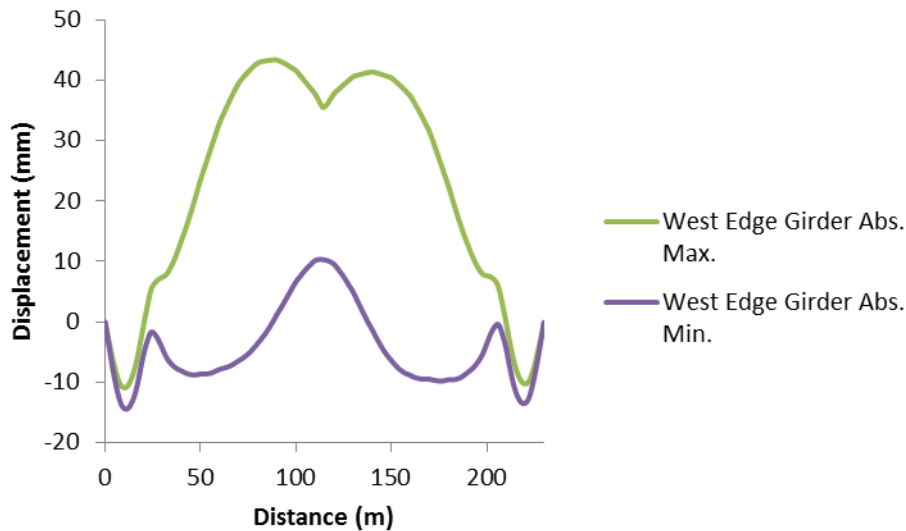


Figure 4-11: SLS2 West Walkway Displacement Envelope

#### 4.2.6.2 Stresses

In the edge girders, the highest normal stresses occur at the end spans and inner bearing locations since the end-spans are not connected to the arches, which can aid in supporting the load. The largest normal stress is roughly -200 MPa at 24 m and 206 m along the length of the edge girders (Figure 4-12). From Figure 4-13, the arches experience the largest negative normal stresses at mid-span, with a normal stress of -130 MPa at the east arch location. The SUP is subject to its highest stresses at 30 m and 203 m, with a stress of -70 MPa (Figure 4-14), which are near the delta-pier locations. The east hangers carry the largest normal stresses, with the maximum normal stress of 760 MPa occurring in east hanger 12 (Figure 4-15). The east hangers carry significantly more stress than the west hanger locations. This can be attributed to the smaller areas of the east hangers relative to the west hangers, and the fact that the bridge may not behave as a perfectly rigid structure. From the drawings provided, it seems that the west hangers were designed to carry a larger share of load due to the larger size of their cross-section compared to the east hangers, as shown in Table 3-11. This assumption is correct if the bridge deck behaves as perfectly rigid. However, this design assumption may not be completely accurate, as the bridge deck does not seem to act as a fully rigid under this analysis. When the flexibility of the bridge deck/floor beam is considered, the east hangers carry

the higher share of load as compared to the west hangers. Appendix C provides an investigation into this concept.

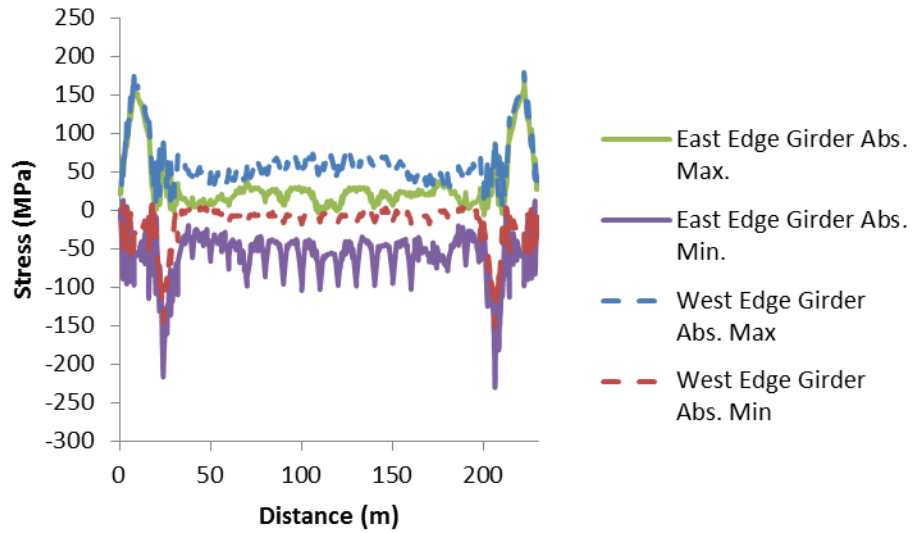


Figure 4-12: Normal Stress Envelope of Edge Girders under SLS1 Load

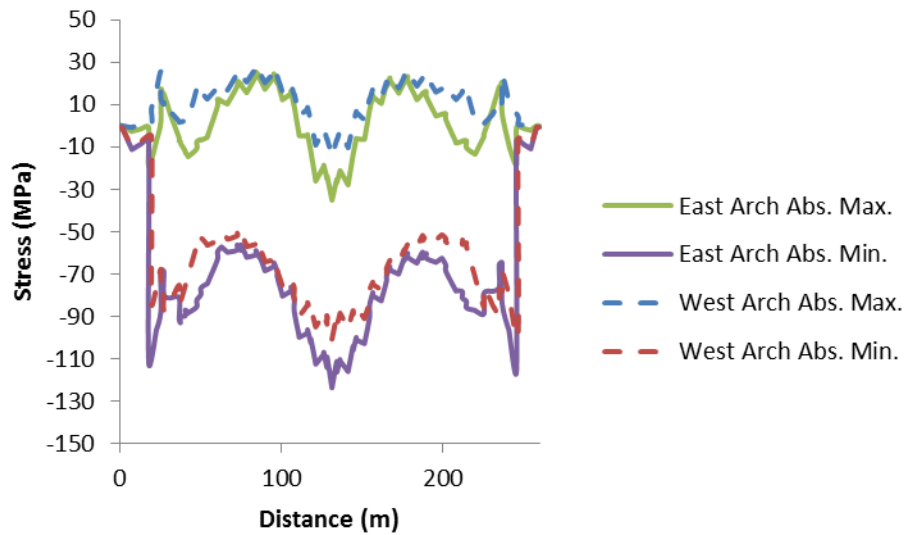


Figure 4-13: Normal Stress Envelope of Arches under SLS1 Load

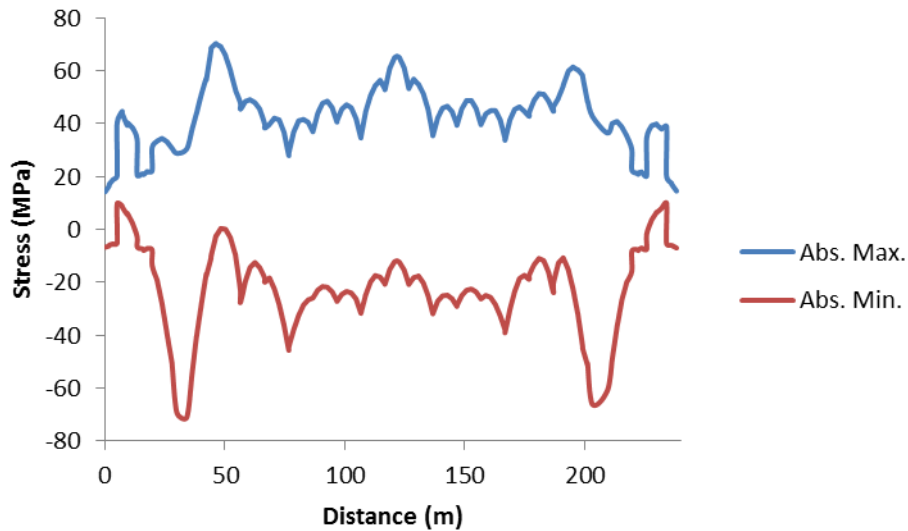


Figure 4-14: Normal Stress Envelope of SUP under SLS1 Load

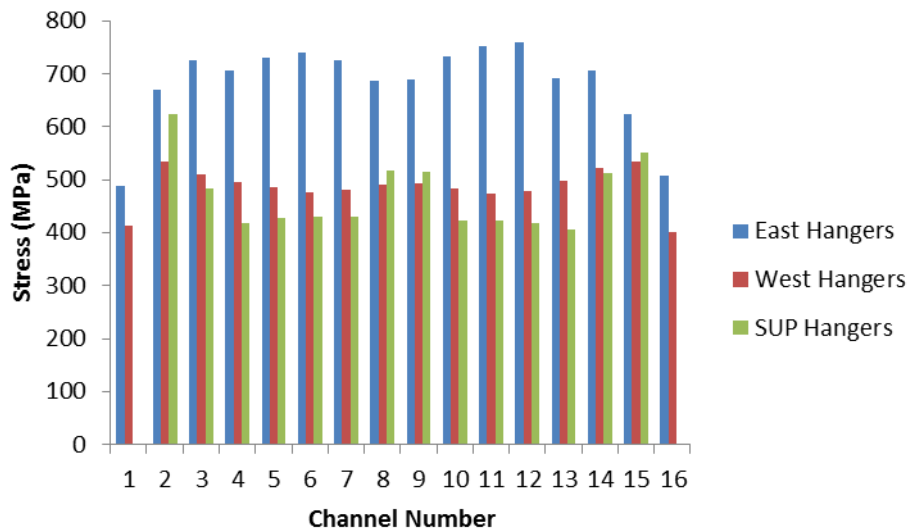


Figure 4-15: Normal Stress of Hangers under SLS1 Load

### 4.3 Predicted Vehicle Load Analysis

Predicted vehicle load refers to the expected loads that will be present on the Walterdale Bridge. These predicted loads were chosen based on the Average Annual Weekday Traffic (AAWT) volume of 2013. Average daily traffic was used to have a better understanding of the in-situ behaviour that will occur on the structure Traffic flow was

taken from a flow map from Edmonton.ca (2015). A volume of approximately 2,300 vehicles was reported during peak traffic hours.

Using this information, an estimated number of 12 vehicles are present on the bridge at one time during high volume periods. The 12 vehicles were then divided equally into the three traffic lanes, for a total of 4 vehicles in each lane. It was assumed that the 4 vehicles in each lane will be 3 seconds apart. The vehicles were simulated to travel at 50 km/hr, as this is the speed limit designated.

The vehicles crossing the bridge were designed to have a length of 5.5 m and a weight of 40 kN, distributed evenly by 4 point loads. This weight is representative of a large SUV or truck, plus any additional weight it may be carrying. The top and side views are given in Figure 4-16 and Figure 4-17. The results shown below reflect the behaviour due to the predicted loading and dead loading.

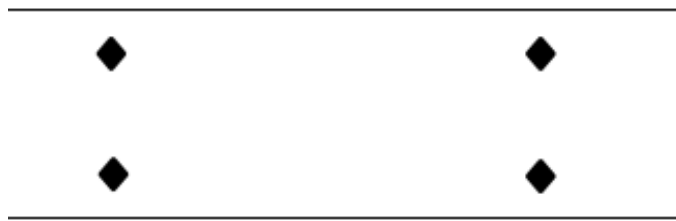


Figure 4-16: Predicted Truck Top View

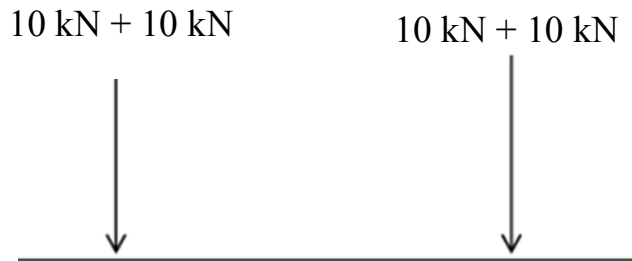


Figure 4-17: Predicted Truck Side View

### 4.3.1 Displacements

The deflected shape of the Walterdale Bridge under predicted traffic load is shown in Figure 4-18. Maximum negative vertical displacement of the edge girders of -10 mm occurs at 50 m and 180 m of the east edge girder, along its length (Figure 4-19). Maximum positive vertical deflection of the edge girders occurs at mid-span of the west edge girder, with a deflection of 30 mm. The bridge deck experiences the highest transverse displacement of 35 mm at mid-span, which is expected, since the bridge deck is the least transversely restraint at mid-span (Figure 4-20). From Figure 4-21, the maximum longitudinal displacement of the bridge deck is approximately 10 mm. The highest vertical displacement of the SUP occurs at 102 m and 132 m along its length (Figure 4-22).

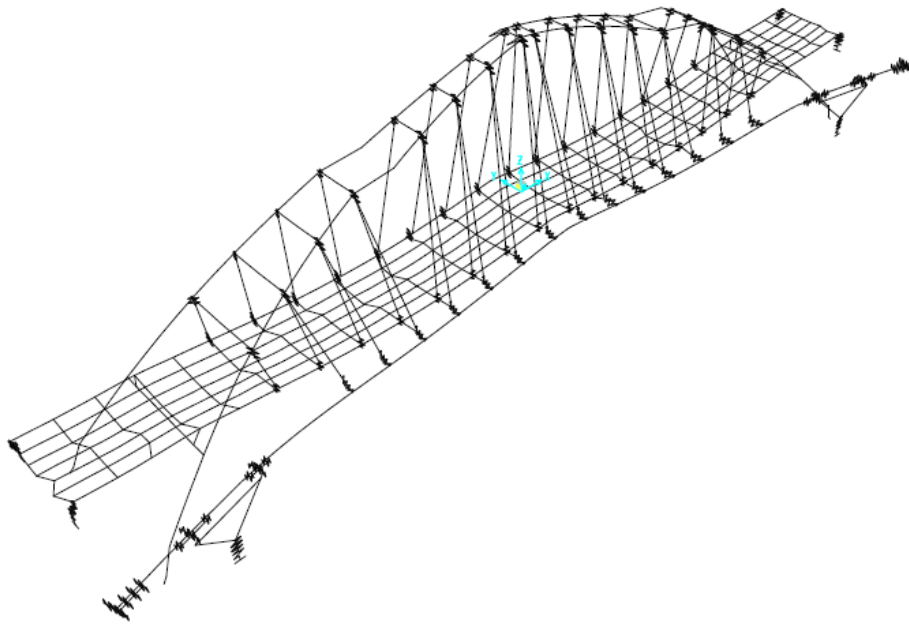


Figure 4-18: Deflected Shape Envelope under Predicted Traffic Load

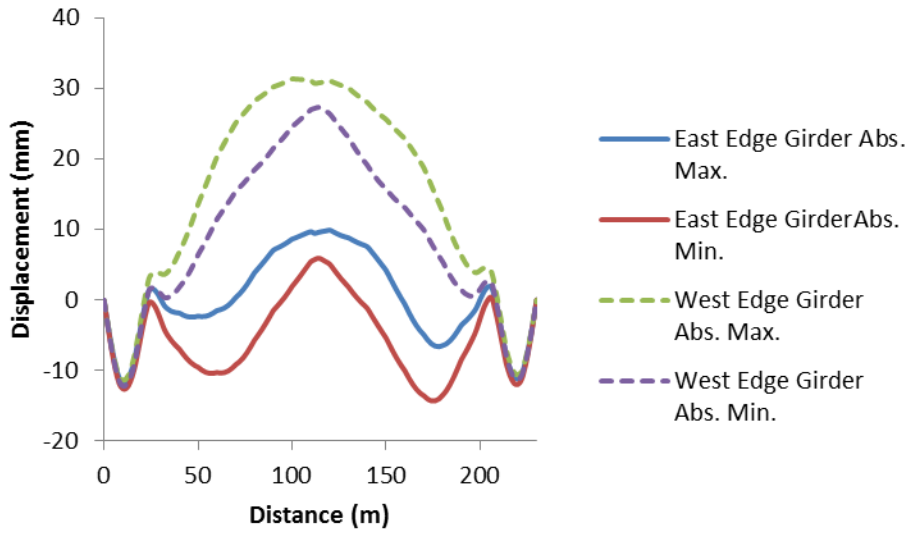


Figure 4-19: Vertical Displacement Envelope of the Bridge Deck under Predicted Traffic

Load

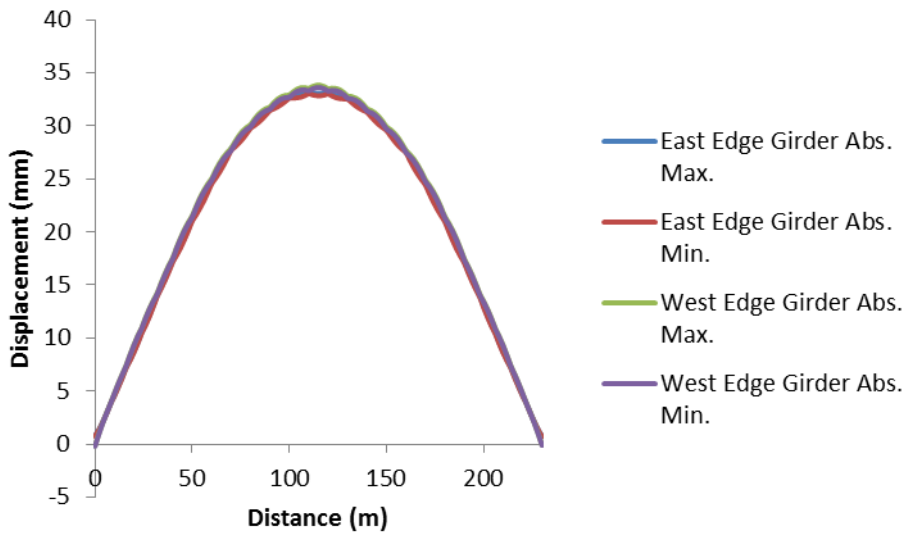


Figure 4-20: Transverse Displacement Envelope of Bridge Deck under Predicted Traffic

Load

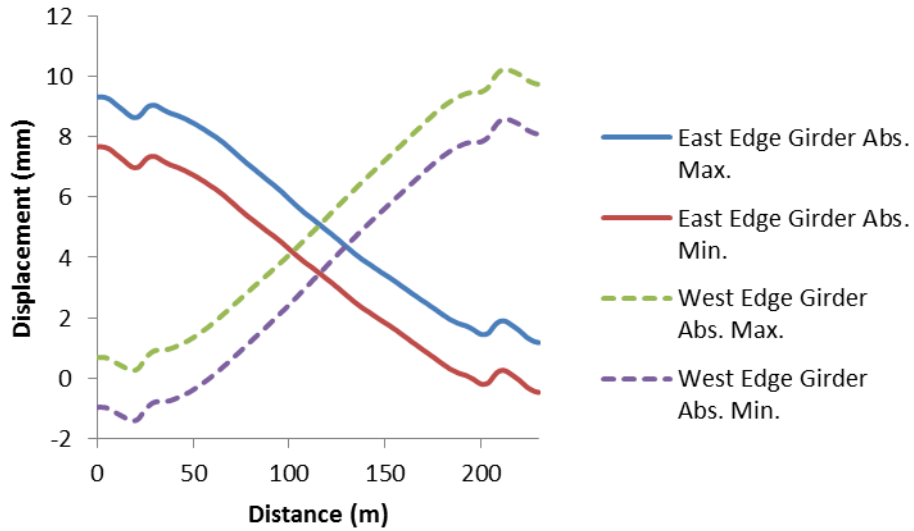


Figure 4-21: Longitudinal Displacement Envelope of the Bridge Deck under Predicted Traffic Load

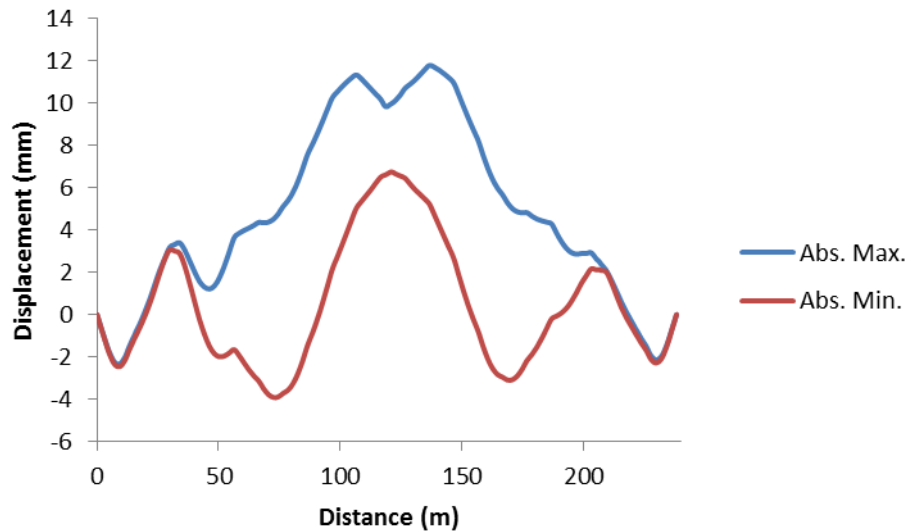


Figure 4-22: Vertical Displacement Envelope of SUP under Predicted Traffic Load

### 4.3.2 Stresses

The maximum normal stress of the bridge deck occurs at end-span locations, which is expected since the end spans are not connected to the arch with hangers. A maximum positive normal stress of 70 MPa occurs at the mid-section of the end-spans. A maximum negative normal stress of -70 MPa occurs at the inner bearing locations (Figure 4-23).

The mid-span of the edge girders, which are connected to hangers, experiences a relatively constant stress throughout its length. The inner girders experience the largest amount of normal stress at inner girder 3, which is the stringer located directly below the middle traffic lane, with a relatively constant value of 100 MPa throughout its length. Peaks occur at locations of the floor beams that run through the inner girder, as this is where the loads are transferred to the floor beam locations. The stresses of inner girder 3 only are displayed in Figure 4-24 for clarity. Maximum normal stress of -80 MPa in the east arch occurs at mid-span (Figure 4-25). The largest normal stress of approximately 640 MPa in the bridge hangers occurs at east hanger 12 (Figure 4-26).

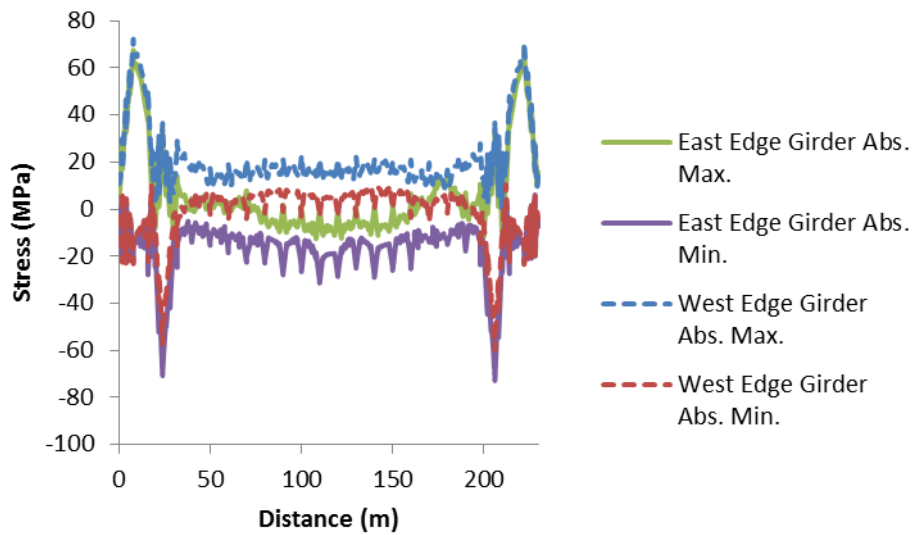


Figure 4-23: Normal Stress Envelope of the Edge Girders under Predicted Traffic Load

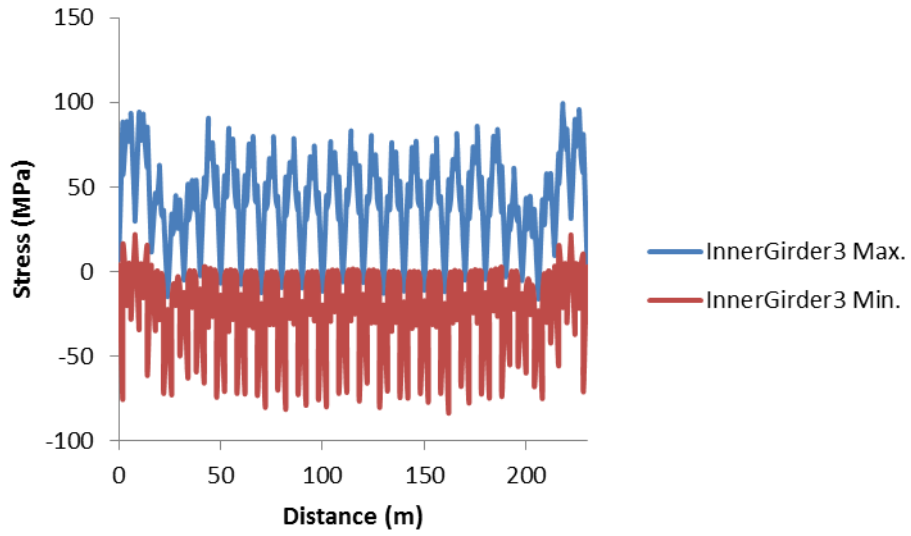


Figure 4-24: Normal Stress Envelope of Inner Girders under Predicted Traffic Load

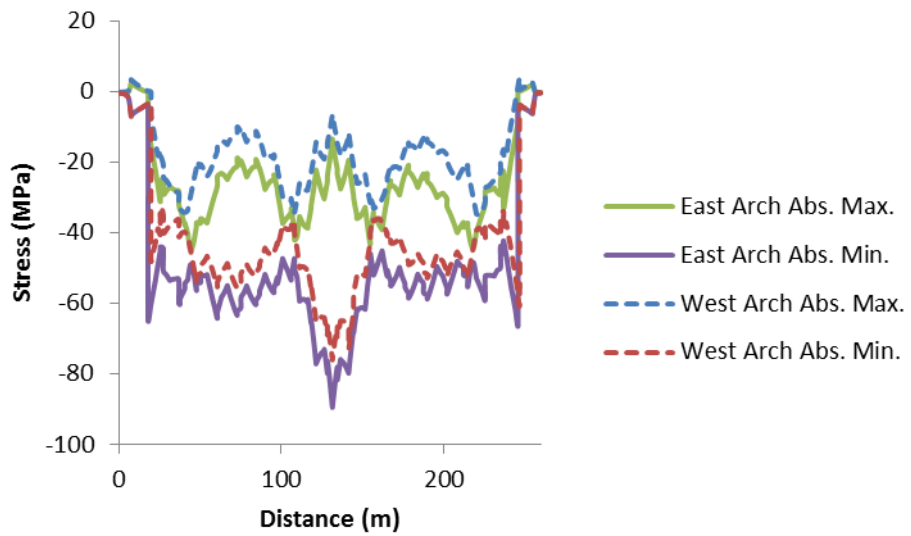


Figure 4-25: Normal Stress Envelope of Arches under Predicted Traffic Load

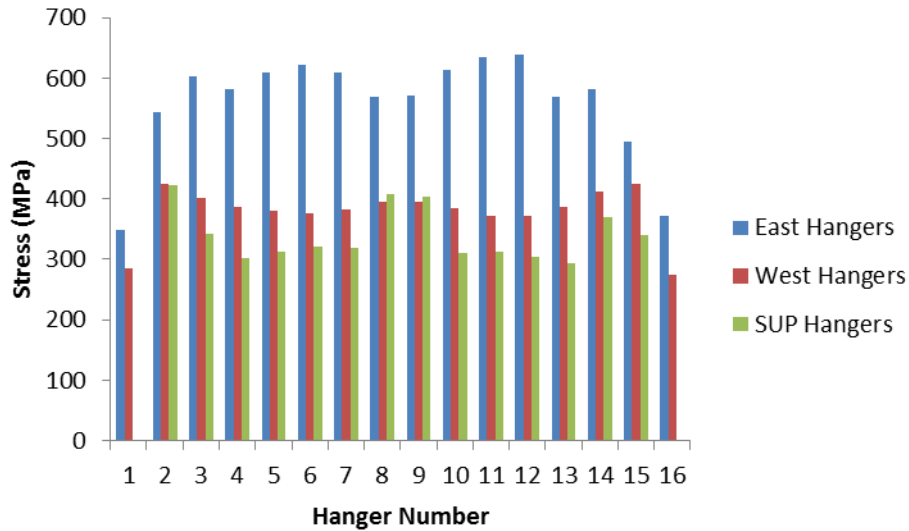


Figure 4-26: Normal Stress of Hangers under Predicted Traffic Load

### 4.3.3 Vibrations

The results show that maximum positive and negative vertical accelerations under vehicle loading occur at the south and north ends of the bridge deck. Figure 4-27 shows the maximum vertical accelerations at the south end, with a maximum positive and negative acceleration of  $0.4515 \text{ m/s}^2$  and  $-0.3163 \text{ m/s}^2$ , respectively. It is evident from this figure that each vehicle passing the bridge deck causes a spike in accelerations. Examining vertical accelerations at the mid-section of the bridge deck, the accelerations are a 10 times smaller than the accelerations at the end spans (Figure 4-28). Peaks in accelerations are still present when vehicles drive over that section. Maximum horizontal acceleration of the bridge is  $0.0218 \text{ m/s}^2$  and maximum longitudinal acceleration is  $-0.0161 \text{ m/s}^2$ , both occurring on the bridge deck.

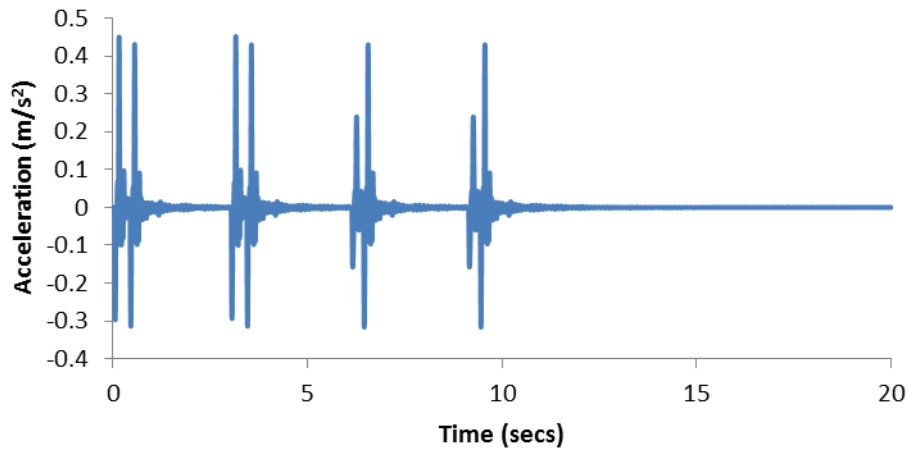


Figure 4-27: Vertical Acceleration of Bridge Deck at South End due to Predicted Traffic Load

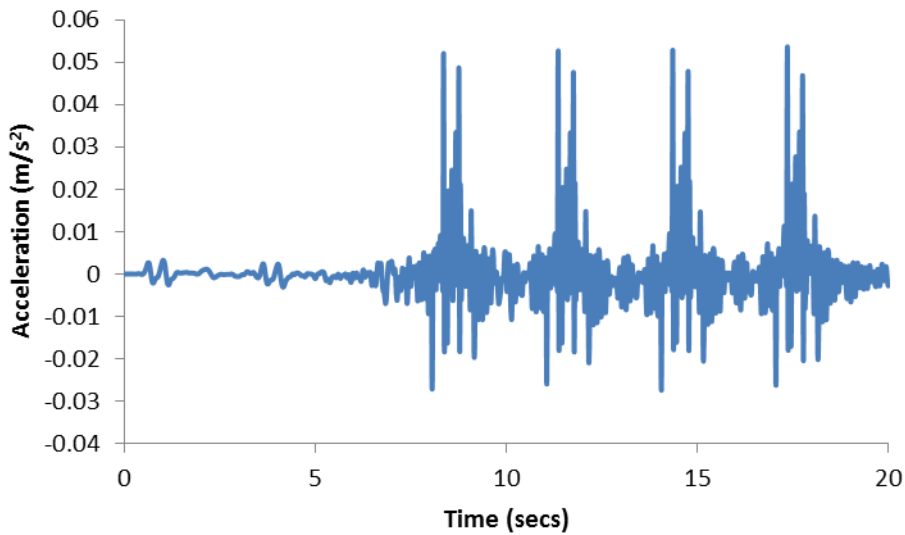


Figure 4-28: Vertical Acceleration of Bridge Deck at Mid-span due to Predicted Traffic Load

To better understand the accelerations experienced on the structure, vertical accelerations from various points along the bridge deck, arches and SUP for a 20 second period were extracted and shown in Figure 4-29,. The points chosen varied from the 30 m, mid-span

and 170 m from the south end of the bridge, shown from top to bottom in the figure columns respectively. From this figure, it is evident that the arches and SUP experience considerably less acceleration than the bridge deck, which is expected, since the source of accelerations is applied directly to the bridge deck and should be excited more than the surrounding members.

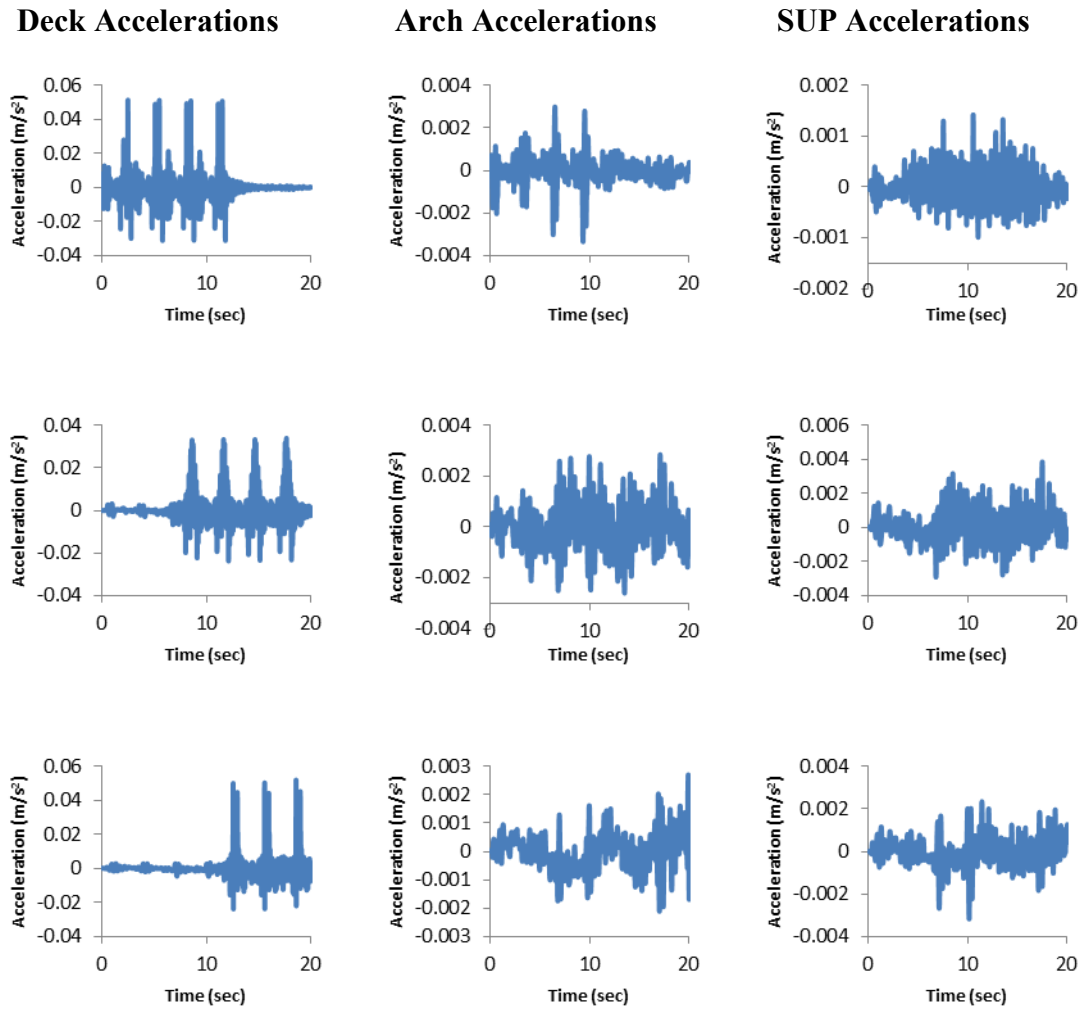


Figure 4-29: Accelerations at 30 m, mid-span and 170 m along the Walterdale Bridge under Predicted Vehicle Loading

#### **4.4 Conclusion**

In this chapter, the CSiBridge model created was analyzed under design loads as well as predicted traffic load. Analysis clearly demonstrated the tensile forces experienced in the cables as well as the compressive forces experienced by the arches, as described in Chapter 2. From analysis under design loading, the areas that experience higher maximum stresses and displacements were discovered. The areas of higher stress under design load include the end spans of the bridge deck, the end locations and mid-span of the arches, the areas near the delta piers on the SUP, as well as the east hangers. Analyzing the model under predicted traffic volumes using nonlinear time-history analysis, the vibrations that the structure is likely to experience were determined. The highest amount of vibration was experienced at the south and north ends of the bridge deck, when the vehicles begin to enter and exit the bridge. The analysis conducted in this chapter is preliminary, and the results and interpretations may change in further studies and investigations, although it is out of the scope of this research.

## **CHAPTER 5: PROPOSED SENSOR LAYOUT PLAN**

Based on the structural analysis from Chapter 4, which analysed the structural response of the Walterdale Bridge under design and predicted loading, two structural health monitoring systems were developed. The sensor locations were selected based on locations that experience higher levels of stress, vibration and displacement. This proposed sensor layout plan is intended to provide further information into the behaviour of the bridge and the design assumptions. The sensor layout can also be used for fatigue monitoring once the cyclic loads, accelerations and stresses experienced on the live structure are better understood. The first system is designed using no budgetary limitations and most aspects desired are monitored, including vibrations, strain, displacement, and the vehicle and environmental loads applied to the structure. Although this system had no financial restrictions, consideration into practicality of purchasing and placing sensors is considered. The second system presented considers financial restrictions, and is capable of monitoring structure vibrational response using 16 triaxial accelerometers only. .

### **5.1 Proposed Sensor Layout Plan**

The following sensor plan is designed under no financial restrictions, and is capable of monitoring the three main aspects of: the environmental conditions, the vehicular loads applied to the structure, and the structural response under both the environment and the loads applied. The sensors used in this system include strain sensors, accelerometers, displacement sensors, anemometers, a weather station, weigh-in-motion sensors, corrosion sensors, GPS units and video cameras. The placement and type of sensor is explained in more detail below. A visual layout of the sensors is then presented in Figure 5-1, Figure 5-2 and Figure 5-3 below.

#### **5.1.1 Strain Monitoring**

Structures will be subject to two types of strains: slow and fast. Slow strain refers to strain that happens over a wider time frame caused mainly by temperature effects, while

fast strain happens rapidly due to changes in vehicle and wind loads. This section presents a layout of strain sensors for both types of strain measurements.

#### ***5.1.1.1 Vibrating-Wire Strain Gauge***

Vibrating-wire strain gauges are capable of measuring slow-rate strain, caused mainly by daily temperature changes. They can be welded to the structural steel surface, and are usually equipped with a temperature sensor in order to measure the structural temperature and the effects that temperature have on strain (Bergmeister and Santa 2001).

Vibrating-wire strain gauges equipped with temperature sensors were proposed to be placed at 20 m intervals on both east and west ends of the bridge deck at the centre span and along the shared-use pathway (SUP), as the centre span of the bridge deck does not experience a large amount of stress variation, 20 m intervals should be sufficient, as to measure the stress distribution but not to have measurement redundancy. The gauges should be placed at 15 m intervals at the end spans, as they experience a higher amount of stress and a larger variation in stress along the span than the centre span. This closer interval will give a better measurement of the stress distribution at the end spans. Vibrating-wire strain gauges are also proposed to be placed at 10 m intervals along the length of the arches, as the arches experience higher amounts of stress under serviceability loading. This 10 m interval is also to measure the effects of temperature on the change in height along the arches. Attention should be paid to the end spans of the edge girders. On the arches, attention should be given to the mid-point and the locations nearest to the thrust-blocks of the arches, as these are the areas that experience the highest amount of stress under serviceability loads.

#### ***5.1.1.2 Dynamic Strain Gauge***

Fast strain occurs over a short period of time, and is primarily caused by vehicle loading. Foil strain gauges are typically used to measure fast strain, although they can measure slow strain, they do not have a reliable performance under harsh environmental conditions (Xu and Xia 2011). They are installed on the object to be measured using a suitable adhesive, alternatively weldable strain gauges can be used. The circuitry of the strain gauge, temperature compensation of the sensor and measurement range are just a few things to

consider when selecting a dynamic strain gauge for measurement, although this is out of scope of this research.

Foil strain gauges were proposed to be placed at 8 m intervals at the end span locations at 20 m intervals at the mid-span locations on inner girders 2, 3, 4 and 5, as these are the inner girders that are directly below the traffic lanes to monitor the strain induced from traffic loads, and to investigate the stress distribution at every other floor beam location. The strain gauges are proposed at a closer spacing along the end span locations, as these locations experience larger stresses and variations in stresses than the mid-span, which experiences a relatively constant stress under traffic loads.

The SUP should also be equipped with dynamic strain gauges with a proposed spacing of 20 m intervals to measure the effects from live loads along its entire span. On the arches, the foil strain gauges are proposed to be placed at the locations that experience a larger amount of stress on the arches under traffic loading to monitor for the stress experienced at these locations, although for fatigue measurements, the arch should not be greatly affected, since it is in compression. These locations include the accessible areas nearest to the thrust blocks and the mid-point of the arches.

### **5.1.2 Vibration Monitoring**

The vibration of a structure is most easily measured with the use of an accelerometer. (Xu and Xia (2011) describe the four main types of accelerometers available, which are piezo-electric type, piezo-resistive type, capacitive type and servo force-balanced type. The type of accelerometer used is dependent on the desired frequency range to be measured. For the application on the Walterdale Bridge, a servo force-balanced type accelerometer capable of measuring low-frequency vibration is recommended, as the first natural frequency is 0.2568 Hz. A few other considerations pertaining to the selection of an accelerometer include: the sensor's sensitivity, the acceleration measurement range, and the temperature range, although this is out of the scope of this research.

An accelerometer layout plan consisting of 50 force-balanced type accelerometers with 90 channels was designed to measure the accelerations of the structure in order to capture its natural frequencies and mode shapes. The system includes 20 triaxial and 30 uniaxial accelerometers. In terms of their placement, 11 accelerometers were proposed on each

edge girder at 20 m intervals, 9 accelerometers on each steel arch at approximately 20 m intervals, and 10 accelerometers on the SUP at 20 m intervals. The accelerometer layout has been designed in a way that is capable of capturing the natural frequency and mode shapes of the structure at each primary member location. The final interval of 20 m was selected to be consistent with every other floor beam location and in order to capture the global behaviour of the structure without collecting redundant information and placing an abundance of sensors on the structure, since the global behaviour does not change drastically in small increments. There are more accelerometers placed to measure the vertical movement of the bridge, since the east and west side of the bridge may move differently in the vertical direction and encounter more changes in displacements along the length. As the longitudinal and transverse movement does not vary as significantly along the structure's length, there are less accelerometer channels for these points, while the longitudinal and transverse movement can still be measured at all the primary steel member locations. This accelerometer layout is analyzed in the next chapter.

### **5.1.3 Displacement Monitoring**

The most common sensor for measuring linear displacements, such as bearing movement, is the linear variable differential transducer (LVDT) (Bergmeister and Santa 2001). In this case, four LVDT sensors could be placed at the bridge deck bearing and SUP locations at the end span to monitor the longitudinal movement of the bridge deck and the SUP elastomeric bearings. Sensitivity, operating temperature, repeatability and resolution are some considerations that are involved in the proper selection of an LVDT sensor, although not identified in this research.

### **5.1.4 Layout**

The layout of the slow and fast rate strain gauges, accelerometers and LVDT sensors is displayed below in Figure 5-1, Figure 5-2, and Figure 5-3 for the bridge deck, arches and SUP, respectively. The sensor legend is provided in Table 5-1.

Table 5-1: Sensor Legend

<b>Symbol</b>	<b>Sensor Type</b>	<b>Total</b>
	Vibrating-wire Strain Gauge	77
	Dynamic Strain Gauge	90
	Uniaxial Accelerometer	30
	Triaxial Accelerometer	20
	LVDT Sensor	8

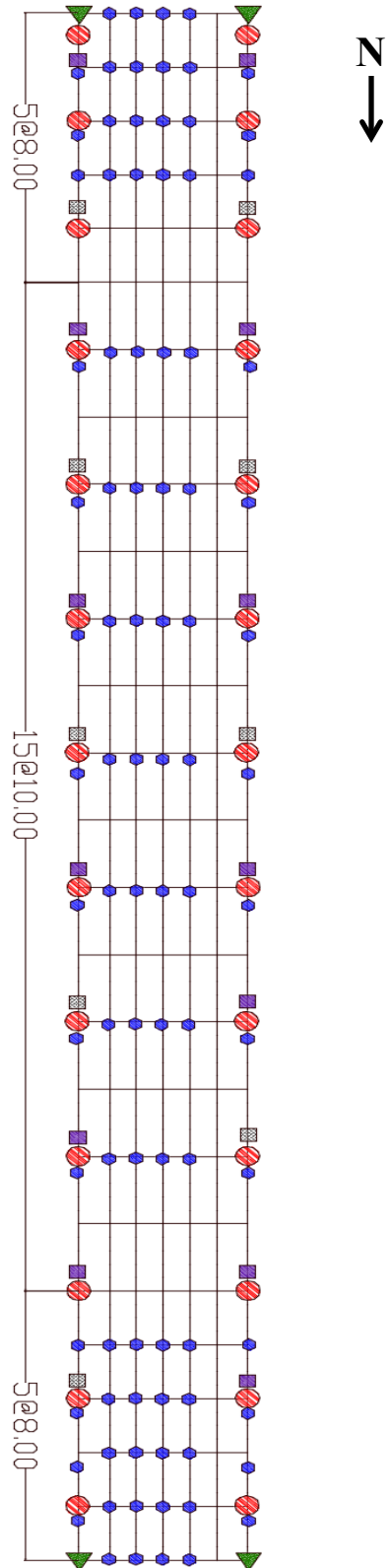


Figure 5-1: Bridge Deck Sensor Layout (Plan View)

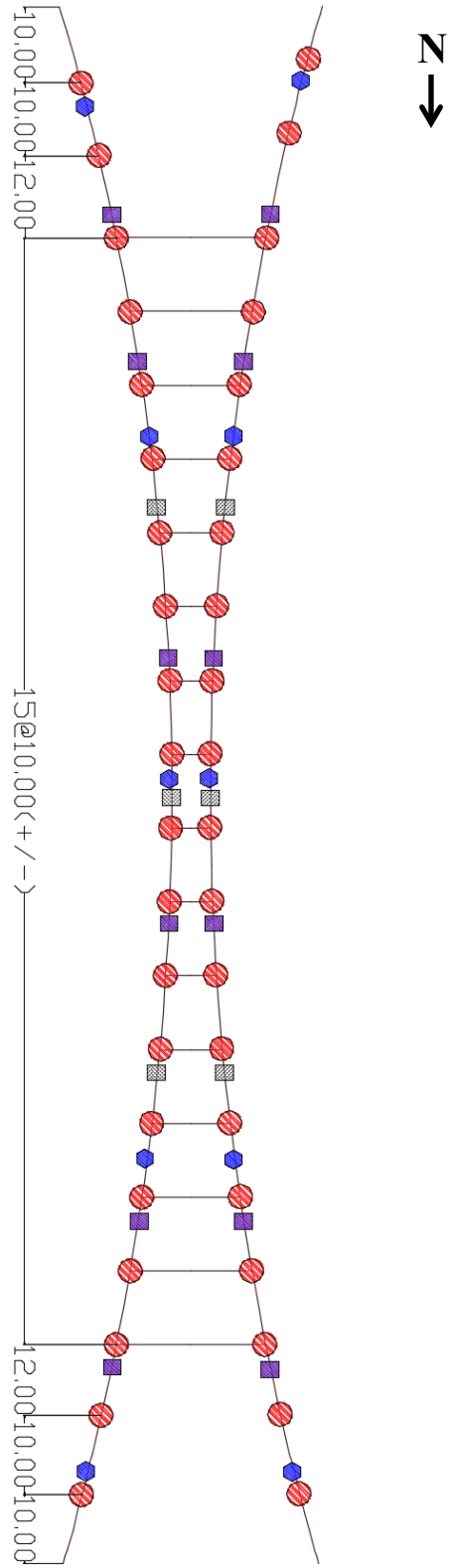


Figure 5-2: Arch Sensor Layout

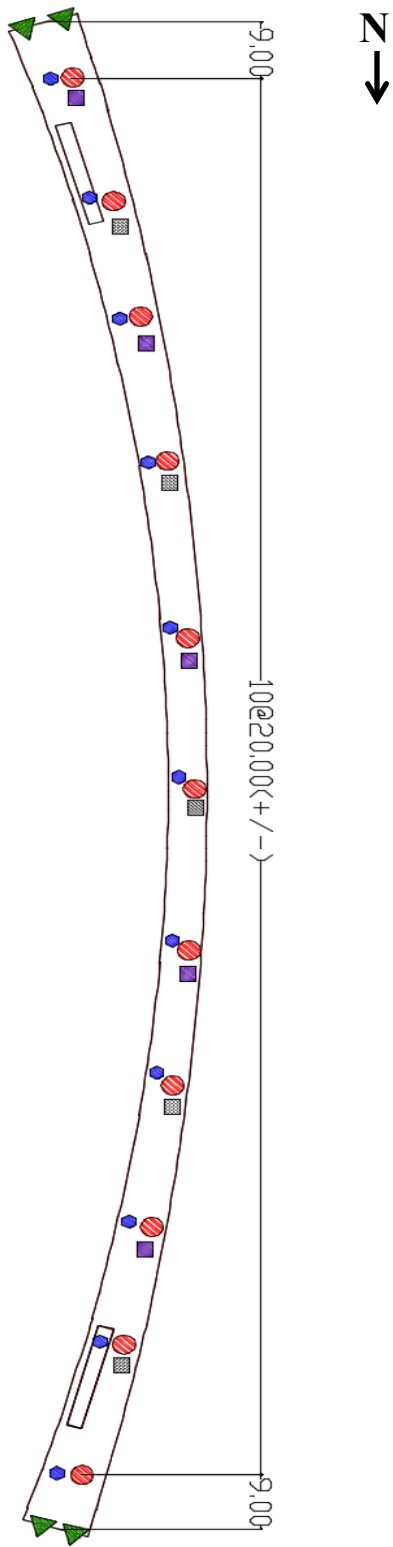


Figure 5-3: SUP Sensor Layout

### **5.1.5 Other Monitoring Considerations**

The following section includes other items that are recommended to be monitored on the structure, although they are not included in the layout plan presented above.

#### ***5.1.5.1 Cable Monitoring***

The tensile force in the cables should be monitored to verify their working status. 24 of the 46 cables were selected for monitoring based on the amount of stress they carry. The cables recommended to be monitored are cables 3, 5, 6, 8, 9, 11, 12 and 14 at the east, west and SUP locations, as these cables generally experience the highest amount of stress compared to the other cables on the same side. Monitoring the cables directly would also help to determine the amount of load the cables at each side are carrying. The cables should be equipped with micro electro-mechanical system (MEMS) capacitive type triaxial accelerometers, due to the small size of MEMS sensors, to measure the vibration shifts over time, as this may be indicative of damage. In order to measure the stress applied on the cables directly, foil strain gauges could also be mounted to the cables. When mounting the foil strain gauges to monitor the cables, the wire strands that make up the cable must be considered. A foil strain gauge can be mounted to one strand directly, or the average strain in the cable can be measured with the use of an extensometer that can measure the elongation of the entire cable.

#### ***5.1.5.2 Weather Monitoring***

To monitor the environmental conditions surrounding the structure, a weather station and anemometers should be placed on site. It can be placed on the structure to measure ambient temperature, humidity, visibility, precipitation, and solar radiation. Measuring the environmental conditions surrounding the structure can give greater insight into the specific surroundings of the structure and how these surroundings influence the structure's behaviour.

Ultrasonic anemometers are capable of measuring wind turbulence, speed and direction. They can be placed at incremental locations along the main span of the bridge deck and arch strut sections to measure the pressure and wind difference at both heights. A few considerations into the selection of an appropriate anemometer include the effects of noise, and weather conditions. Some solutions to these problems include: placing the

anemometers a few meters away from the structure using booms that extend outward and that are easily retrievable (Xu and Xia 2011). Due to extreme weather conditions in Edmonton, the ultrasonic anemometers may need to be equipped with a heating device to avoid the effects of snow and frost, as an unheated anemometer may experience ice accretion that can block the wind measurements (Battisti 2015).

#### ***5.1.5.3 Vehicle Load Monitoring***

A weigh-in-motion sensor could be installed at the south end of the bridge deck, where vehicles begin to drive across the bridge. This device is capable of recording traffic conditions, as well as measuring vehicle axle and gross weights. Having knowledge into the vehicle loads applied to the structure can aid in determining cyclic loads applied to the bridge deck, which can aid in fatigue monitoring. Chen et al. (2014) explains that it is good practice for a video camera to be installed at a location that is unobstructed from the view of traffic driving over the bridge deck, yet is protected from harsh environments. The video camera is capable of capturing vehicles driving over the bridge, and can be very useful to capture license plate numbers in the event that overweight vehicles drive over the structure. Considerations into the type of weigh-in-motion sensor to apply to the bridge include the ability to measure static or dynamic loads, as well as the type of sensor embedded, such as bending plate, piezoelectric, load cell, capacitive and fibre optic (Xu and Xia 2011). These details have not been specified in this research.

#### ***5.1.5.4 Corrosion Monitoring***

Corrosion of reinforcing bars should be measured at locations exposed to higher amounts of chlorides and water, such as the south and north end of the deck, the thrust block locations, and pier locations of the SUP. If desired, corrosion can be measured at 20 m intervals, in similar locations to the temperature sensors along the deck, to measure possible corrosion along the east and west ends of the bridge deck due to the possible exposure to deicing salts, a major cause of corrosion, although the rebar used in the bridge deck is stainless steel and should not experience a large amount of corrosion. The interval of 20 m was chosen using engineering judgement and consistency, as to not have redundancy in measurement, as the amount of corrosion experienced along the bridge deck should not change significantly at each location if the bridge deck is exposed to the

same amount of moisture and chlorides. The ends of the bridge deck are of more interest due to the 2.5% slope of the bridge deck, and water pooling is more likely to occur at the ends. Most corrosion sensors are embedded within the concrete, and cannot be installed in the bridge deck after construction. In the absence of corrosion sensors or to complement corrosion monitoring using sensors, non-destructive techniques, such as ultrasonic pulse velocity measurements, x-ray and gamma radiography, and infrared thermography are commonly used to monitor corrosion (Song and Saraswathy 2007).

#### ***5.1.5.5 GPS Monitoring***

GPS mobile units can be placed at locations along the structure that may experience settlement over time, such as the thrust blocks, approaches and delta-piers. This may also give insight into the soil conditions surrounding the structure. The Real Time Kinematic (RTK) technique with a base station receiver and multiple mobile units is typically used and the location precision can approach 5-10 mm (Kaloop and Li 2009). Using GPS to monitor small displacements is not recommended due to its precision, but is useful when monitoring larger deformations, such as potential settlement over time.

#### ***5.1.5.6 Surveillance***

With the potential risk of vandalism to the equipment mounted on the structure, or to the structure itself, the use of a video camera and surveillance equipment would help deter the threat to defacement of the structure.

#### **5.1.6 Data-Acquisition System**

Data acquisition (DAQ) hardware will be required to complete the SHM system. DAQ hardware acts as the interface between a computer and the signals measured from the sensors. It is used primarily for signal acquisition and conditioning. Many factors influence the type of DAQ setup that should be used, including the amount of data to be streamed, signal synchronization, portability of the DAQ, and the distance between measurements and the computer system (NI.com 2015). Based on the application, the appropriate connection between the DAQ hardware and the computer can be chosen. The connection options between the DAQ and the computer include: a standalone system, a USB connection, an Ethernet connection, and a wireless connection. For a SHM system

on a large civil structure, such as the Walterdale Bridge, the most practical choice would be a wireless connection, as cabling between the DAQ and the computer would be eliminated, reducing the cost and time of installation. A wireless connection would also reduce the amount of cables running through the structure, given that sensors and the DAQ is suggested to be connected using cables. These specifications are out of the scope of this research, but must be considered when implementing a full SHM system to the bridge.

## **5.2 Limited Budget Sensor Layout Plan**

The following sensor layout plan considers financial limitations and is designed to monitor vibrations at 16 points on the bridge. The first step in determining an appropriate SHM given fiscal boundaries was to decide what type of sensor would give the most beneficial information for the best cost. It was decided to focus on accelerometers, as the global behaviour of a recently built structure could be identified soon after construction. Having the global behaviour, such as natural frequencies and mode shapes, can be extremely useful in further analysis and research. A change in these established parameters over time may be a good indication of overall health of the bridge.

After deciding that accelerometers would be the main focus, financial parameters of a SHM system were considered by looking into price quotations of various sensors. A wired sensor system was the first type that was examined. It was concluded that the cost for a DAQ, sensors and cabling was too high and would it not be feasible to apply this system to the Walterdale Bridge given a budget restriction.

An alternative to a wired SHM system is a wireless sensor network (WSN). The configuration of a WSN consists of wireless sensors that measure the response of the structure, and a gateway that wirelessly collects the signals from the sensors. The signals can then be downloaded to a computer system using an Ethernet or wireless connection, where they can be processed and analyzed. Wireless sensors are becoming a feasible alternative to a wired system, as it eliminates the cost of cables and a data acquisition system, and reduces installation time (Cho and Spencer 2015).

Four wireless SHM systems from different companies, all meeting the necessary criteria, were investigated. Examining the cost of each system, it was estimated that under a budgetary constraint, a WSN with a total of 16 wireless triaxial accelerometers and a wireless gateway could be purchased. Preliminary investigation into the effects of placement for all 16 accelerometers is available in Appendix D..

### **5.3 Conclusion**

In this chapter, two different sensor layout plans were presented. The first does not consider budgetary considerations directly. This layout plan is presented in order to demonstrate all the aspects that could be monitored by a SHM system if money was not a limiting factor. These aspects include: environmental loads, vehicle loads, and the structural response in terms of strains, vibrations, and displacements. This system would be able to give insight into the vibrations and stress distribution of the structure, as well as the vehicle load cycles applied, and the environment surrounding the structure. Information into the cyclic loads, along with vibrations and strain can provide information into areas that are more critical to fatigue in future studies. The accelerometer layout of this system is studied in the next chapter. The second layout plan presented considers the limits presented by a budget and includes the use of accelerometers only. Table 5-2 summarizes and compares the capabilities of the two systems. Before implementing a permanent SHM system on the structure, dynamic and static field tests should be performed to ensure sensor calibration and to validate analysis assumptions. Also, many factors are involved in the design of a complete SHM system, including: detailed configuration of the sensors to the DAQ, the communication between the DAQ and software, signal processing and data analysis methods, just to name a few. This chapter offers a suggestion on sensor placement based on analysis conducted in chapter 4 and knowledge into common sensor applications, although further investigation into completing the SHM system should be considered, but it is out of the scope of this research.

Table 5-2: Comparison of Unlimited and Limited Sensor Layout Plan

Capability	Proposed Sensor Layout	Limited Budget Sensor Layout
Capable of measuring vibrations?	√ <b>50</b> Accelerometers (90 Channels)	√ <b>16</b> Accelerometers (48 Channels)
Capable of measuring longitudinal displacements of deck and SUP?	√	X
Capable of measuring slow and fast strain types?	√	X
Capable of measuring environmental effects?	√	X
Capable of measuring vehicle loading?	√	X
Capable of monitoring cables directly?	√	X
Equipped with GPS monitoring?	√	X
Equipped with video camera monitoring?	√	X
Sensor to DAQ connection?	Wired	Wireless
DAQ to computer connection?	Wireless	Wireless

# CHAPTER 6: DAMAGE SIMULATIONS USING THE FINITE ELEMENT MODEL

This chapter investigates the effects of different types of damage on the modal parameters of the structure with the use of the Complex Mode Indicator Function (CMIF), explained in further detail below. Both global and local damage was simulated, and the change in modal parameters from the healthy to damage cases were compared in order to understand what extent of damage can be monitored using the 50 accelerometers with 90 channels presented in chapter 5. From this analysis, a better understanding into the global behaviour of the structure that can be measured was developed. The effects of global and local damage on the overall global behaviour of the structure were also studied.

## 6.1 CMIF Modal Identification Analysis

The CMIF method was used as a modal identification algorithm to identify the natural frequencies and mode shapes of the Walterdale Bridge. Since the Walterdale Bridge is currently under construction, modal identification was simulated using the acceleration data from the FE model created. CMIF was used as a multi-input multi-output (MIMO) method, meaning that the input forces that excited the structure along with the response of the structure to these forces were both known.

According to Shih et al. (1988), the CMIF performs singular value decomposition (SVD) on the frequency response function (FRF) matrix to identify the eigenvalues that exist at each spectral line. The eigenvalues are solved from the normal matrix, which is formed from the FRF matrix at each spectral line. The CMIF is the plot of the eigenvalues on a logarithmic scale as a function of frequency. The peaks of the CMIF plot indicate the presence of modes and contain information of their unscaled mode shapes. Enhanced FRFs (eFRF) are used to find the scaled mode shapes.

An FRF expresses the response of the structure in terms of frequency. The FRF matrix is a complex matrix formed from collecting the response of multiple reference channels, known as output locations,  $N_o$ . The measured response is based on multiple excitation locations, known as input locations,  $N_i$ . Using SVD, the FRF matrix can be written as:

$$[H(j\omega)]_{N_o \times N_i} = [U(j\omega)]_{N_o \times N_i} [S(j\omega)]_{N_i \times N_i} [V(j\omega)]_{N_i \times N_i}^H \quad [6 - 1]$$

Equation 6-1 expresses the FRF matrix in terms of  $[U(j\omega)]$  and  $[V(j\omega)]$  which are unitary matrices called left and right hand vectors, respectively, and  $[S(j\omega)]$  which is the singular value matrix. The left hand vector contains unscaled mode shape information and right hand vectors contain unscaled modal participation factors.  $j\omega$  is the sampling frequency. The FRF matrix can also be expressed as:

$$[H(j\omega)]_{N_o \times N_i} = [\Psi]_{N_o \times 2N} \left[ \frac{Q_r}{j\omega - \lambda_r} \right]_{2N \times 2N} [L]_{2N \times N_i}^T \quad [6 - 2]$$

Equation 6-1 expresses the FRF in terms of unitary vectors, while Equation 6-2 expresses FRF in terms of physical characteristics, where  $[\Psi]$  is the mode shape matrix,  $[L]$  is the modal participation factor matrix,  $Q_r$  is the scaling factor for the  $r^{\text{th}}$  mode,  $\lambda_r$  is the system pole for the  $r^{\text{th}}$  mode,  $j\omega$  is the frequency domain variable and  $N$  is the number of modes. In order to compare Equation 6-1 and Equation 6-2, the mode shape vectors and modal participation factor vectors must be scaled to be unitary vectors. The singular values from Equation 6-1 are then the scaling factor divided by the difference between the sampling frequency and the system poles. So, since the scaling factor is constant, the closer the sampling frequency is to the system pole, the larger singular value will be obtained. This is essentially the peaks seen in a CMIF plot.

The CMIF plot generates the eigenvalues, obtained from the normal matrix, on a logarithmic scale as a function of frequency. The plot indicates where the modes are located. Since eigenvalues are the square of the singular values, and larger singular values indicate the location of modes, the peaks of the CMIF plot are the mode locations. A CMIF plot is generated for each input location.

In order to produce scaled modal information from the FRF matrix computations, eFRFs are calculated for each single degree of freedom (SDOF) system. The eFRFs contains the scaling factor needed to correctly scale each mode shape obtained.

The eFRF for the  $m^{\text{th}}$  mode can be defined as:

$$e\hat{H}(j\omega)_m = \{U(j\omega)\}_m^H [H(j\omega)] \{V(j\omega)\}_m \quad [6 - 3]$$

$\{U(j\omega)\}_m$  is the unscaled mode shape and  $\{V(j\omega)\}_m$  is the equivalent mode participation factor for the  $m^{\text{th}}$  mode. Substituting Equation 6-2 into Equation 6-3 gives:

$$e\hat{H}(j\omega)_m = \frac{Q_m}{(j\omega - \lambda_m)} \quad [6 - 4]$$

Equation 6-4 then gives the scaling factor for the mode shapes,  $Q_m$ .

CMIF modal identification was carried out using MATLAB R2015a computation software. The CMIF codes used were provided from Gul and Catbas (2008). To identify the modal parameters of the Walterdale Bridge, an impact force of 50 kN for a duration of 0.02 seconds was placed at 11 input locations on the bridge deck and steel arches, otherwise known as impact locations of the FE model. The measured accelerations from all 50 accelerometer locations, mentioned in Chapter 5, for all 11 impact loads were collected from the model to generate a CMIF plot where the natural frequencies and mode shapes were obtained. The 11 impact locations and the direction of the impact loads can be seen in Figure 6-2 for the bridge deck and Figure 6-3 for the arches. No impact loads were placed on the SUP, but the accelerometer layout is presented in Figure 6-4. The total number of input or impact channels is 11, and the total number of output channels refers to the accelerometer locations and the directions they are able to measure, for a total of 90, see Table 6-1. The number of impact loads and locations of impact were chosen in order to avoid impacts at a node points, which would led to no structural excitation, and to ensure that modes from all three directions were being excited. The sampling rate used was 50 Hz, with a total number of Fast Fourier Transforms (nFFT) of 8000. The change in frequency then corresponds to the sampling rate divided by the nFFT value, for a change in frequency of 0.00625 Hz. Sample acceleration data is presented in Appendix E. It must also be realized that impact testing is often impractical and expensive on large structures (Peeters and De Roeck 1999).

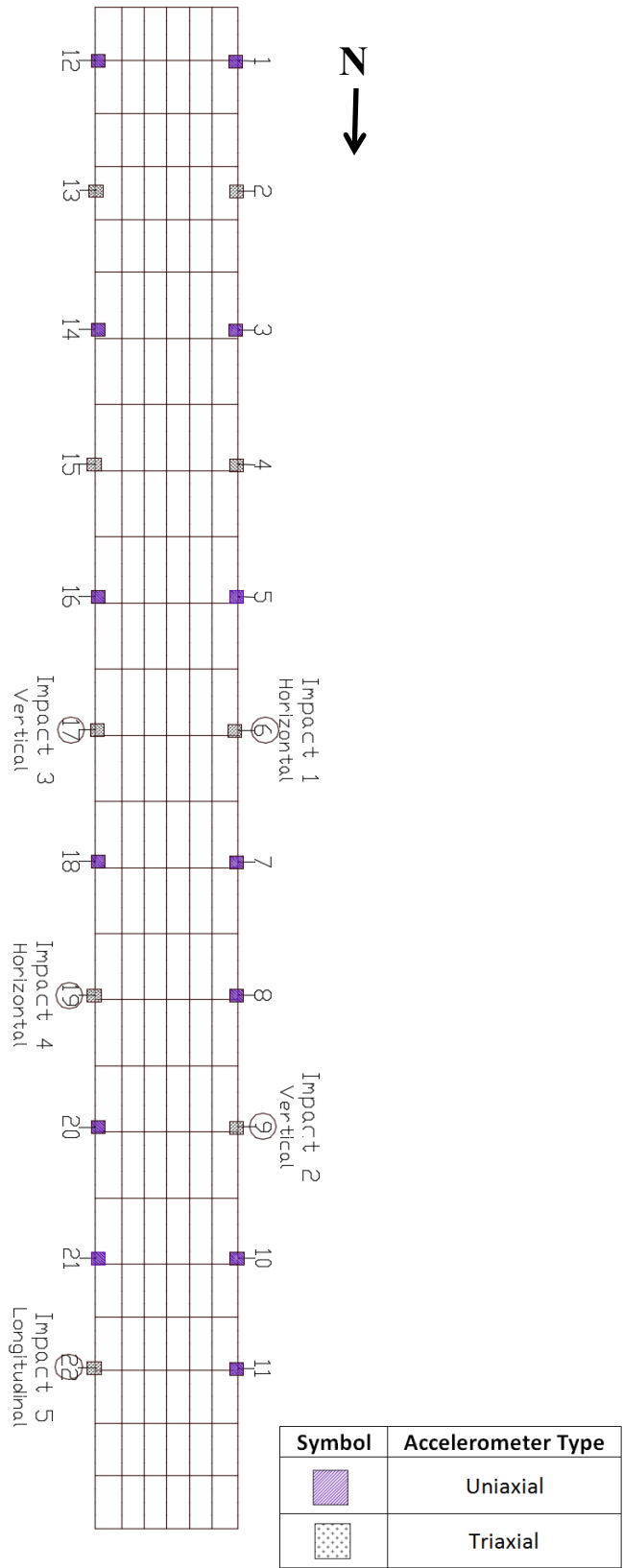


Figure 6-1: Top View of Bridge Deck Accelerometer Layout and Impact Locations

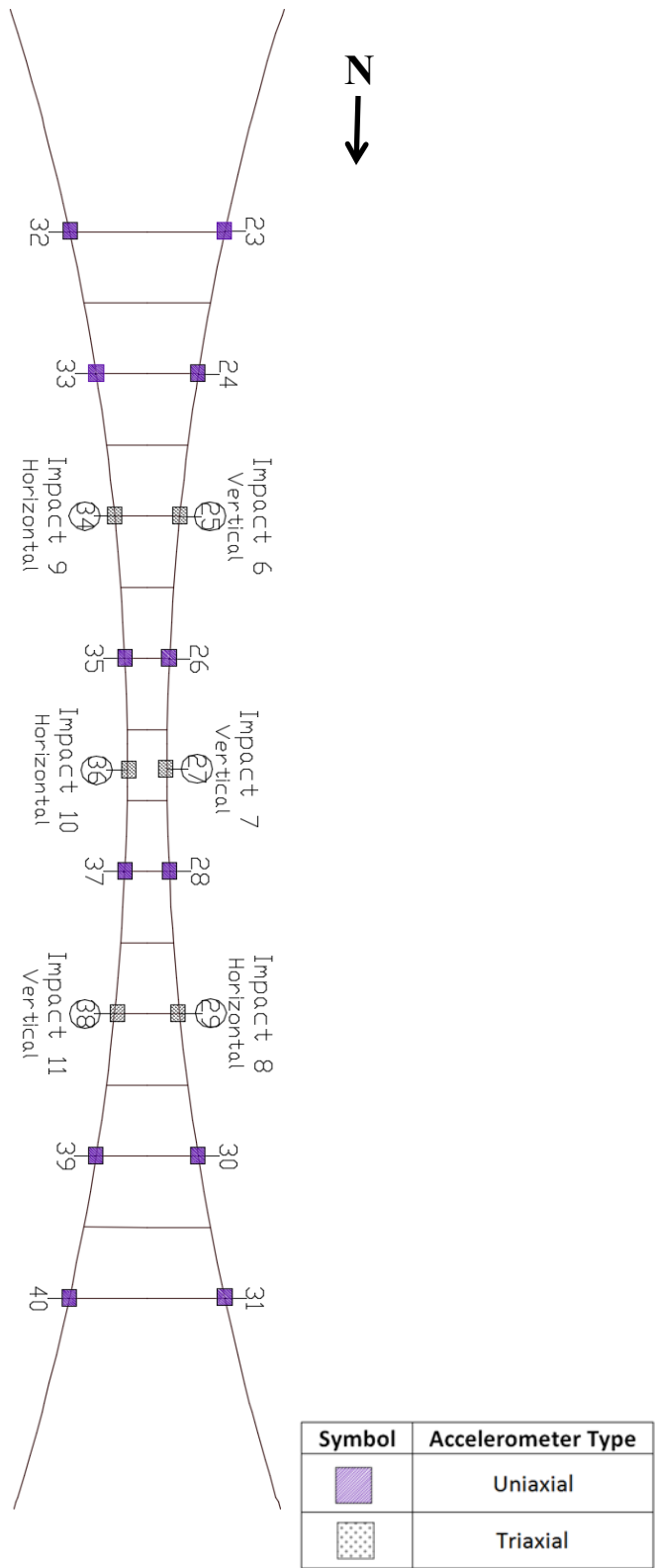


Figure 6-2: Top View of Steel Arches Accelerometer Layout and Impact Locations

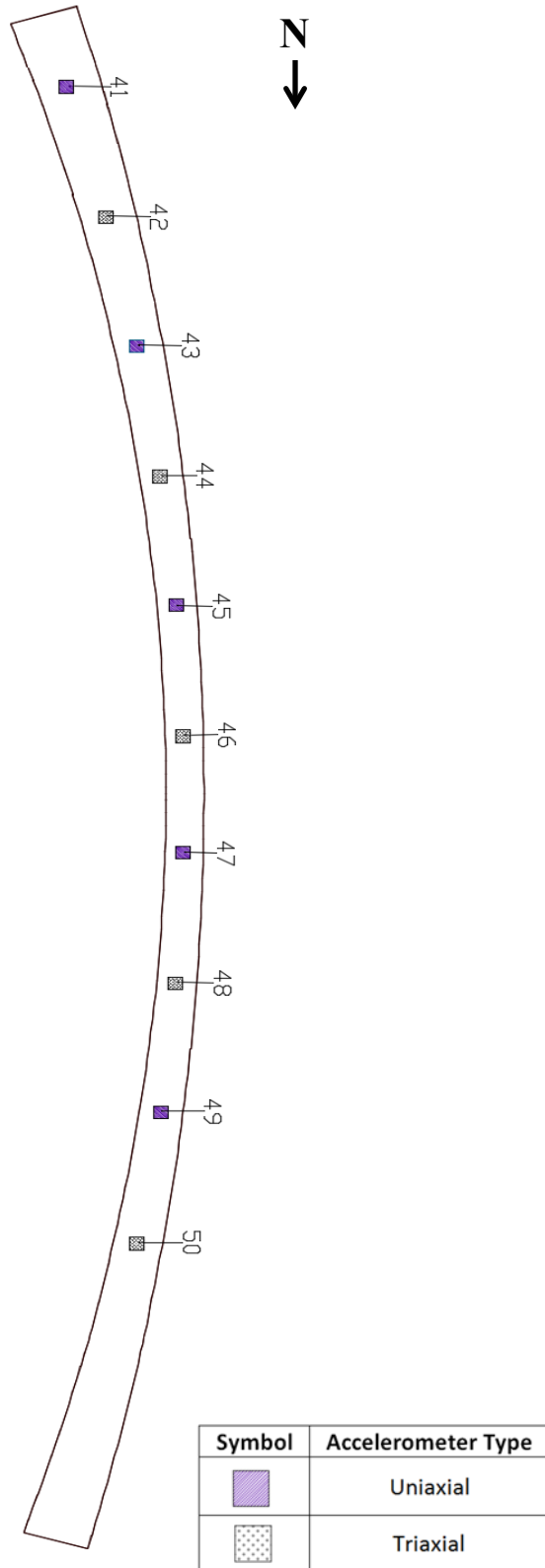


Figure 6-3: SUP Accelerometer Layout

Table 6-1: Summary of Channel Direction Measurements

<b>Channels</b>	<b>Location</b>	<b>Direction</b>
<b>1-11</b>	West Edge Girder	Vertical
<b>12-22</b>	East Edge Girder	Vertical
<b>23-31</b>	West Arch	Vertical
<b>32-40</b>	East Arch	Vertical
<b>41-50</b>	SUP	Vertical
<b>51-54</b>	West Edge Girder	Horizontal
<b>55-58</b>	East Edge Girder	Horizontal
<b>59-61</b>	West Arch	Horizontal
<b>62-64</b>	East Arch	Horizontal
<b>65-70</b>	SUP	Horizontal
<b>71-74</b>	West Edge Girder	Longitudinal
<b>75-78</b>	East Edge Girder	Longitudinal
<b>79-81</b>	West Arch	Longitudinal
<b>82-84</b>	East Arch	Longitudinal
<b>85-90</b>	SUP	Longitudinal

## 6.2 Full Accelerometer Layout with No Damage

CMIF analysis was first conducted on the healthy FE model, with no simulated damage using the full accelerometer layout mentioned in Chapter 5. Using MATLAB to conduct CMIF modal identification, 11 modes were identified and compared with the modes from the software using Modal Assurance Criterion (MAC) value. The modes identified are shown in Table 6-2, and they were then used as the benchmark for damage identification analysis. The MAC value of mode 3 is significantly lower than the others measured. This mode may be more sensitive to the impact loads simulated or to the placement of the accelerometers. Some modes, such as modes 7, 9, 14 and 15, were not identified from the CMIF plot. The reason for this can be due to the mode's sensitivity to the impact loads, poor mass participation values and the fact that higher modes are generally more difficult to excite.

Table 6-2: No Damage CMIF Natural Frequencies

<b>Mode</b>	<b>CSiBRIDGE (Hz)</b>	<b>MATLAB (Hz)</b>	<b>MAC Value</b>	<b>Direction</b>
<b>1</b>	0.2568	0.2563	0.9997	Longitudinal
<b>2</b>	0.4586	0.4688	0.9998	Flexural
<b>3</b>	0.5919	0.6000	0.5997	Transverse
<b>4</b>	0.6225	0.6250	0.8345	Torsional
<b>5</b>	0.7798	0.7813	0.9970	Flexural
<b>6</b>	0.8111	0.8188	0.9999	Torsional
<b>7</b>	0.9834	--	--	Longitudinal
<b>8</b>	1.2690	1.2750	0.9999	Torsional
<b>9</b>	1.3081	--	--	Flexural
<b>10</b>	1.4443	1.4500	0.9997	Flexural
<b>11</b>	1.7575	1.7500	0.9974	Combination
<b>12</b>	1.8637	1.8563	0.9927	Combination
<b>13</b>	1.9319	1.9313	0.8975	Combination
<b>14</b>	1.9558	--	--	Combination
<b>15</b>	2.0954	--	--	Combination

### 6.3 Damage Simulations

Global and local damage was simulated to the bridge model. Simulated damage includes: bridge deck bearing damage, cable damage, arch strut damage and connection damage, as described in the following sections. This damage was simulated in order to understand how it could be monitored using this sensor layout plan and to what extent it could be measured.

### 6.4 Bearing Damage

Bearing damage was simulated to the south-east bridge deck bearing by changing the bearing stiffness of the south-east bridge deck bearing in the longitudinal direction. This type of damage should be easily detectable using a shift in modal parameters since a change in boundary conditions corresponds to a shift in the overall global behaviour of the structure. An increase in bearing stiffness could correspond to obstruction of the bearing due to debris, or weakness in the elastomeric pad due to fatigue. Two stiffness cases were investigated: completely fixed in all directions and 2X longitudinal bearing stiffness. The modal property changes were investigated and compared to the benchmark case.

#### 6.4.1 Complete Longitudinal Stiffness Fixity

When the bearing stiffness is changed to completely fixed, the first mode is no longer present because the bridge can no longer move in the longitudinal direction, Table 6-3. This change in natural frequency would be a very good indication that changes to the boundary conditions may be present in the structure. Investigation into the mode shapes reveals that damage is evident due to the difference in longitudinal displacements. The longitudinal displacements of the edge girders in mode 2, Figure 6-4, show a large discrepancy between the benchmark and damaged structure, as expected since the bridge deck can no longer move as freely in the longitudinal direction. The transverse displacement is also slightly affected, since the rotation at the bearing location is altered. The change in displacements, along with the absence of the first mode, would all be good indications that damage is present. The MAC values do not change considerably, because changing the longitudinal stiffness only causes a large change in the longitudinal direction, and does not affect the vertical and transverse behaviour as significantly.

Table 6-3: Fully Fixed South-East Deck Bearing Natural Frequency Comparison

<b>Mode</b>	<b>Healthy (Hz)</b>	<b>Damaged (Hz)</b>	<b>MAC Value</b>	<b>CSiBRIDGE Healthy (Hz)</b>	<b>CSiBRIDGE Damaged (Hz)</b>
<b>1</b>	0.2563	--	--	0.2568	--
<b>2</b>	0.4688	0.4625	0.9941	0.4586	0.4569
<b>3</b>	0.6000	0.5875	0.9356	0.5919	0.5823
<b>4</b>	0.6250	0.6250	0.9954	0.6225	0.6203
<b>5</b>	0.7813	0.7813	0.9281	0.7798	0.7798
<b>6</b>	0.8188	0.8125	0.9999	0.8111	0.8111
<b>7</b>	--	--	--	0.9834	--
<b>8</b>	1.2750	1.2688	0.9997	1.2690	1.2689
<b>9</b>	--	--	--	1.3081	1.3052
<b>10</b>	1.4500	1.4438	0.9999	1.4443	1.4443
<b>11</b>	1.7500	1.7250	0.9559	1.7575	1.7417
<b>12</b>	1.8563	1.8500	0.8755	1.8637	1.8419
<b>13</b>	1.9313	1.9188	0.9418	1.9319	1.9360
<b>14</b>	--	--	--	1.9558	2.0107
<b>15</b>	--	--	--	2.0954	2.1710

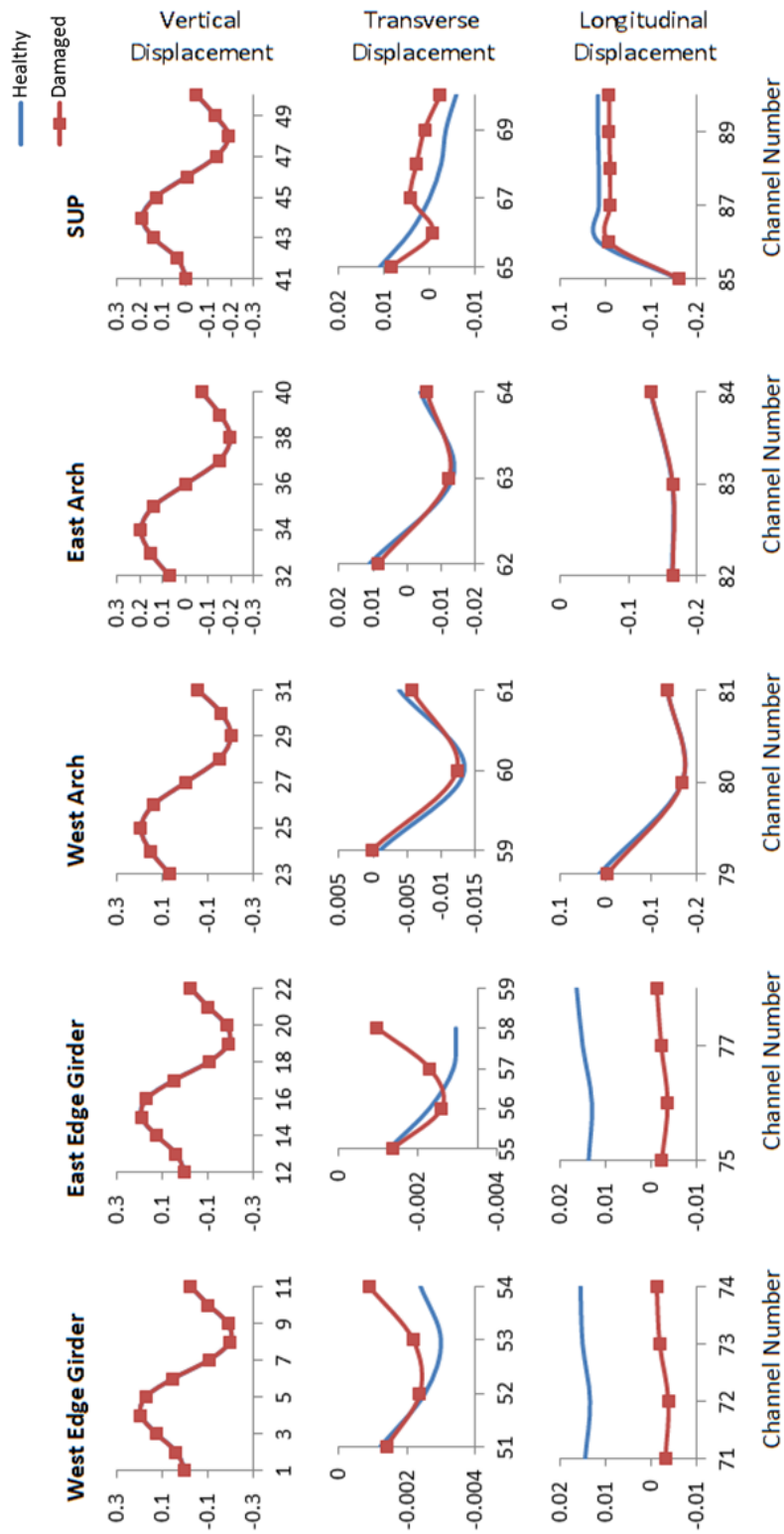


Figure 6-4: Full Bearing Stiffness Mode Shape 2 Comparison

#### 6.4.2 2X Bearing Longitudinal Stiffness Increase

The bearing stiffness was increased by 2 times the original value. In doing so, all 11 original modes could be identified in the CMIF plot. Although there was a significant change in natural frequency value for the first mode, the longitudinal mode, the MAC values correlate well, (Table 6-4). The reason for a good MAC correlation is because the other displacements are not affected considerably by this change in longitudinal stiffness. This shift in longitudinal natural frequency value could be the first sign that a change is present in the bearing in the longitudinal direction. When comparing the east edge girder displacements of mode 1, it can also be seen that the bridge deck is not as free to move longitudinally as well as transverse since the rotation at the bearing is altered from this longitudinal stiffness change, Figure 6-5, although this displacement shift is not very significant. There are a few signs that a shift in boundary conditions is taking place, the increase in mode 1 natural frequency value being the largest indication.

Table 6-4: 2X Bearing Stiffness Natural Frequency Comparison

<b>Mode</b>	<b>Healthy (Hz)</b>	<b>Damaged (Hz)</b>	<b>MAC Value</b>	<b>CSiBRIDGE Healthy (Hz)</b>	<b>CSiBRIDGE Damaged (Hz)</b>
<b>1</b>	0.2563	0.2813	0.9999	0.2568	0.2725
<b>2</b>	0.4688	0.4563	1.0000	0.4586	0.4587
<b>3</b>	0.6000	0.6000	0.9889	0.5919	0.5921
<b>4</b>	0.6250	0.6250	1.0000	0.6225	0.6226
<b>5</b>	0.7813	0.7813	0.9634	0.7798	0.7798
<b>6</b>	0.8188	0.8125	1.0000	0.8111	0.8111
<b>7</b>	--	--	--	0.9834	0.9848
<b>8</b>	1.2750	1.2688	1.0000	1.2690	1.2690
<b>9</b>	--	--	--	1.3081	1.3081
<b>10</b>	1.4500	1.4375	1.0000	1.4443	1.4443
<b>11</b>	1.7500	1.7500	1.0000	1.7575	1.7575
<b>12</b>	1.8563	1.8688	1.0000	1.8637	1.8637
<b>13</b>	1.9313	1.9438	1.0000	1.9319	1.9319
<b>14</b>	--	--	--	1.9558	1.9558
<b>15</b>	--	--	--	2.0954	2.0955

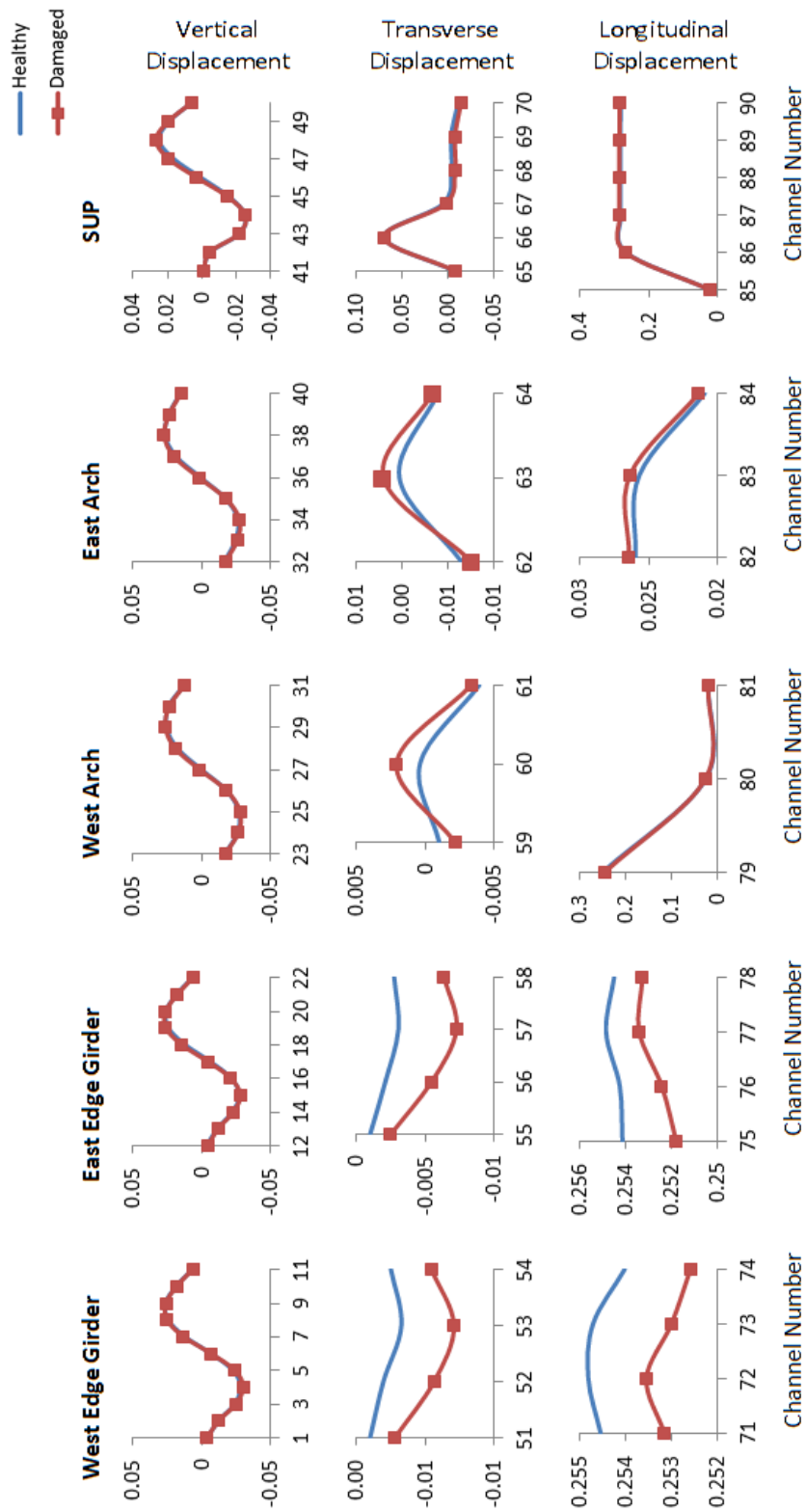


Figure 6-5: 2X Bearing Stiffness Mode Shape 1 Comparison

## **6.5 Cable Damage**

Two damage cases were simulated in the cables. The first involved severe damage of total cable removal. The second damage case was less severe, with a 20% reduction in stiffness of the cable member. Damage in the cables was selected in order to investigate the influence of a primary member on the structure behaviour. Although the removal of a cable, or a partial change in the cable properties should not cause a large change in overall global behaviour of the structure, the effects of local changes were nevertheless studied in order to obtain a better understanding on how these small local changes may result in a modest shift in the global behaviour.

### **6.5.1 Removal of Cable Member**

Damage was simulated on east hanger 12 by removing the element completely. Total removal of the cable element signifies that the cable is no longer capable of carrying any load. This could occur due to significant corrosion, or a loss in connection between a steel member and the cable. By removing the cable element, little change in natural frequencies and MAC values occurs, as expected and demonstrated in Table 6-5. Although discrepancies can be seen when comparing mode shape displacements. For example, examining the bridge deck transverse displacement of mode 4, a change in displacement is observed, as seen in Figure 6-6.

Table 6-5: Removal of East Hanger 12 Natural Frequency Comparison

<b>Mode</b>	<b>Healthy (Hz)</b>	<b>Damaged (Hz)</b>	<b>MAC Value</b>	<b>CSiBRIDGE Healthy (Hz)</b>	<b>CSiBRIDGE Damaged (Hz)</b>
<b>1</b>	0.2563	0.2688	1.0000	0.2568	0.2571
<b>2</b>	0.4688	0.4625	1.0000	0.4586	0.4587
<b>3</b>	0.6000	0.6000	0.9999	0.5919	0.5919
<b>4</b>	0.6250	0.6250	0.9972	0.6225	0.6221
<b>5</b>	0.7813	0.7875	0.9998	0.7798	0.7791
<b>6</b>	0.8188	0.8188	1.0000	0.8111	0.8111
<b>7</b>	--	--	--	0.9834	0.9831
<b>8</b>	1.2750	1.2625	1.0000	1.2690	1.2691
<b>9</b>	--	--	--	1.3081	1.3067
<b>10</b>	1.4500	1.4313	1.0000	1.4443	1.4308
<b>11</b>	1.7500	1.7438	0.9961	1.7575	1.7538
<b>12</b>	1.8563	1.8563	0.9983	1.8637	1.8618
<b>13</b>	1.9313	1.9375	0.9992	1.9319	1.9317
<b>14</b>	--	--	--	1.9558	1.9542
<b>15</b>	--	--	--	2.0954	2.0939

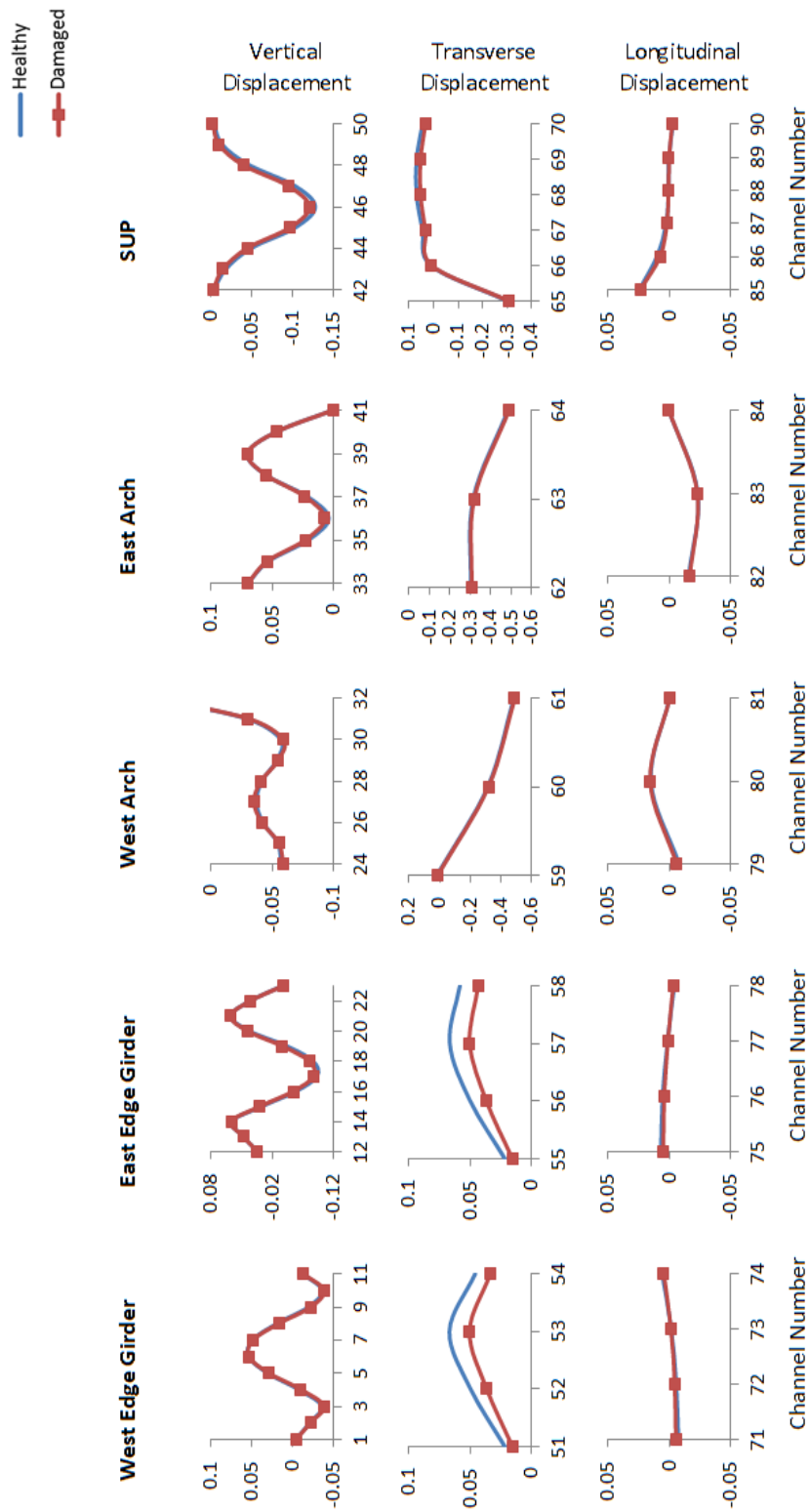


Figure 6-6: Full E12 Hanger Removal Mode Shape 4 Comparison

### 6.5.2 20% Stiffness Reduction of Cable

The stiffness of east hanger 12 was reduced by 20% of its original value to examine if cable damage could be detected in a less severe case than deleting the entire member, as described above. A reduction of stiffness could occur in the structure if corrosion were to occur to the cables, or if a few hanger wires are weakened. Comparing the modes to the benchmark case, Table 6-6, no significant changes occur, as expected. Looking at the transverse displacement of the bridge deck, the difference in displacements is significantly reduced compared to when the cable is fully deleted, Figure 6-7. This severity of damage may be difficult to detect on the structure using modal identification methods.

Table 6-6: 20% Stiffness Reduction to East Hanger 12 Natural Frequency Comparison

<b>Mode</b>	<b>Healthy (Hz)</b>	<b>Damaged (Hz)</b>	<b>MAC Value</b>	<b>CSiBRIDGE Healthy (Hz)</b>	<b>CSiBRIDGE Damaged (Hz)</b>
<b>1</b>	0.2563	0.2625	0.9999	0.2568	0.2569
<b>2</b>	0.4688	0.4688	1.0000	0.4586	0.4586
<b>3</b>	0.6000	0.6000	1.0000	0.5919	0.5919
<b>4</b>	0.6250	0.6250	1.0000	0.6225	0.6224
<b>5</b>	0.7813	0.7813	1.0000	0.7798	0.7797
<b>6</b>	0.8188	0.8188	1.0000	0.8111	0.8111
<b>7</b>	--	--	--	0.9834	0.9833
<b>8</b>	1.2750	1.2750	0.9999	1.2690	1.2690
<b>9</b>	--	--	--	1.3081	1.3079
<b>10</b>	1.4500	1.4500	1.0000	1.4443	1.4421
<b>11</b>	1.7500	1.7500	0.9999	1.7575	1.7569
<b>12</b>	1.8563	1.8625	1.0000	1.8637	1.8634
<b>13</b>	1.9313	1.9375	0.9993	1.9319	1.9319
<b>14</b>	--	--	--	1.9558	1.9555
<b>15</b>	--	--	--	2.0954	2.0952

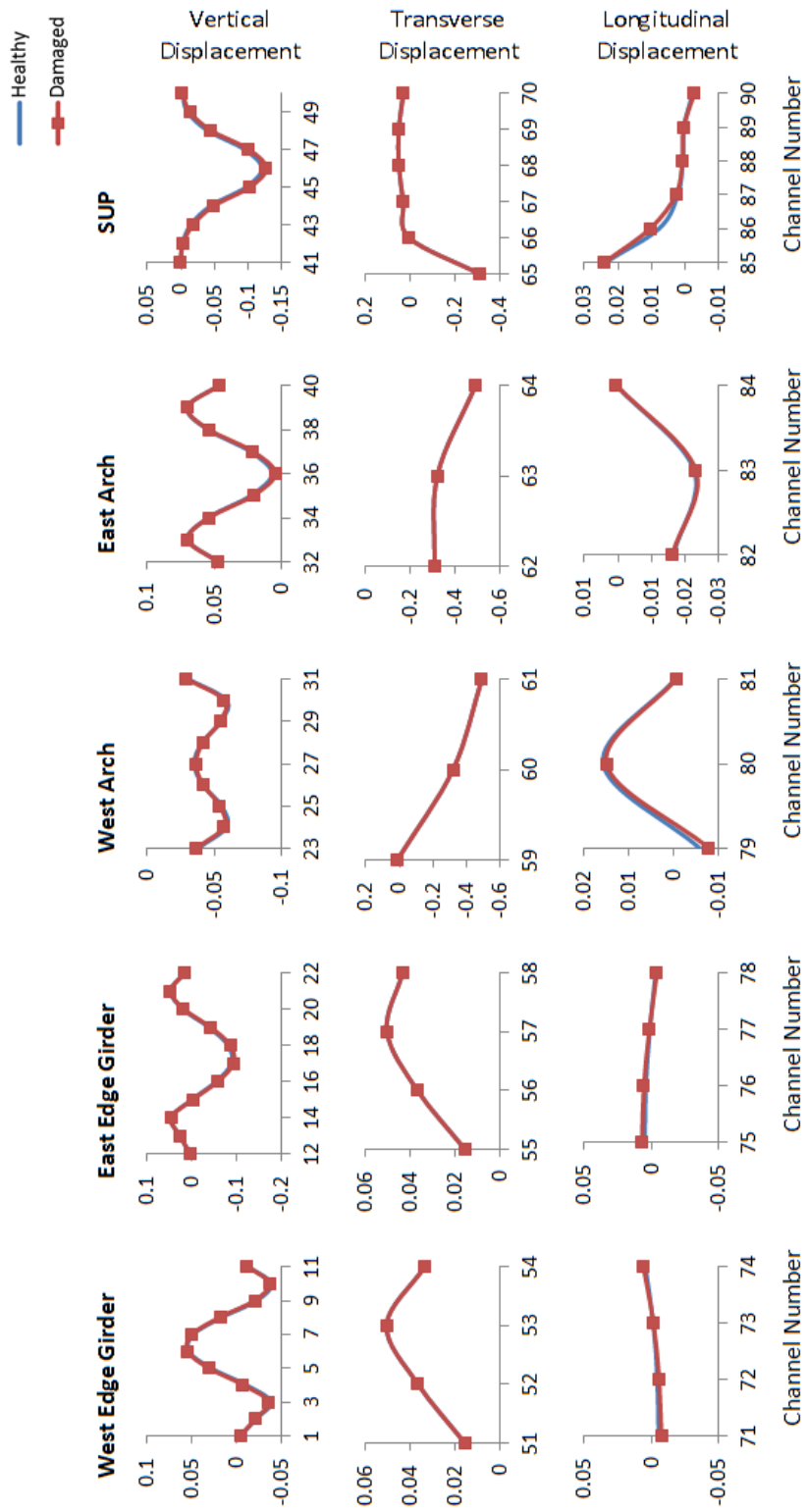


Figure 6-7: 20% Reduction in Stiffness of E12 Hanger Mode Shape 4 Comparison

## **6.6 Arch Strut Damage**

Damage was simulated in the arch struts under two different scenarios. The first case reduced the stiffness of the entire 4<sup>th</sup> arch strut member by 80%. The second case only reduced the stiffness of half of the member by 20%. Damage in the arch strut was simulated in order to understand the effects of a secondary member on the overall structure behaviour, and how a change in these members may influence the behaviour of primary members. Similar to cable damage, it is expected that a change in the arch struts should not greatly affect the global behaviour of the structure, although still examined.

### **6.6.1 80% Stiffness Reduction to Full Arch Member**

Simulating damage to the 4<sup>th</sup> arch strut member was achieved by changing the stiffness of the steel material to 20% of its original value. This reduction in stiffness could occur due to corrosion or fatigue. Although the natural frequencies and MAC values compare well and no significant change in modal behaviour is significantly obvious, Table 6-7, a large change in displacement can be noted for mode 5 in the transverse direction of the arches, Figure 6-8. This change in displacement shows that a change in the arch strut has a potentially significant influence on the global behaviour of the structure. A large change to this secondary member could possibly be identified using modal identification methods.

Table 6-7: 80% Stiffness Reduction to Full Arch Strut 4 Natural Frequency Comparison

<b>Mode</b>	<b>Healthy (Hz)</b>	<b>Damaged (Hz)</b>	<b>MAC Value</b>	<b>CSiBRIDGE Healthy (Hz)</b>	<b>CSiBRIDGE Damaged (Hz)</b>
<b>1</b>	0.2563	0.2688	0.9999	0.2568	0.2568
<b>2</b>	0.4688	0.4625	1.0000	0.4586	0.4586
<b>3</b>	0.6000	0.6000	0.9930	0.5919	0.5893
<b>4</b>	0.6250	0.6188	0.9980	0.6225	0.6159
<b>5</b>	0.7813	0.7875	0.9820	0.7798	0.7796
<b>6</b>	0.8188	0.8063	0.9968	0.8111	0.8012
<b>7</b>	--	--	--	0.9834	0.9834
<b>8</b>	1.2750	1.2688	1.0000	1.2690	1.2687
<b>9</b>	--	--	--	1.3081	1.3080
<b>10</b>	1.4500	1.4500	1.0000	1.4443	1.4442
<b>11</b>	1.7500	1.7375	0.9975	1.7575	1.7454
<b>12</b>	1.8563	1.8563	0.9961	1.8637	1.8619
<b>13</b>	1.9313	1.9375	0.9337	1.9319	1.9250
<b>14</b>	--	--	--	1.9558	1.9521
<b>15</b>	--	--	--	2.0954	2.0900

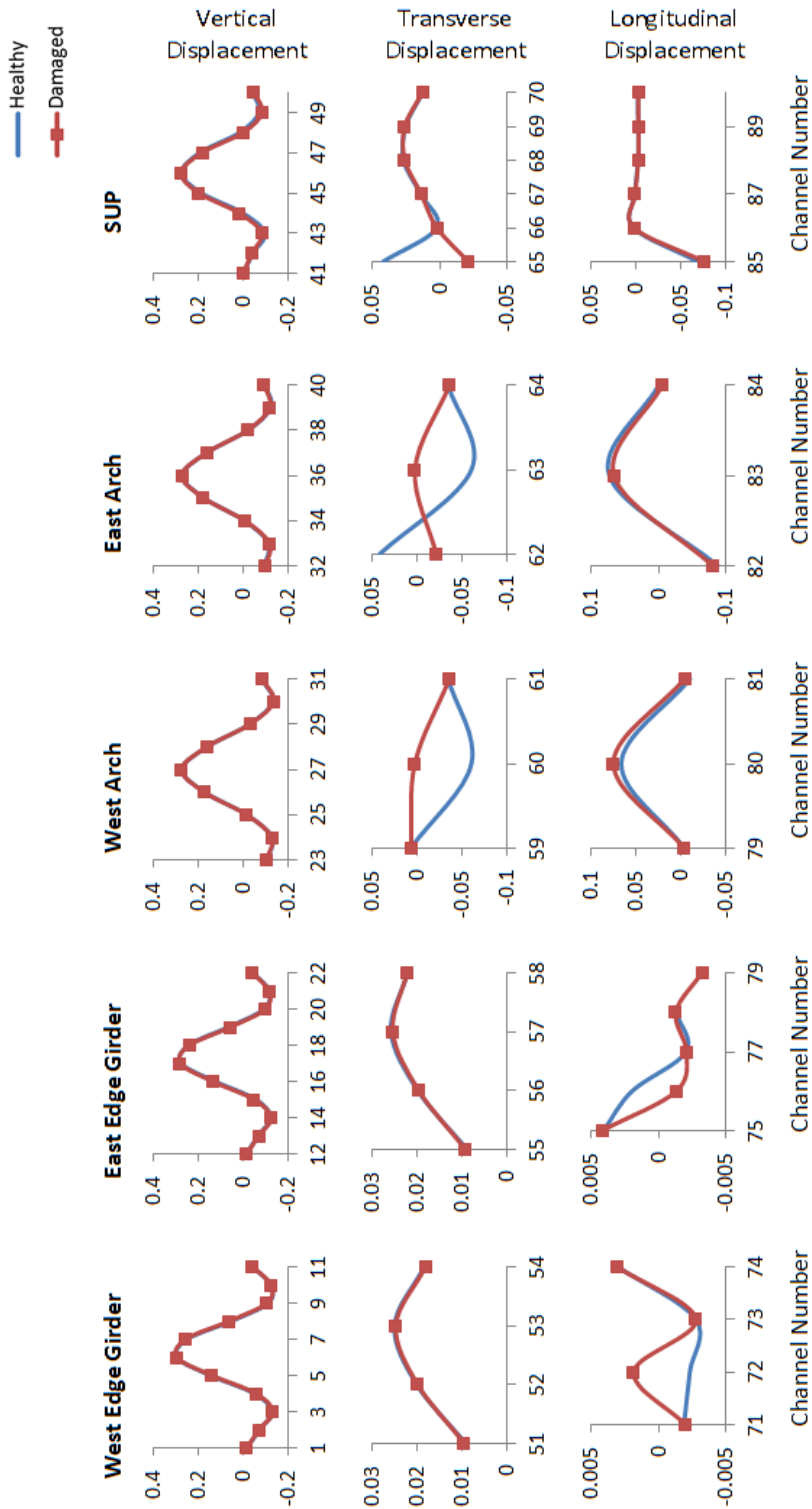


Figure 6-8: 80% Stiffness Reduction of Full Arch Strut 4 Member Mode Shape 5 Comparison

### 6.6.2 20% Stiffness Reduction to Half Arch Member

Less severe damage was simulated to the 4<sup>th</sup> arch strut member by reducing the stiffness by 20% and applying the change in material properties to only half of the strut, in order to investigate if the monitoring system would be capable of detecting smaller, localized damage. The modes obtained and their MAC values are presented in Table 6-8. When comparing the mode 5 transverse arch displacements, the difference between the healthy and damaged case becomes more difficult to detect than the previous damage scenario, see Figure 6-9. This small change in a secondary member would likely not be severe enough to identify using modal identification methods since it does not have a significant effect on the structure's overall behaviour.

Table 6-8: 20% Stiffness Reduction to Half of Arch Strut 4 Natural Frequency Comparison

<b>Mode</b>	<b>Healthy (Hz)</b>	<b>Damaged (Hz)</b>	<b>MAC Value</b>	<b>CSiBRIDGE Healthy (Hz)</b>	<b>CSiBRIDGE Damaged (Hz)</b>
<b>1</b>	0.2563	0.2625	0.9999	0.2568	0.2568
<b>2</b>	0.4688	0.4625	1.0000	0.4586	0.4586
<b>3</b>	0.6000	0.6000	0.9999	0.5919	0.5917
<b>4</b>	0.6250	0.6250	0.9999	0.6225	0.6217
<b>5</b>	0.7813	0.7813	0.9995	0.7798	0.7798
<b>6</b>	0.8188	0.8125	1.0000	0.8111	0.8099
<b>7</b>	--	--	--	0.9834	0.9834
<b>8</b>	1.2750	1.2688	1.0000	1.2690	1.2690
<b>9</b>	--	--	--	1.3081	1.3081
<b>10</b>	1.4500	1.4313	1.0000	1.4443	1.4443
<b>11</b>	1.7500	1.7438	1.0000	1.7575	1.7562
<b>12</b>	1.8563	1.8625	0.9992	1.8637	1.8635
<b>13</b>	1.9313	1.9375	0.9971	1.9319	1.9312
<b>14</b>	--	--	--	1.9558	1.9552
<b>15</b>	--	--	--	2.0954	2.0949

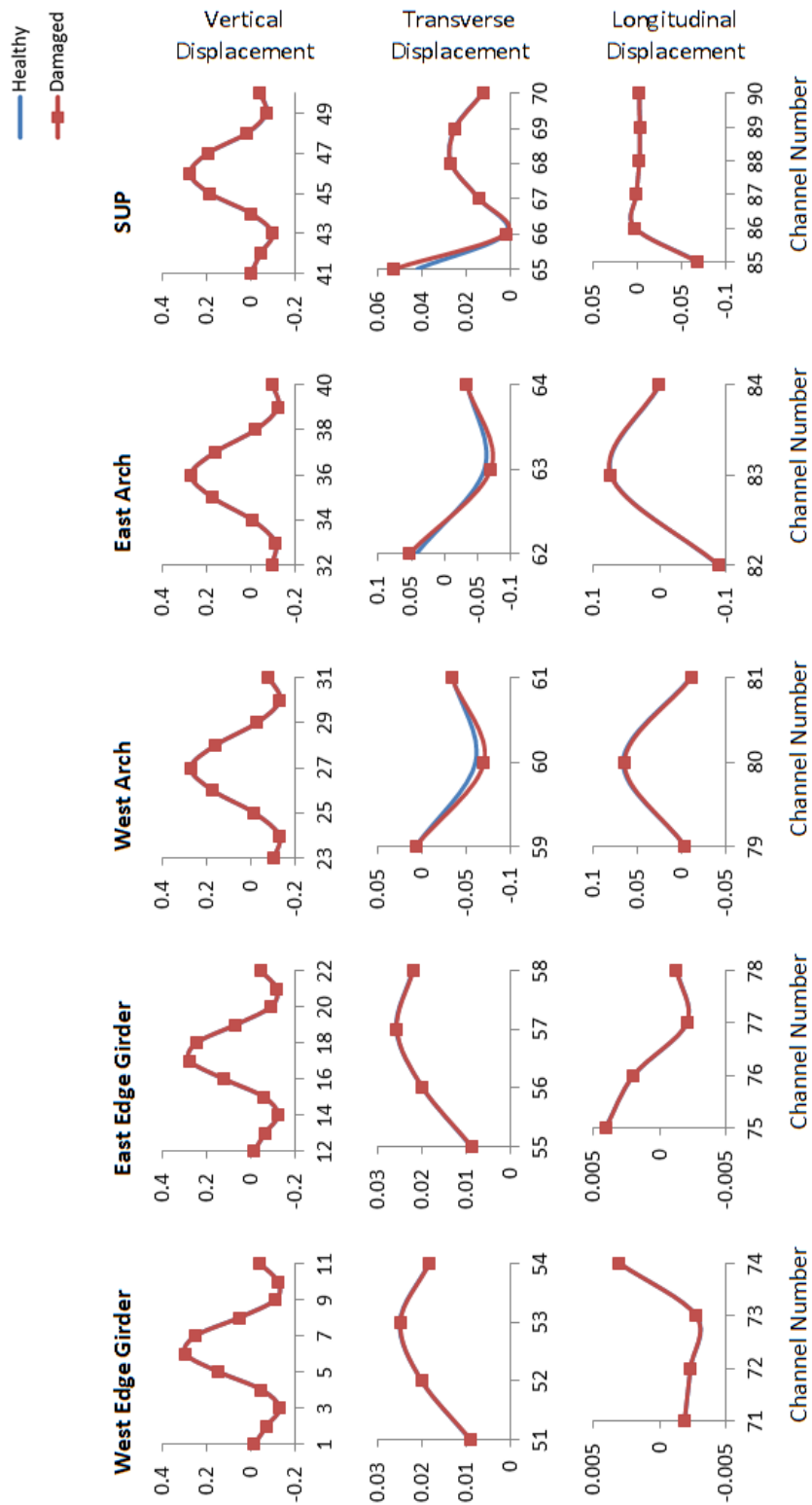


Figure 6-9: 20% Stiffness Reduction of Half Arch Strut 4 Member Mode Shape 5

Comparison

## 6.7 Connection Damage

Damage was simulated to the connection between floor beam 1 and the east edge girder, at 8 m along the east edge girder length, by releasing the moments at this joint location in the model. This loss in moment connection could be caused by corrosion, bolt failure or fatigue cracks. Similar to the local changes examined above, a small change in connection should not greatly affect the overall global behaviour of the structure. Connection damage was investigated to examine the effects of sensor placement and how connectivity may influence a small change in the structure's modal properties. Comparing the CMIF results of the benchmark case with the damaged case, the natural frequencies and MAC values are in good comparison, Table 6-9. In order to determine that damage is present, the modal displacements must be compared. The changes in displacements can only be seen at the sensor locations near the damaged connection. For example, by looking at the change in mode 1 displacements from the benchmark to the damaged case in Figure 6-10, a small shift in modal displacement is present, more so at the east edge girder near the damaged location. This would indicate that the detection of local damage is dependent on the sensor locations, as this damage could go undetected if a sensor had not been at the location of damage, although this shift is still extremely small and the use of modal identification may not be a good method for determining this highly localized damage, since it does not affect the overall global behaviour.

Table 6-9: Connection Damage Natural Frequency Comparison

<b>Mode</b>	<b>Healthy (Hz)</b>	<b>Damaged (Hz)</b>	<b>MAC Value</b>	<b>CSiBRIDGE Healthy (Hz)</b>	<b>CSiBRIDGE Damaged (Hz)</b>
<b>1</b>	0.2563	0.2563	1.0000	0.2568	0.2567
<b>2</b>	0.4688	0.4625	1.0000	0.4586	0.4585
<b>3</b>	0.6000	0.6000	1.0000	0.5919	0.5919
<b>4</b>	0.6250	0.6250	1.0000	0.6225	0.6225
<b>5</b>	0.7813	0.7813	1.0000	0.7798	0.7798
<b>6</b>	0.8188	0.8125	1.0000	0.8111	0.8111
<b>7</b>	--	--	--	0.9834	0.9834
<b>8</b>	1.2750	1.2688	1.0000	1.2690	1.2690
<b>9</b>	--	--	--	1.3081	1.3081
<b>10</b>	1.4500	1.4500	1.0000	1.4443	1.4442
<b>11</b>	1.7500	1.7375	1.0000	1.7575	1.7575
<b>12</b>	1.8563	1.8625	0.9994	1.8637	1.8635
<b>13</b>	1.9313	1.9438	0.9913	1.9319	1.9318
<b>14</b>	--	--	--	1.9558	1.9557
<b>15</b>	--	--	--	2.0954	2.0954

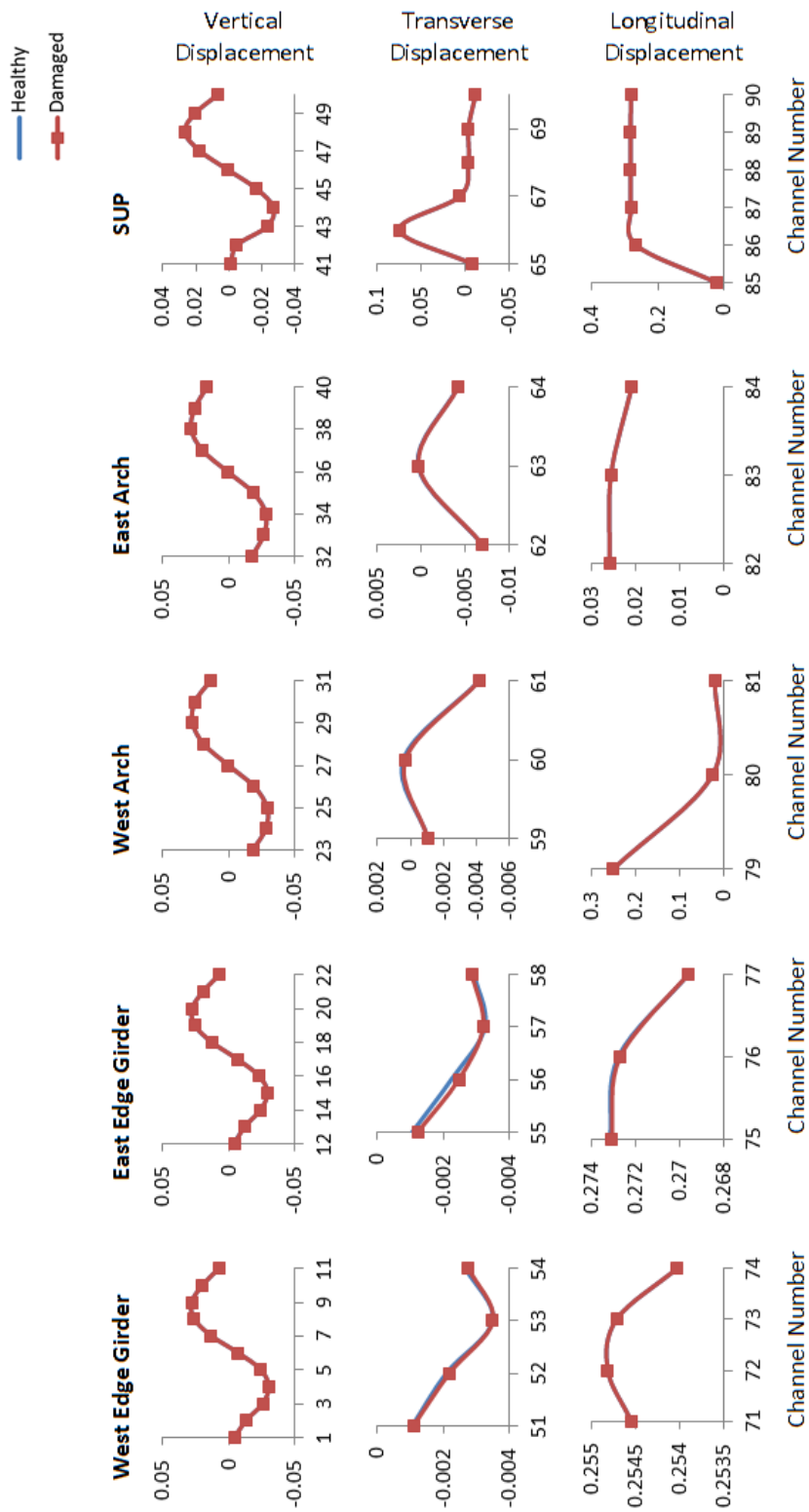


Figure 6-10: Connection Damage at East Edge Girder Mode 1 Comparison

## 6.8 Conclusion

The damage detection simulated in this chapter shows that 11 modes can successfully be identified using the full accelerometer layout described. Using this modal information, global damage, such as boundary condition change, was identified. The detection of local damage, such as arch strut damage and connection damage, was harder to detect and is dependent on accelerometer location. Shifts in natural frequency and MAC value criterion are not good indicators of local damage, and a comparison of mode shapes must be made in order to identify that a large amount of local damage is present within the structure, although when the local damage is not severe, modal identification is not a good indicator for local damage.

The analysis presented in this chapter is very preliminary damage detection. Further analysis and different damage algorithms, such as ARX models that use sensor clusters to extract damage features (Gul and Catbas 2011), will need to be performed in future research, although it is out of the scope of this thesis. Other measurement types, such as strain, can also be used and compared in future studies. Catbas et. al (2012) proposed an approach of tracking correlation coefficients between strain time histories and locations along the structure to detect damage using strain data. Also, the use of impact testing is not recommended on large scale structures, due to impracticality, and the use of ambient vibrations on the CMIF algorithm with use of the random decrement method (Gul and Catbas 2008b) should also be examined. Other algorithms and techniques may be more effective at measuring a larger amount of modes compared to the 11 measured using CMIF, as well as detecting the presence of local damage.

# CHAPTER 7: CONCLUSIONS AND RECOMMENDATIONS

## 7.1 Conclusions

This thesis presented the modeling and analysis of the Walterdale Bridge in order to investigate the behaviour of the structure under design and predicted loading. The structure was also analyzed under serviceability limit state loading combinations to identify the highest areas of stress and displacement. From analysis, it was realized that areas of highest stress were: the end-spans of the bridge girders, the mid-section and end locations of the arches, as well as the east hangers.

Using the preliminary analysis results, two sensor layout plans were proposed in order to determine the importance of the number and placement of sensors. The first system was a sensor layout plan under no budgetary constraints. In addition to loading response, this system was capable of measuring the environmental and vehicle loads that are applied to the structure using a weather station and a weigh-in-motion sensor. The sensors used for response measurements include: 77 vibrating wire strain gauges, 64 dynamic strain gauges, 8 LVDT sensors, 20 triaxial accelerometers and 30 uniaxial accelerometers (90 channels), for a total of 199 sensors. A second sensor layout plan was designed based on budgetary constraints, using 16 triaxial accelerometers (48 channels). The main sensor layout plan, designed with no financial restrictions, was analyzed with 11 impact loads at various locations along the bridge deck and arches. The measured response of the structure under the various impact loads was used to determine the modal behaviour of the structure. These modes were used as a benchmark for damage detection analysis. The ability to measure and excite the bridge modes was dependent on the impact load locations, and the modes sensitivity to the impact load.

Various types of damage were then simulated to the structure in order to better understand how the change in a structural member, both severe and mild, may have an influence on the overall global behaviour. Under damage detection analysis, global damage created a noticeable change in the modes measured, as a large shift in global

behaviour created a noticeable change in natural frequencies and mode shapes. It was demonstrated that natural frequency shifts and the MAC value criterion are not good indicators of the local damage simulated, such as a change in arch strut and cable stiffness, since their change is insignificant on the overall behaviour of the structure. In order to better determine if local change is present within the structure, the comparison of mode shapes must be performed. Although in some cases studied, such as connection damage, it was shown that modal comparisons was not sufficient in detecting local damages and should not be measured using modal identification methods. The placement of sensors was discovered to be of importance, as damage can go undetected if a sensor is not placed near the damaged location. In order to measure local changes in the structure, other techniques should be explored.

## **7.2 Recommendations**

This study investigated the general behaviour of the Walterdale Bridge under several preliminary design and predicted loads under ideal scenarios. As mentioned in Chapter 2, temperature can have a significant effect on the natural behaviour of a structure. Since the Walterdale Bridge will be placed in an environment subject to drastic temperature changes throughout the year, these effects should be analyzed in future work. The investigation into the influence of temperature can give more insight into the extent of damage that can be detected employing the sensor layout plan used in this study.

Also, this study focused on preliminary analysis using CMIF modal identification with the use of impact loading to excite the structure only in order to investigate the sensor layout plan's ability to detect damage using mode shapes. Future work should consider measurements under ambient vibrations, such as vehicle and wind loads. Additionally, different algorithms that use acceleration data or algorithms that incorporate strain measurements can be used to create benchmark behaviour. Multiple algorithms can be compared and the effects of using several algorithms to detect the presence of damage should be explored. Better results are expected by incorporating other types of damage analysis and further analysis of the structure.

It should be noted that the layout plan described in this thesis is capable of measuring the global behaviour of the structure. If the behaviour of a specific member is desired, additional analysis into localized behaviour of specific members should be implemented.

Furthermore, the analysis conducted in this research is based solely on a model created in CSiBridge software under ideal conditions. The results obtained in this research may not fully reflect the true behaviour of the in-situ structure and may change in future studies or with the use of other analysis software. Model updating is also required once the construction of the bridge is complete that may result in a more accurate representation of the structure.

## REFERENCES

- Battisti, L. (2015). *Wind Turbines in Cold Climates: Icing Impacts and Mitigation Systems*. Springer, Switzerland, 64.
- Bergmeister, K., and Santa, U. (2001). "Global monitoring concepts for bridges." *Structural Concrete*, 2(1), 29-39.
- CAN/CSA-S6. (2006). *Canadian Highway Bridge Design Code & Commentary*. Canadian Standards Association, Mississauga, ON.
- Cardini, A., and DeWolf, J. T. (2008). "Long-term structural health monitoring of a multi-girder steel composite bridge using strain data." *Structural Health Monitoring*, 8(1), 47-58.
- Catbas, F. N., Gokce, H. B., and Gul, M. (2012). "Nonparametric analysis of structural health monitoring data for identification and localization of changes: Concept, lab, and real-life studies." *Structural Health Monitoring*, 11(5), 613-626.
- Catbas, F. N., Susoy, M., and Frangopol, D. M. (2008). "Structural health monitoring and reliability estimation: Long span truss bridge application with environmental monitoring data." *Eng.Struct.*, 30(9), 2347-2359.
- Cbc.ca,. (2015). 'New Waltherdale Bridge delayed a full year, city says'. <<http://www.cbc.ca/news/canada/edmonton/new-waltherdale-bridge-delayed-a-full-year-city-says-1.3024978>> (Sep. 5, 2015).
- Çelebi, M., Purvis, R., Hartnagel, B., Gupta, S., Clogston, P., Yen, P., O'Connor, J., and Franke, M. (2004). "Seismic instrumentation of the Bill Emerson Memorial Mississippi River Bridge at Cape Girardeau (MO): A cooperative effort." *Proceedings of the 4th International Seismic Highway Conference*, Memphis, TN.
- Chang, P. C., Flatau, A., and Liu, S. (2003). "Review paper: health monitoring of civil infrastructure." *Structural Health Monitoring*, 2(3), 257-267.
- Chen, B., Wang, X., Sun, D., and Xie, X. (2014). "Integrated System of Structural Health Monitoring and Intelligent Management for a Cable-Stayed Bridge." *The Scientific World Journal*, 2014.
- Cheung, M., and Naumoski, N. (2002). "The first smart long-span bridge in Canada—health monitoring of the Confederation Bridge." *Structural Health Monitoring Workshop*, Winnipeg, MN., 31-44.

Chintalapudi, K., Fu, T., Paek, J., Kothari, N., Rangwala, S., Caffrey, J., Govindan, R., Johnson, E., and Masri, S. (2006). "Monitoring civil structures with a wireless sensor network." *Internet Computing, IEEE*, 10(2), 26-34.

Cho, S., and Spencer, B. F. (2015). "Sensor Attitude Correction of Wireless Sensor Network for Acceleration-Based Monitoring of Civil Structures." *Computer-Aided Civil and Infrastructure Engineering*, 00 (2015), 1-13.

*Civil Infrastructure Systems Technology Road Map*. (2013). 14-15.

Clark, M. R., McCann, D. M., and Forde, M. C. (2003). "Application of infrared thermography to the non-destructive testing of concrete and masonry bridges." *NDT E Int.*,36(4), 265-275.

CSI Analysis Reference Manual. (2013). Computers and Structures, Inc., Berkley, California, USA, 145.

CSiBridge Version 16.1.0 (2014). Computers and Structures, Inc., Berkeley, California, USA.

DeWolf, J. T. (2009). *Field Strain Monitoring to Evaluate Unexpected Cracking in a Non-Redundant Steel Plate Girder Bridge Report No. CT-2251-2-09-4*, CN.

Doebling, S. W., Farrar, C. R., and Prime, M. B. (1998). "A summary review of vibration-based damage identification methods." *Shock Vib Dig*, 30(2), 91-105.

Doebling, S. W., Farrar, C. R., Prime, M. B., and Shevitz, D. W. (1996). *Damage Identification and Health Monitoring of Structural and Mechanical Systems from Changes in their Vibration Characteristics: A Literature Review*, Los Angeles, CA .

dos Santos, Fábio Luis Marques, Peeters, B., Menchicchi, M., Lau, J., Gielen, L., Desmet, W., and Góes, L. C. S. (2014). "Strain-Based Dynamic Measurements and Modal Testing." *Topics in Modal Analysis II, Volume 8*, Springer, 233-242.

Edmonton.ca,. (2015). 'John Walter Biography: City of Edmonton'. <[http://www.edmonton.ca/attractions\\_events/john\\_walter\\_museum/john-walter-bio.aspx](http://www.edmonton.ca/attractions_events/john_walter_museum/john-walter-bio.aspx)> (May 20, 2015).

Edmonton.ca,. (2015). 'Walterdale Bridge Replacement Project History :: City of Edmonton'. <[http://www.edmonton.ca/transportation/road\\_projects/walterdale-bridge-project-history.aspx](http://www.edmonton.ca/transportation/road_projects/walterdale-bridge-project-history.aspx)> (May 20, 2015).

Edmonton.ca,. (2015). 'Traffic Flow Maps & Reports :: City of Edmonton'. <[http://www.edmonton.ca/transportation/traffic\\_reports/traffic-reports-flow-maps.aspx](http://www.edmonton.ca/transportation/traffic_reports/traffic-reports-flow-maps.aspx)> (January 25, 2015).

Edmonton.ctvnews.ca,. (2015). 'Opinions split on what should be done with the aging Walterdale Bridge'. <<http://edmonton.ctvnews.ca/opinions-split-on-what-should-be-done-with-the-aging-walterdale-bridge-1.668899>> (May 20, 2015).

Galvín, P., and Domínguez, J. (2007). "Dynamic analysis of a cable-stayed deck steel arch bridge." *Journal of Constructional Steel Research*, 63(8), 1024-1035.

Gul, M., and Catbas, F. N. (2011). "Structural health monitoring and damage assessment using a novel time series analysis methodology with sensor clustering." *J.Sound Vibrat.*, 330(6), 1196-1210.

Gul, M., and Catbas, F. N. (2008). "Ambient vibration data analysis for structural identification and global condition assessment." *J.Eng.Mech.*, 134(8), 650-662

Harms, T., Sedigh, S., and Bastianini, F. (2010). "Structural health monitoring of bridges using wireless sensor networks." *Instrumentation & Measurement Magazine, IEEE*, 13(6), 14-18.

Infrastructurereportcard.org,. (2015). 'ASCE | 2013 Report Card for America's Infrastructure'. <<http://www.infrastructurereportcard.org/a/#p/bridges/conditions-and-capacity>> (June 14, 2015).

Kalooop, M. R., and Li, H. (2009). "Monitoring of bridge deformation using GPS technique." *KSCE Journal of Civil Engineering*, 13(6), 423-431.

Ko, J., and Ni, Y. (2005). "Technology developments in structural health monitoring of large-scale bridges." *Eng.Struct.*, 27(12), 1715-1725.

Lee, Y., Phares, B., and Wipf, T. (2007). "Development of a Low-Cost, Continuous Structural Health Monitoring System for Bridges and Components." *Proceedings of the 2007 Mid-Continent Transportation Research Symposium*, Ames, Iowa,

Li, H., and Ou, J. (2015). "The state of the art in structural health monitoring of cable-stayed bridges." *Journal of Civil Structural Health Monitoring*, 1-25.

Liu, C., and DeWolf, J. T. (2007). "Effect of temperature on modal variability of a curved concrete bridge under ambient loads." *J.Struct.Eng.*, 133(12), 1742-1751.

MacKenzie, D., Barker, C., McFadyen, N., and Allison, B. (2005). "Footbridge pedestrian vibration limits-part 2: human sensitivity." *Proceedings of Footbridge Second International Conference*, Venice .

MATLAB Release 2015a, The MathWorks, Inc., Natick, Massachusetts, United States.

Mirza, M. S., and Haider, M. (2003). "The state of infrastructure in Canada: Implications for infrastructure planning and policy." *Infrastructure Canada*, 29(1), 17-38.

Moore, M., Phares, B. M., Graybeal, B., Rolander, D., and Washer, G. (2001). *Reliability of Visual Inspection for Highway Bridges, Volume I*, McLean, Va, USA.

Ni.com.,(2015). 'What Is Data Acquisition? - National Instruments'.  
<<http://www.ni.com/data-acquisition/what-is/>> (Aug. 12, 2015).

Ni.com., (2015). 'How to Choose the Right Bus for Your Measurement System - National Instruments'. <<http://www.ni.com/white-paper/9401/en/>> (August 12, 2015).

Ni, Y., Hua, X., Fan, K., and Ko, J. (2005). "Correlating modal properties with temperature using long-term monitoring data and support vector machine technique." *Eng.Struct.*, 27(12), 1762-1773.

Peeters, B., and De Roeck, G. (1999). "Reference-based stochastic subspace identification for output-only modal analysis." *Mechanical Systems and Signal Processing*, 13(6), 855-878.

Pines, D., and Aktan, A. E. (2002). "Status of structural health monitoring of long-span bridges in the United States." *Progress in Structural Engineering and Materials*,4(4), 372-380.

Potdar, V., Sharif, A., and Chang, E. (2009). "Wireless sensor networks: A survey." *Advanced Information Networking and Applications Workshops, 2009. WAINA'09.*, IEEE, 636-641.

Ren, W., Zhao, T., and Harik, I. E. (2004). "Experimental and analytical modal analysis of steel arch bridge." *J.Struct.Eng.*, 130(7), 1022-1031.

Roeder, C. W., MacRae, G., Crocker, P., Arima, K., and Wong, S. (2000). "Dynamic response and fatigue of steel tied-arch bridge." *J.Bridge Eng.*, 5(1), 14-21.

Sadeghi, F., Kueh, A., Bagheri Fard, A., and Aghili, N. (2013). "Vibration Characteristics of Composite Footbridges under Various Human Running Loads." *International Scholarly Research Notices*, 2013.

Shih, C., Tsuei, Y., Allemang, R., and Brown, D. (1988). "Complex mode indication function and its applications to spatial domain parameter estimation." *Mechanical Systems and Signal Processing*, 2(4), 367-377.

Song, H., and Saraswathy, V. (2007). "Corrosion Monitoring of Reinforced Concrete Structures-A." *Int.J.Electrochem.Sci*, 2 1-28.

Steelconstruction.info (2015). 'Tied-arch bridges'.  
<[http://www.steelconstruction.info/Tied-arch\\_bridges](http://www.steelconstruction.info/Tied-arch_bridges)> (August 12, 2015).

*Walterdale Bridge Rehabilitation Assessment Summary*. (2001). 1-4.

- Wang, L., and Chan, T. H. (2009). "Review of vibration-based damage detection and condition assessment of bridge structures using structural health monitoring." *QUT Conference Proceedings*, Queensland University, 1-15.
- Wardhana, K., and Hadipriono, F. C. (2003). "Analysis of recent bridge failures in the United States." *J.Perform.Constr.Facil.*, 17(3), 144-150.
- Xu, Y. L., and Xia, Y. (2011). *Structural health monitoring of long-span suspension bridges*. CRC Press, New York, NY.
- YEGisHome.ca,(2015). 'The great old Walterdale Bridge'.  
<<http://yegishome.ca/news/2011/01/06/the-great-old-walterdale-bridge>> (May 20, 2015).
- Zhang, Q., Fan, L., and Yuan, W. (2002). "Traffic-induced variability in dynamic properties of cable-stayed bridge." *Earthquake Eng.Struct.Dyn.*, 31(11), 2015-2021.
- Zhou, G., and Yi, T. (2014). "A summary review of correlations between temperatures and vibration properties of long-span bridges." *Mathematical Problems in Engineering*, 2014.
- Zhou, H., Ni, Y., and Ko, J. (2011). "Eliminating temperature effect in vibration-based structural damage detection." *J.Eng.Mech.*, 137(12), 785-796.

## **APPENDIX A: CONSTRUCTION SEQUENCE**

The construction has been divided into 10 separate stages, provided in the bridge drawings. Stage 1 includes the construction of the berms for foundations and construction of the thrust blocks. Stage 2 – 8 involves the installation of the arch segments. This requires the erection of shoring towers that provide support to the arch ribs. The 6 north and south arch segments at each shoring tower are installed first. After the installation of these segments is complete, the mid-section of the arch is erected by rolling the completed assembled segment from the south end to its required location with the use of a barge. Once at the proper location, a temporary tie is installed to the arch segment to reduce its deflections. The segment is then lifted to place using strand jacks. The temporary shoring towers are then removed and the abutments, girder segments, floor beams, stringers and hangers are installed, starting from the north end until the mid-span is reached, repeating the process on the south end. Stage 9 involves casting the deck. Stage 10 is the construction of all the SUP components and surveying the bridge profile geometry and measuring all hanger tensions.



Figure A-1: South-West Thrust Block Construction (August 20<sup>th</sup>, 2015)



Figure A-2: South Abutment Construction (August 20<sup>th</sup>, 2015)



Figure A-3: Temporary Modular Barge (August 20<sup>th</sup>, 2015)



Figure A-4: Mid-arch Section Construction (August 20<sup>th</sup>, 2015)

# APPENDIX B: SAMPLE ANALYSIS RESULTS OF INDIVIDUAL LOADING CASES

## B.1 Negative Effective Temperature Load Normal Stresses

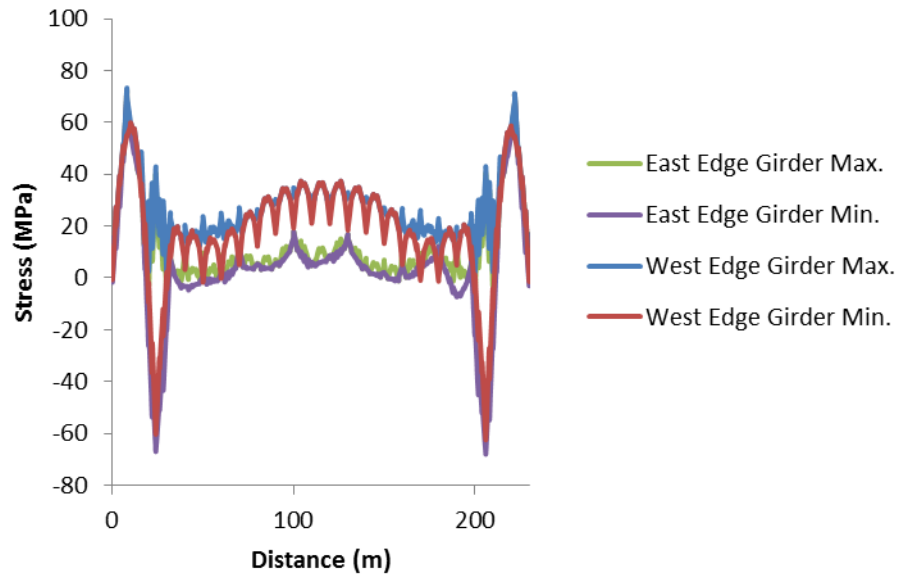


Figure B-1: Edge Girder Normal Stress under Negative Effective Temperature

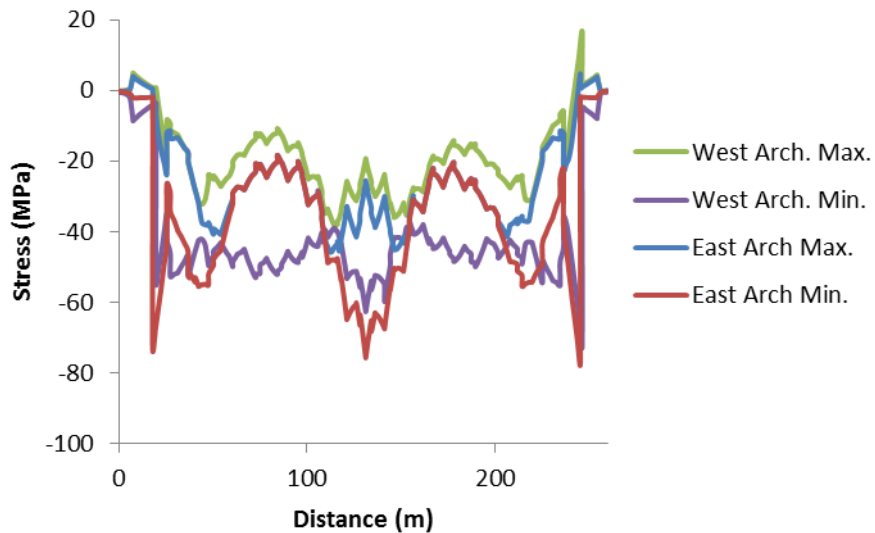


Figure B-2: Arch Normal Stresses under Negative Effective Temperature

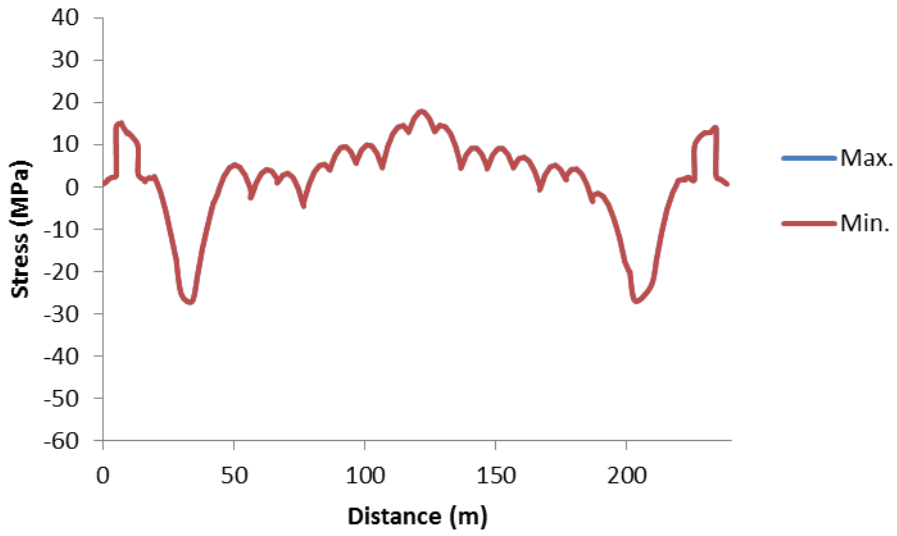


Figure B-3: SUP Normal Stresses under Negative Effective Temperature

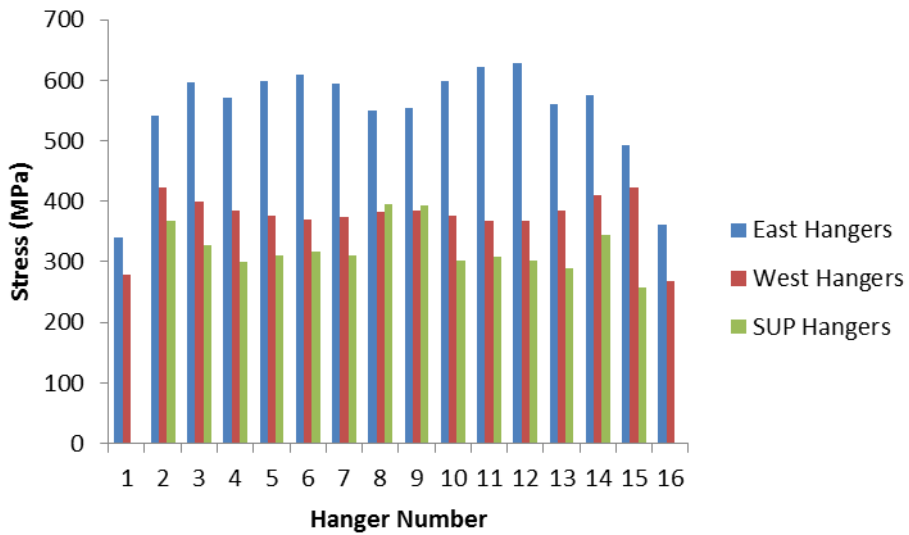


Figure B-4: Hanger Normal Stresses under Negative Effective Temperature

## B.2 Negative Thermal Gradient Temperature Load Stresses

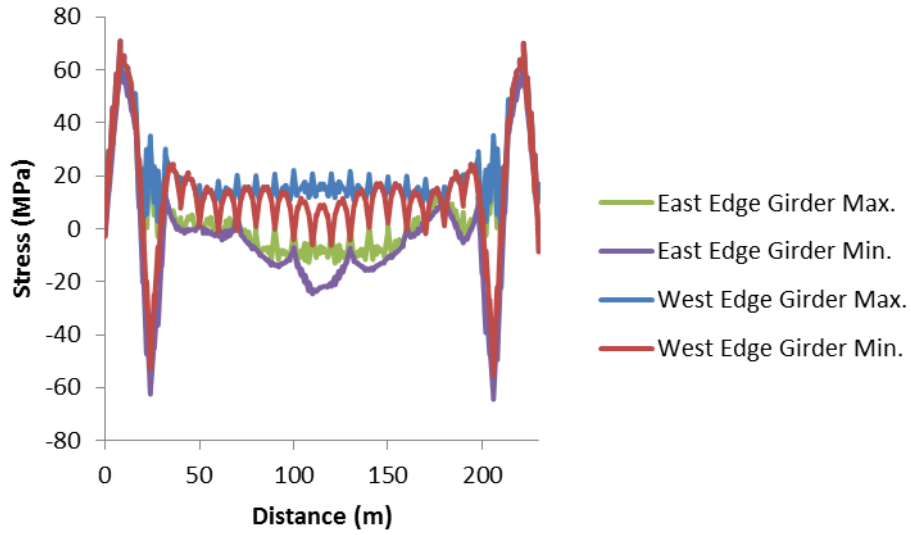


Figure B-5: Edge Girder Normal Stresses under Negative Thermal Gradient

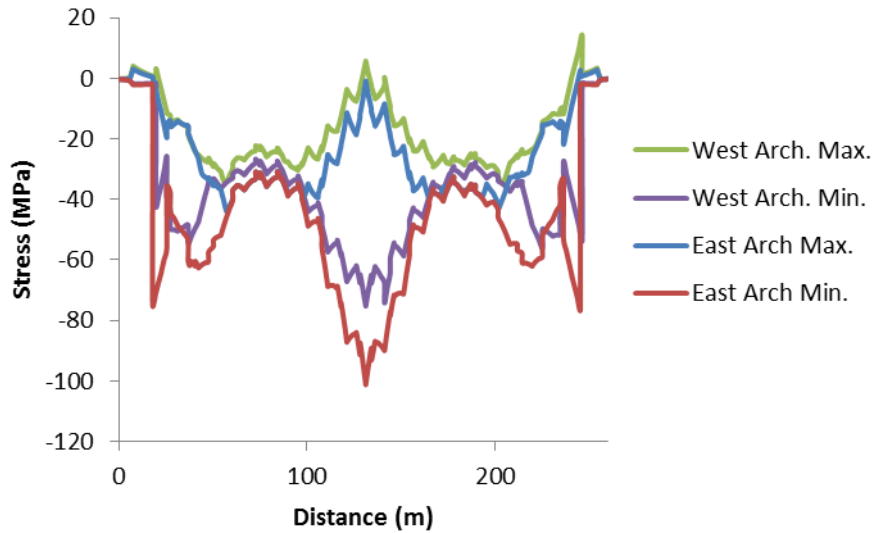


Figure B-6: Arch Normal Stresses under Negative Thermal Gradient

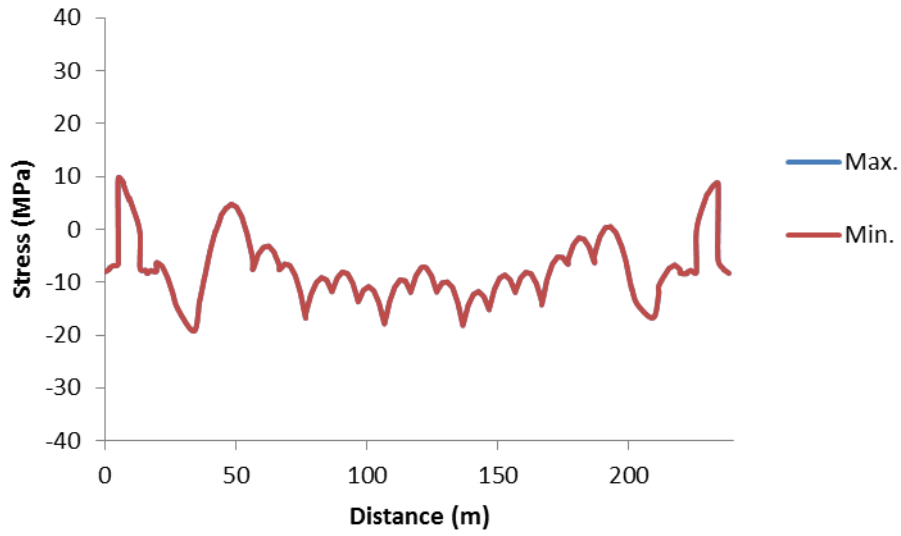


Figure B-7: SUP Normal Stresses under Negative Thermal Gradient

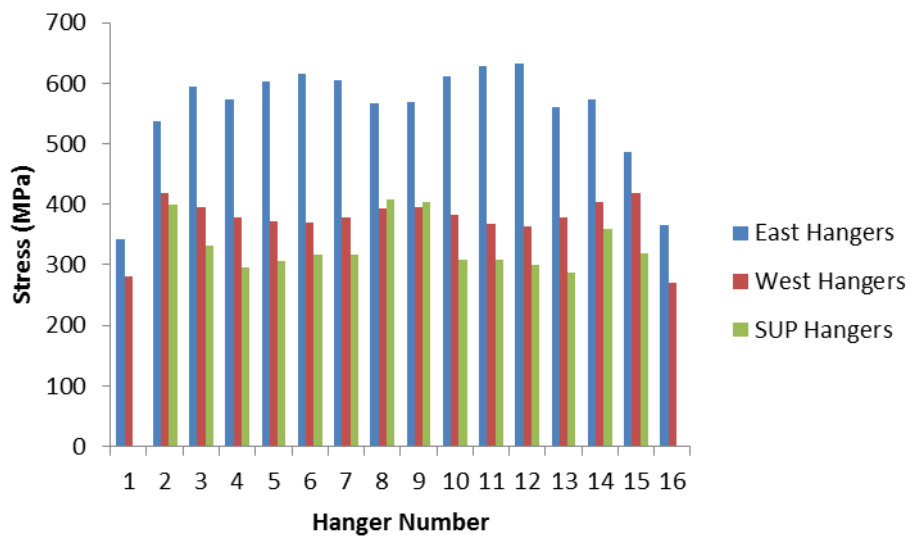


Figure B-8: Hanger Normal Stresses under Negative Thermal Gradient

### B.3 CL-W800 Truck Load Analysis Stresses

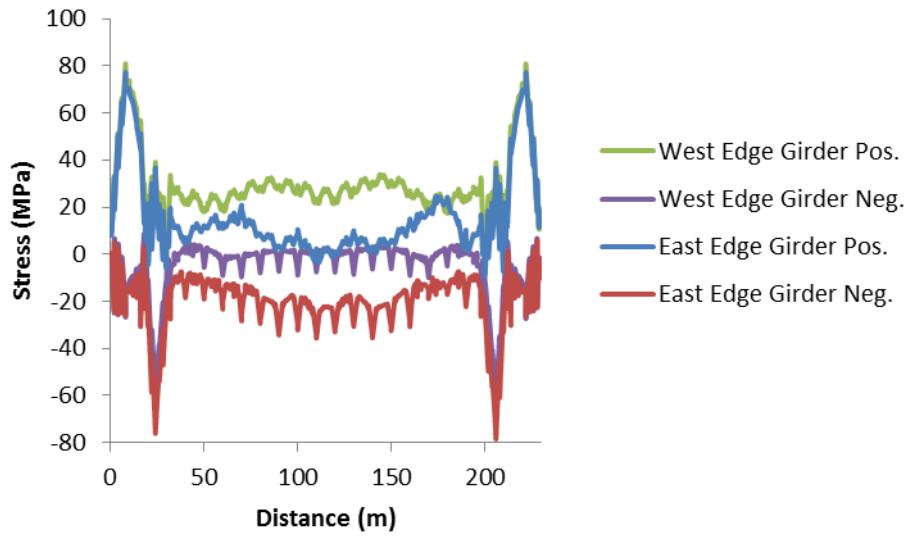


Figure B-9: Edge Girder Normal Stresses under CL-W800 Truck

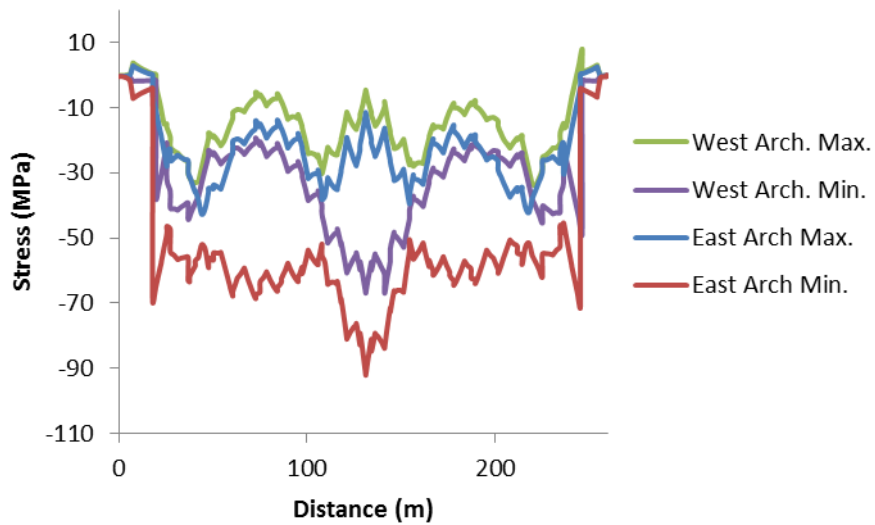


Figure B-10: Arch Normal Stresses under CL-W800 Truck

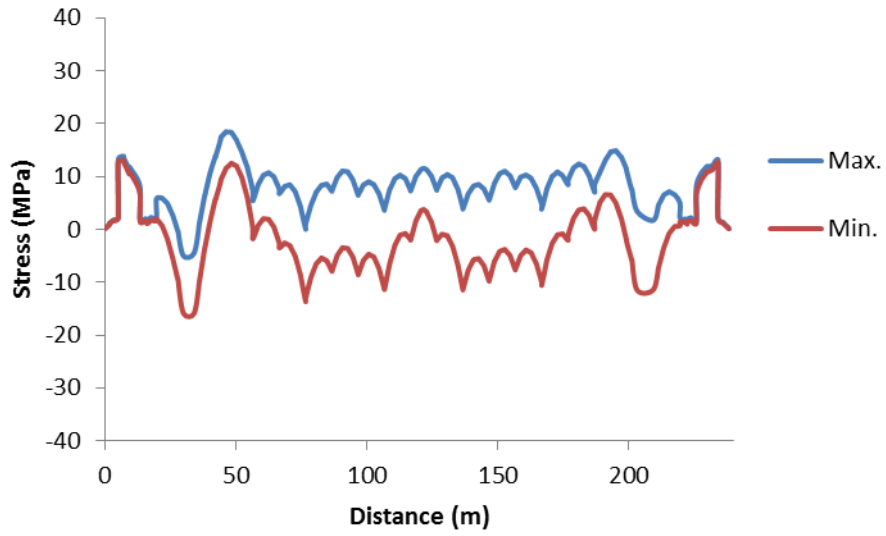


Figure B-11: SUP Normal Stress under CL-W800 Truck

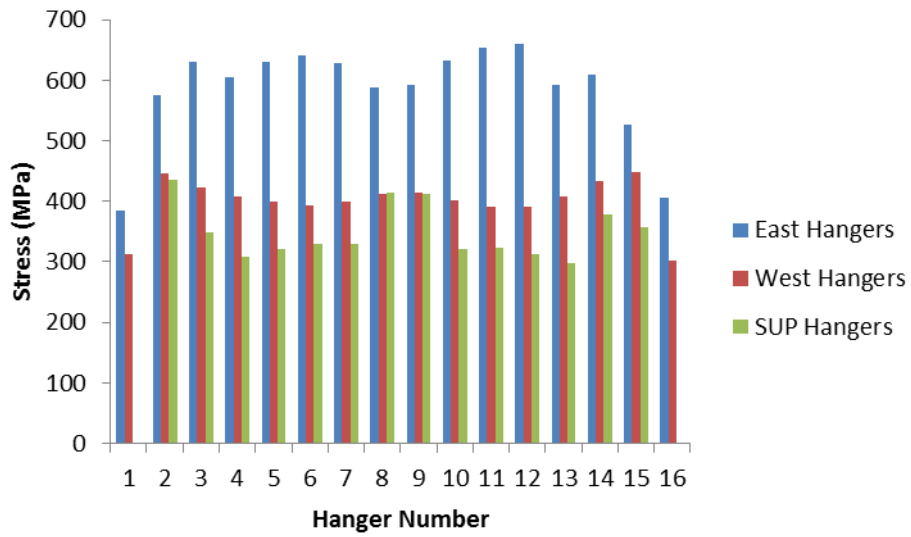


Figure B-12: Hanger Normal Stress under CL-W800 Truck

#### B.4 SUP Pedestrian Load Analysis Stresses

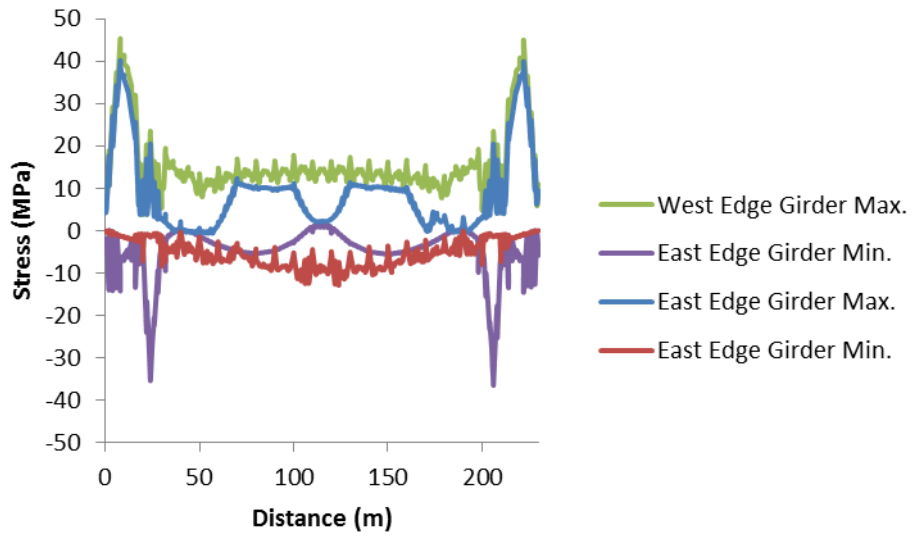


Figure B-13: Edge Girder Normal Stress under SUP Pedestrian Load

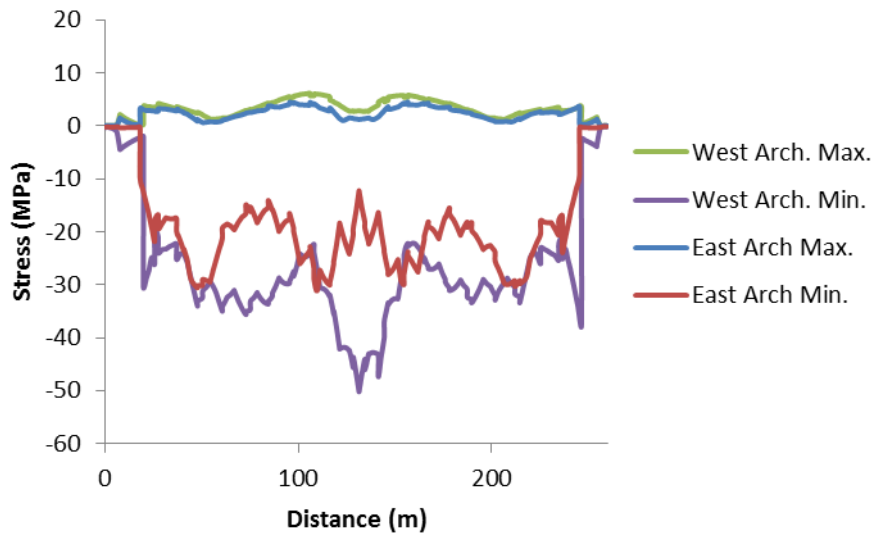


Figure B-14: Arch Normal Stress under SUP Pedestrian Load

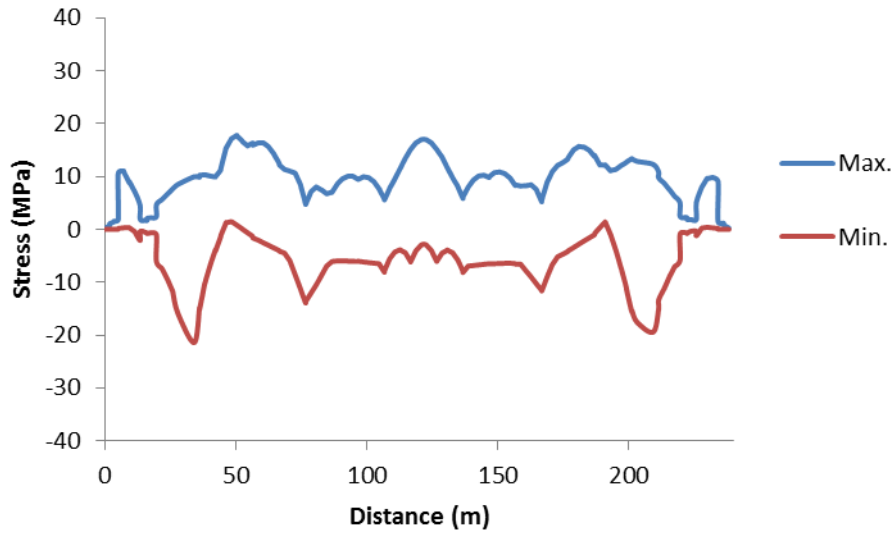


Figure B-15: SUP Normal Stress under SUP Pedestrian Load

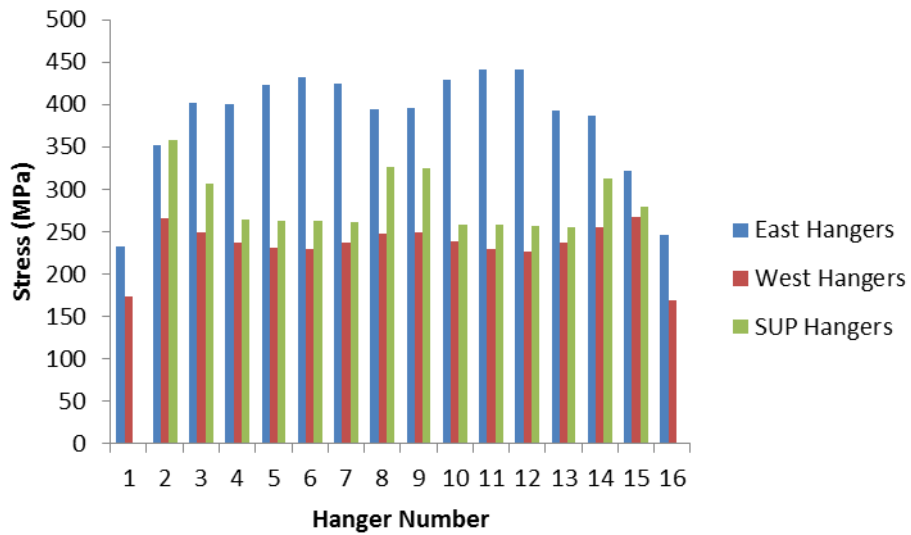


Figure B-16: Hanger Normal Stress under SUP Pedestrian Load

## B.5 Wind Load Envelope Analysis Stresses

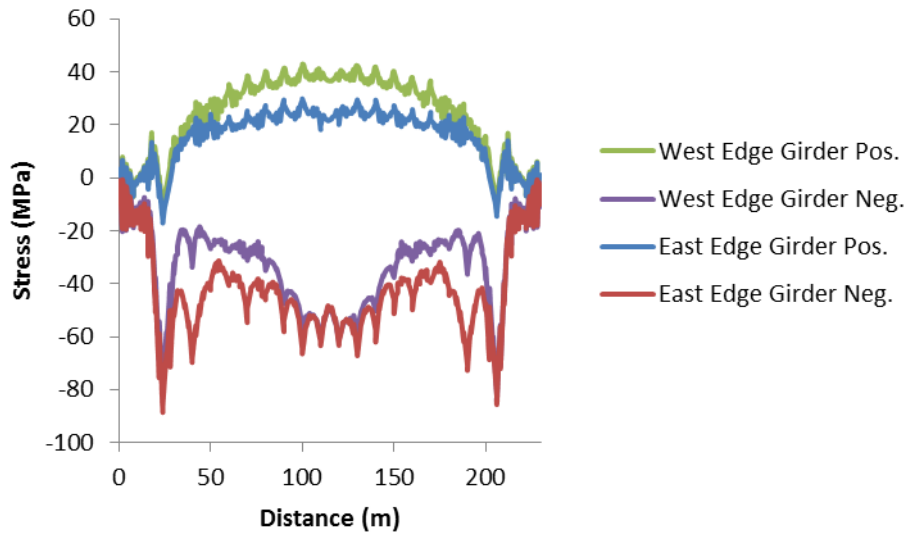


Figure B-17: Edge Girder Normal Stress under Wind Load Envelope

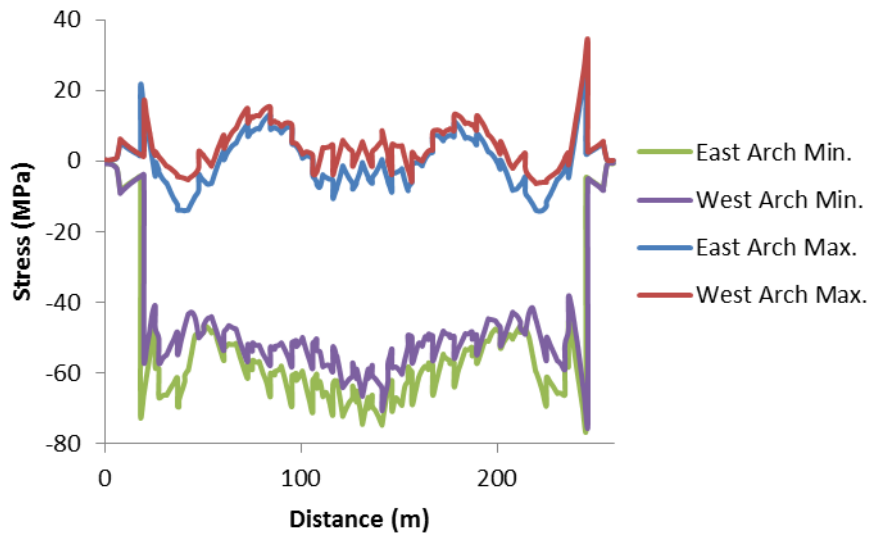


Figure B-18: Arch Normal Stress under Wind Load Envelope

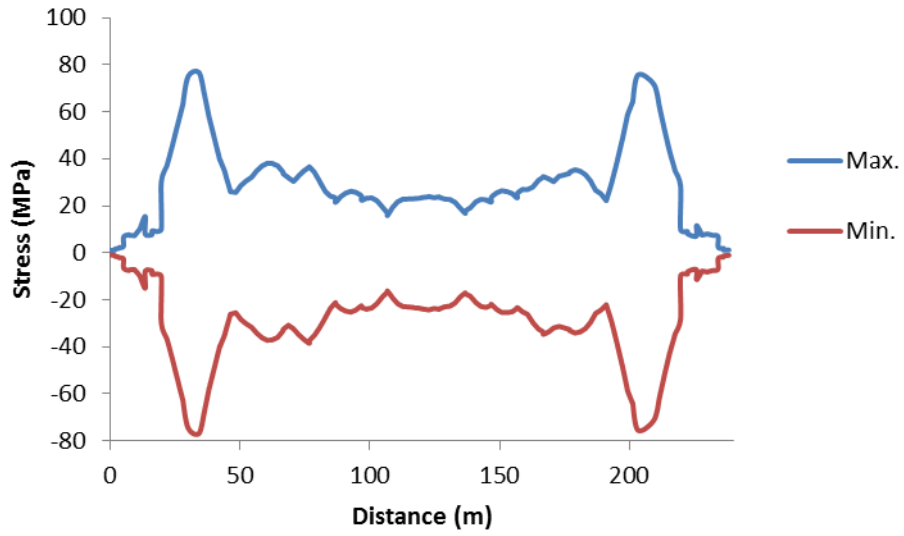


Figure B-19: SUP Normal Stresses under Wind Load Envelope

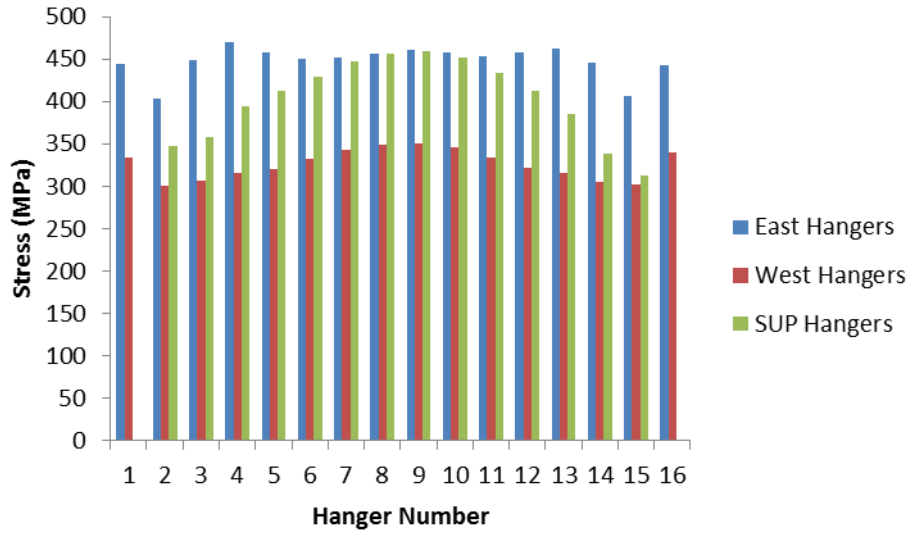


Figure B-20: Hanger Normal Stresses under Wind Load Envelope

### B.6 Serviceability Limit State 1 Analysis Second Member Stresses

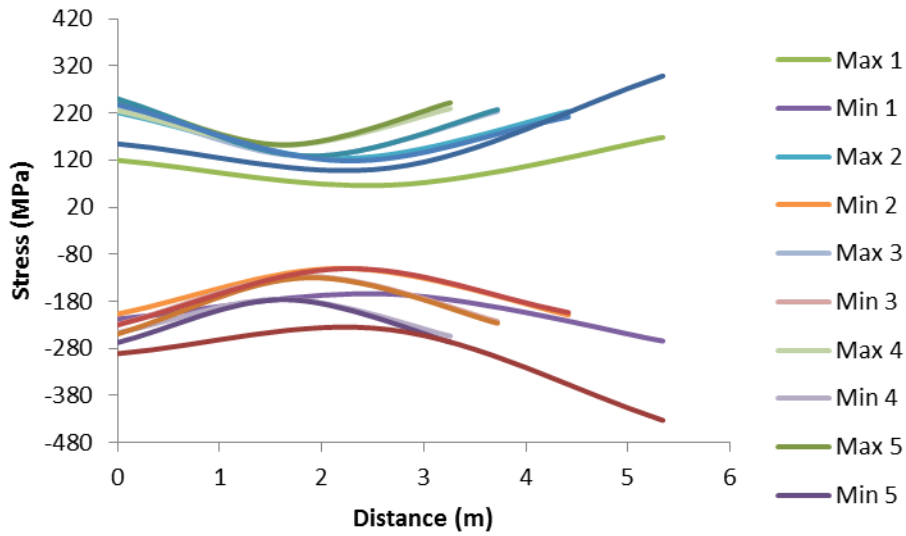


Figure B-21: Floor Beam Extension Normal Stress under SLS1 Load Combination

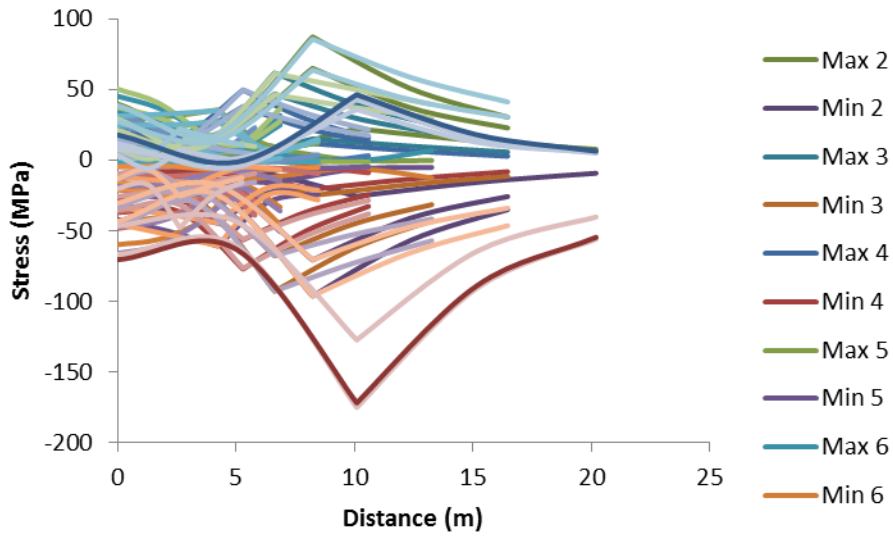


Figure B-22: Arch Strut Normal Stress under SLS1 Load Combination

## APPENDIX C: BEAM RIGIDITY INVESTIGATION

A simple structure was simulated under dead load analysis in order to investigate the effects of rigidity on the load carried by the cables. The structure has the same cross-sectional properties of the Walterdale Bridge deck at the “Hanger 6” location. The cross section was then analyzed under dead load and dead load + live load using a modulus of elasticity of 200 GPa and again simulating a fully rigid beam.

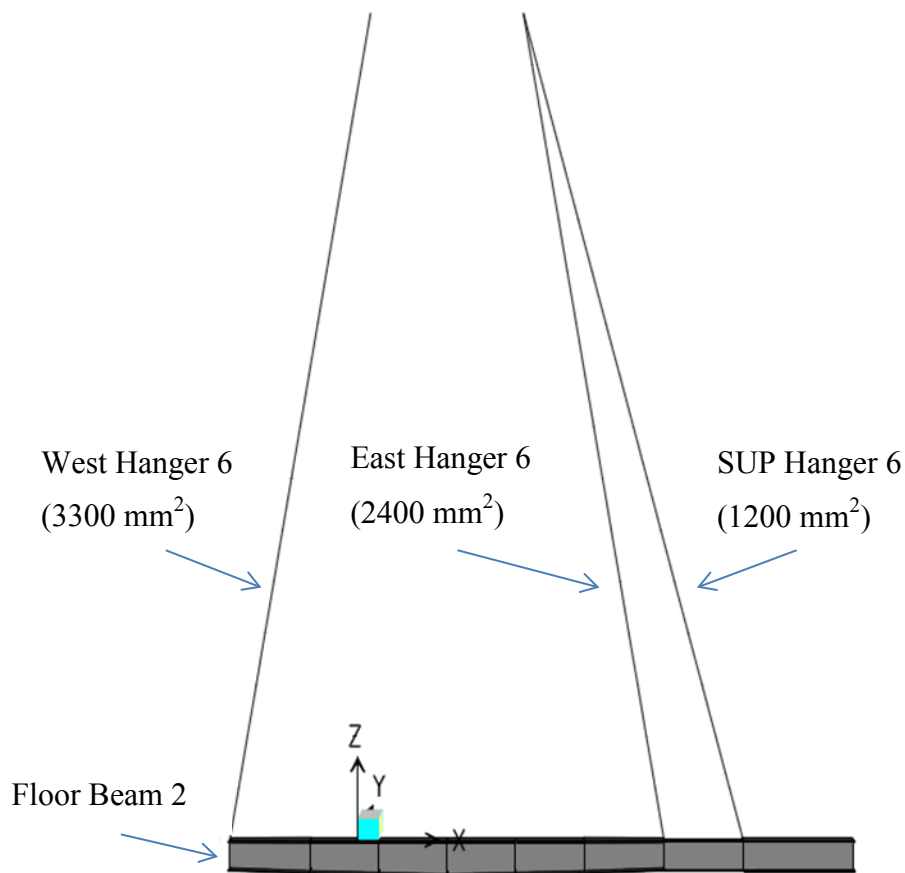


Figure C-1: Cross-Section at Hanger 6 Location

## C.1 Nonlinear Analysis

### C.1.1 Modulus of Elasticity of 200 GPa

The structure was first analyzed using a value of 200 GPa for the modulus of elasticity of steel.

#### C.1.1.1 Dead Load Analysis

Under dead load only, the cables experience the axial forces as demonstrated below. From this, it is evident that the east hanger carries the largest amount of loading, since the deflected shape of the beam is an important factor in how the load is distributed.

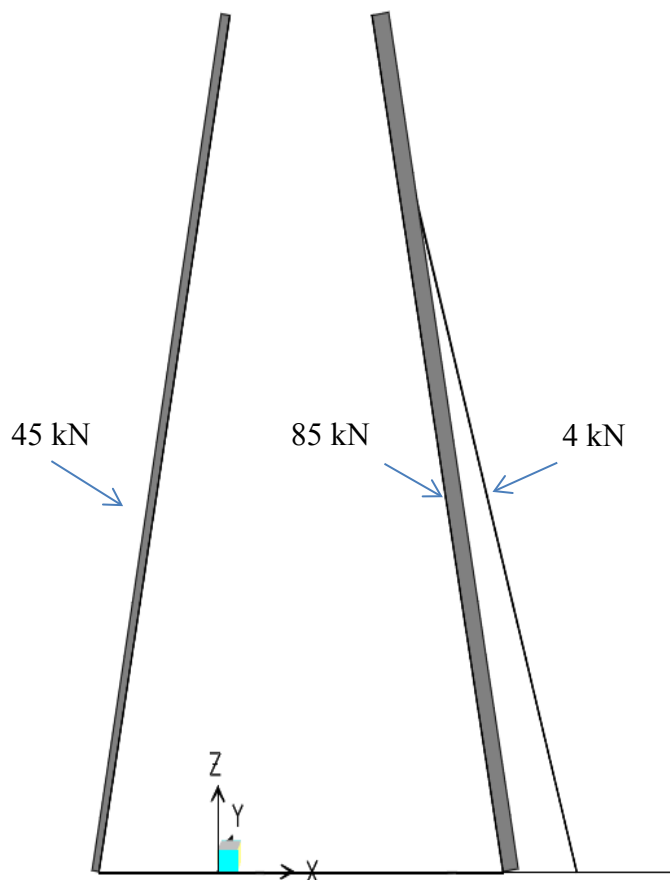


Figure C-2: Nonlinear Dead Load Analysis Results of 200 GPa Member

#### C.1.1.2 Dead Load + Live Load Analysis

The member was then analyzed using a point load of 40 kN, simulating the load of a large vehicle, at the location of traffic lane 2. Similar results as above were obtained. The

east hanger is again responsible for a higher axial force compared to the other two hangers. The results are shown below.

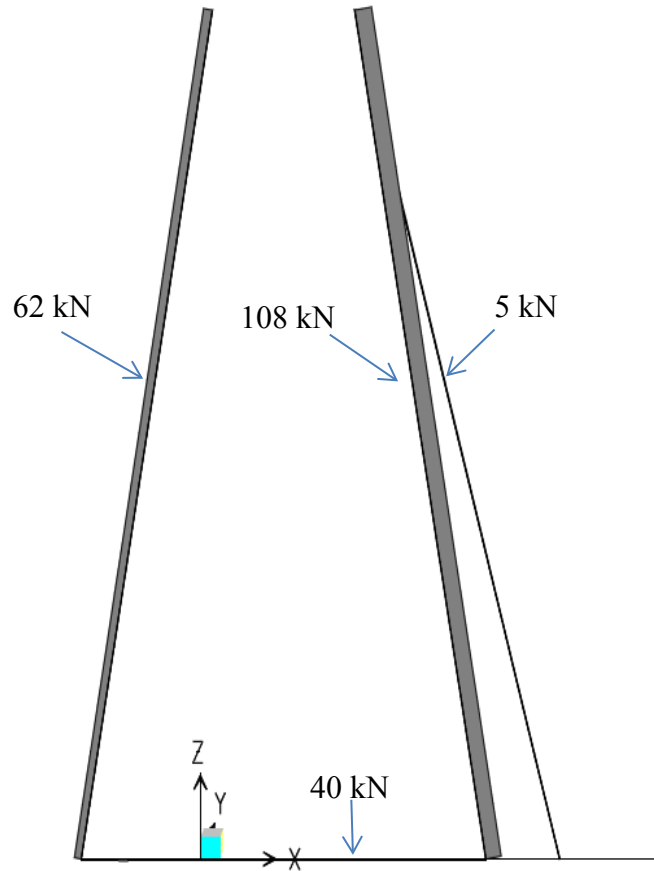


Figure C-3: Nonlinear Dead Load + Live Load Analysis Results of 200 GPa Member

### C.1.2 Fully Rigid Member

The stiffness of the beam was then altered to simulate a fully rigid member. The results under the same load cases as above were then investigated.

#### C.1.2.1 Dead Load Analysis

The same structure was then analyzed by simulating a fully rigid floor beam member. By doing this, the west hanger now carries the largest amount of axial load, as the east and shared-use pathway (SUP) hangers now share the load on the east side, while the west cable is responsible for all the load on the west side of the beam. Although the total load

supported by the beam is the same as the case above, the load is distributed in a different manner than using a modulus of elasticity of 200 GPa.

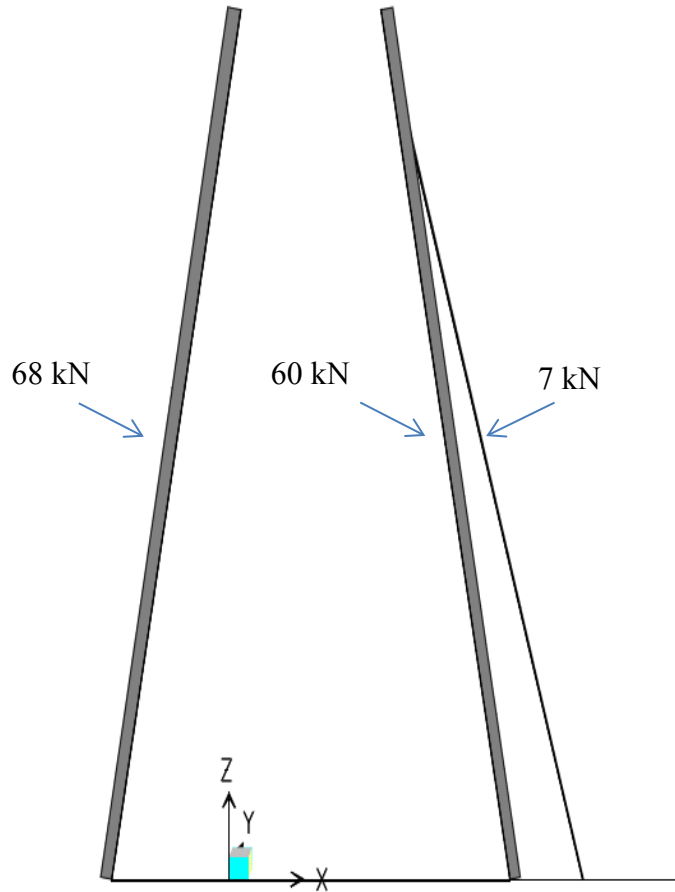


Figure C-4: Nonlinear Dead Load Analysis Results of Fully Rigid Member

#### ***C.1.2.2 Dead Load + Live Load Analysis***

Again, similar results to that of the dead load analysis are obtained. The west hanger still carries the highest amount of load.

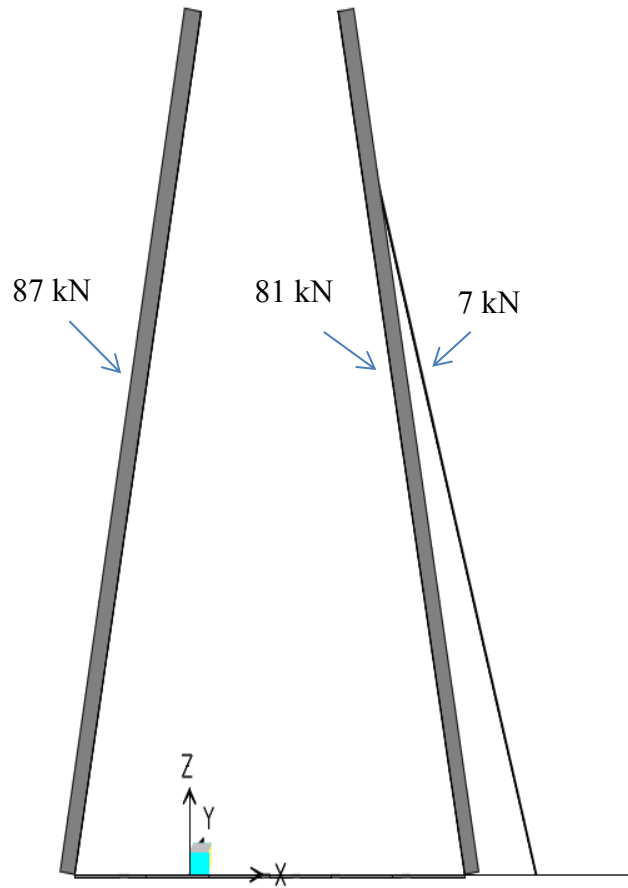


Figure C-5: Nonlinear Dead Load + Live Load Analysis Results of Fully Rigid Member

## C.2 Linear Beam Rigidity Analysis

Linear analysis was performed on the dead load of the structure and a point load of 40 kN for both 200 GPa modulus of elasticity and again for a fully rigid beam. Similar results shown in non-linear analysis were obtained. The axial forces experienced in each hanger for all stiffness and loading cases are shown below.

### C.2.1 Modulus of Elasticity of 200 GPa

For both the dead load and live load analysis, the east hanger carries the highest amount of axial load, demonstrated below.

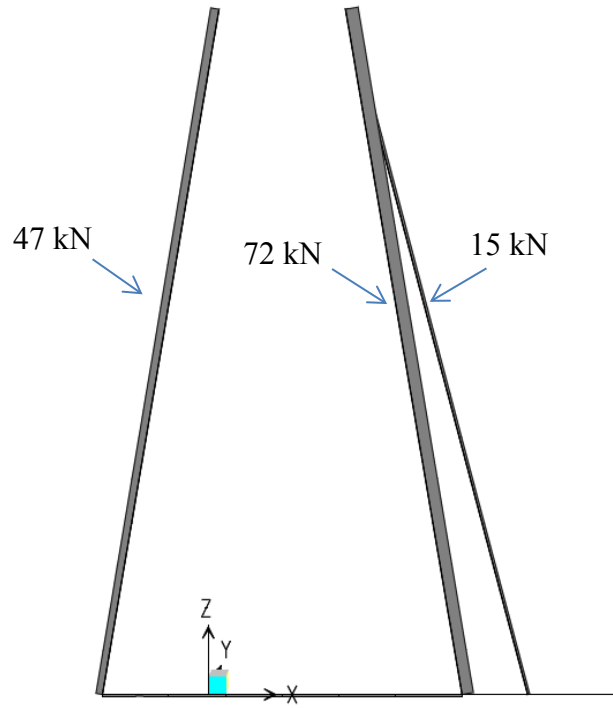


Figure C-6: Linear Dead Load Analysis Results of 200 GPa Member

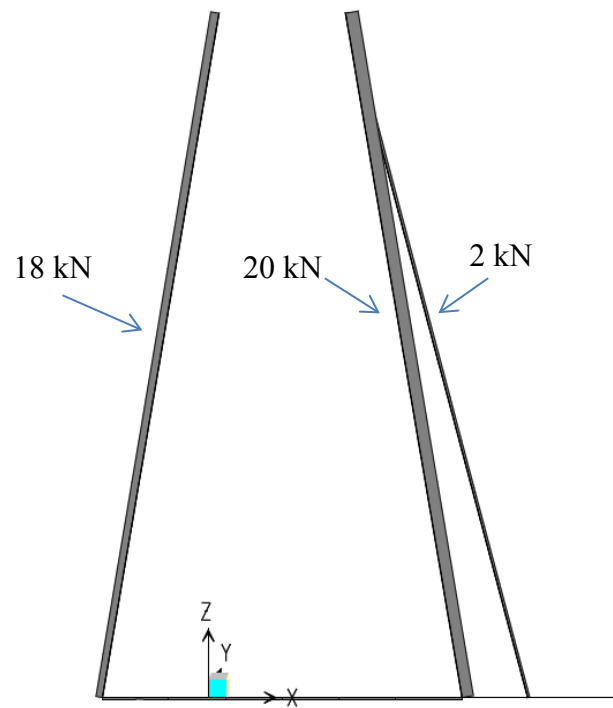


Figure C-7: Linear Live Load Analysis Results of 200 GPa Member

### C.2.2 Fully Rigid Member

When the floor beam is fully rigid, the west hanger carries the largest amount of axial load.

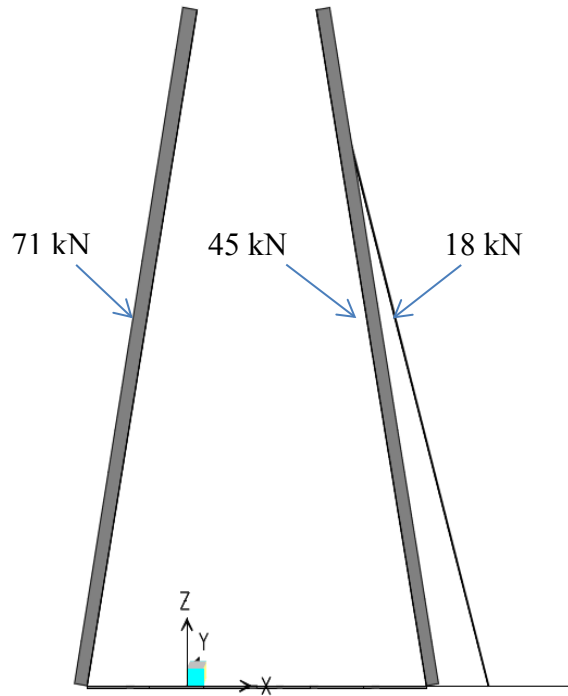


Figure C-8: Linear Dead Load Analysis Results of Fully Rigid Member

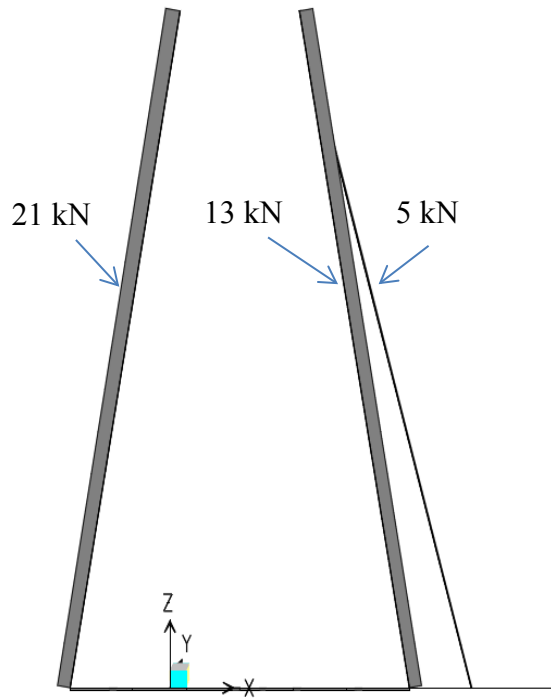


Figure C-9: Linear Live Load Analysis Results of Fully Rigid Member

### C.3 Conclusion

From this analysis, it is demonstrated that the amount of axial load at each hanger location is dependent on the stiffness of the floor beam. When the modulus of elasticity is 200 GPa, the east hanger experiences the highest amount of axial force. When the floor beam is fully rigid, the west hanger experiences a higher amount of axial load compared to the east and SUP hangers. The analysis also shows that the geometric nonlinearity has significant effects on the loads in each cable.

## **APPENDIX D: LIMITED BUDGET ANALYSIS USING CMIF MODAL IDENTIFICATION**

Two budgeted layout plans, both using 16 triaxial accelerometers, are presented below. As discussed in Chapter 5, 16 wireless triaxial accelerometers can be purchased given a financial constraint. The first layout places all 16 accelerometers on the bridge deck only. The second layout places 10 on the bridge deck, and 6 on the two arches, although the practical installation of this system may be challenging, as the steel arches could be difficult to access. . The two layout plans are compared using CMIF modal identification to verify which system can collect the most accurate information as well as the effects of using 16 accelerometers versus 50 accelerometers. The same time-history impact load described in Chapter 6 was used. The sensor and impact locations used are described in further detail below.

### **D.1 Layout Plan 1: 16 Accelerometers on Bridge Deck**

A layout system consisting of 16 triaxial accelerometers placed on the bridge deck at 20 m intervals was considered. A total of 5 impact loads were used for modal identification. The location and direction of the impact loads are shown in Figure 6-12. The results from this system show that 7 modes can be captured, Table 6-10. Other modes that were not measured rely on movement from the arches, where no sensors were placed. Comparing the results of this system with the CSiBridge software model, the MAC values correlate well, though comparing to the full system describe above, 7of the 11were available usingmeasurements on the bridge deck only.

Table D-1: Layout Plan 1 Natural Frequencies

<b>Mode</b>	<b>CSiBridge (Hz)</b>	<b>MATLAB (Hz)</b>	<b>MAC Value</b>
<b>1</b>	0.2568	0.2625	0.9999
<b>2</b>	0.4586	0.4625	0.9970
<b>3</b>	0.5919	0.6063	0.9894
<b>4</b>	0.6225	--	--
<b>5</b>	0.7798	0.7813	0.9997
<b>6</b>	0.8111	--	--
<b>7</b>	0.9834	--	--
<b>8</b>	1.2690	--	--
<b>9</b>	1.3081	--	--
<b>10</b>	1.4443	1.4438	0.9989
<b>11</b>	1.7575	1.7375	0.9994
<b>12</b>	1.8637	1.8563	0.9917
<b>13</b>	1.9319	--	--
<b>14</b>	1.9558	--	--
<b>15</b>	2.0954	--	--

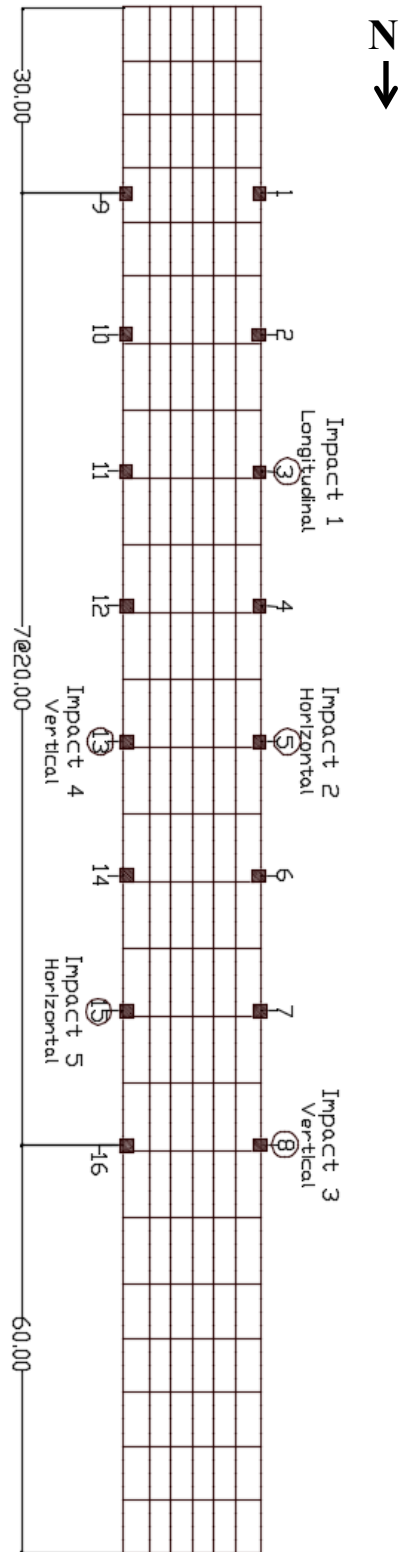


Figure D-1: Bridge Deck Top View of Layout Plan 1

## D.2 Layout Plan 2: 16 Accelerometers on Bridge Deck and Arches

The arches are an important aspect of modal identification because many modes rely on their behaviour. A second layout system, consisting of 10 accelerometers on the bridge deck, 5 placed on each edge girder at 40 m intervals, and 6 accelerometers on the steel arches, 3 on each arch at 40 m intervals, was investigated. 6 impact loads were used for modal identification. See Figure 6-13 and Figure 6-14 for the layout plan and the location and direction of impact loads. This system was capable of capturing 10 modes, most of which compared well to the CSiBridge model, Table 6-11. Although this system can capture more modes than layout plan 1 mentioned above, the sensors are more spaced apart. This means that this system has a better ability of measuring global behaviour, but the increased spacing of sensors could lead to a reduced ability to detect local damage. The use of this system would be a good solution when the overall global behaviour of the structure is needed, although it has overall less precision than 50 accelerometers on the structure, as presented in Chapter 6, due to the smaller amount of accelerometers and the increased spacing between accelerometers

Table D-2: Layout Plan 2 Natural Frequencies

<b>Mode</b>	<b>CSiBridge (Hz)</b>	<b>MATLAB (Hz)</b>	<b>MAC Value</b>
<b>1</b>	0.2568	0.2625	0.9997
<b>2</b>	0.4586	0.4625	0.9999
<b>3</b>	0.5919	0.6000	0.4217
<b>4</b>	0.6225	0.6250	0.9272
<b>5</b>	0.7798	0.7750	0.9998
<b>6</b>	0.8111	0.8125	0.9997
<b>7</b>	0.9834	--	--
<b>8</b>	1.2690	1.2625	0.9986
<b>9</b>	1.3081	--	--
<b>10</b>	1.4443	1.4438	0.9992
<b>11</b>	1.7575	1.7500	0.9960
<b>12</b>	1.8637	1.8688	0.9187
<b>13</b>	1.9319	--	--
<b>14</b>	1.9558	--	--
<b>15</b>	2.0954	--	--

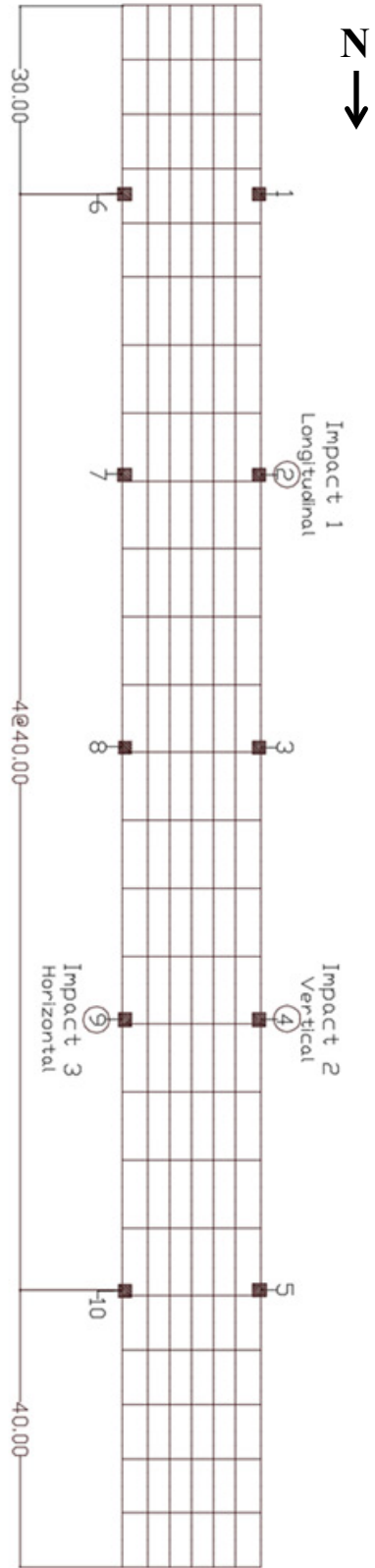


Figure D-2: Bridge Deck Top View of Layout Plan 2

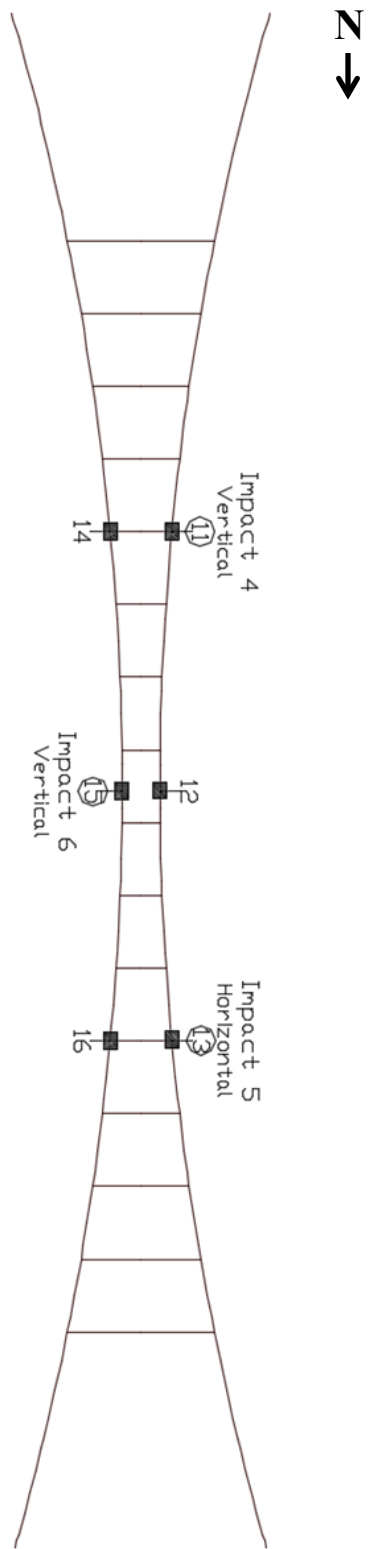


Figure D-3: Steel Arch Top View of Layout Plan 2

# APPENDIX E: SAMPLE IMPACT LOAD ACCELERATION DATA

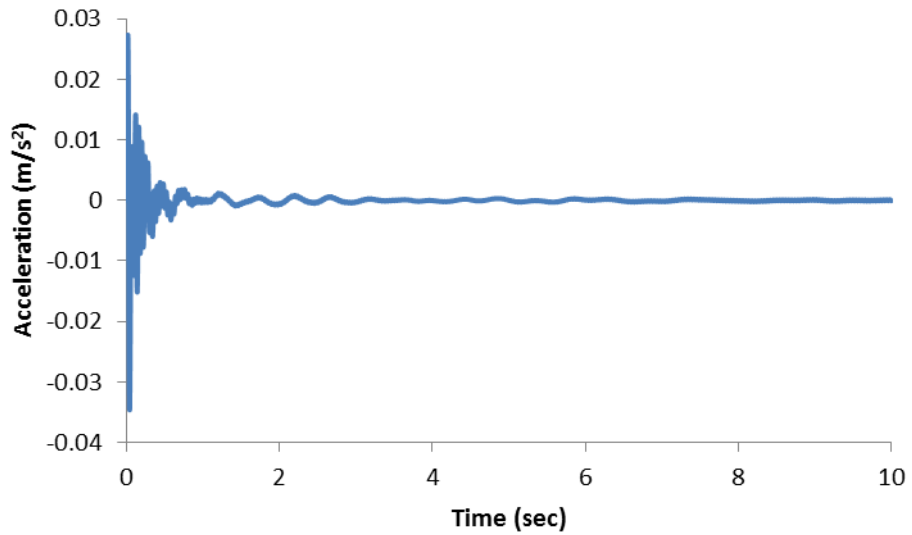


Figure E-1: Impact 1 Channel 6 - Vertical Acceleration

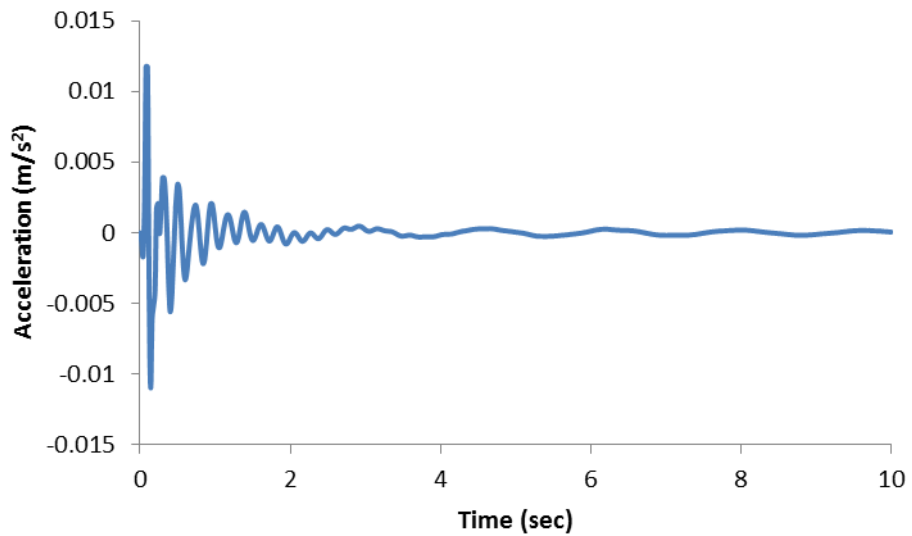


Figure E-2: Impact 1 Channel 56 - Horizontal Acceleration

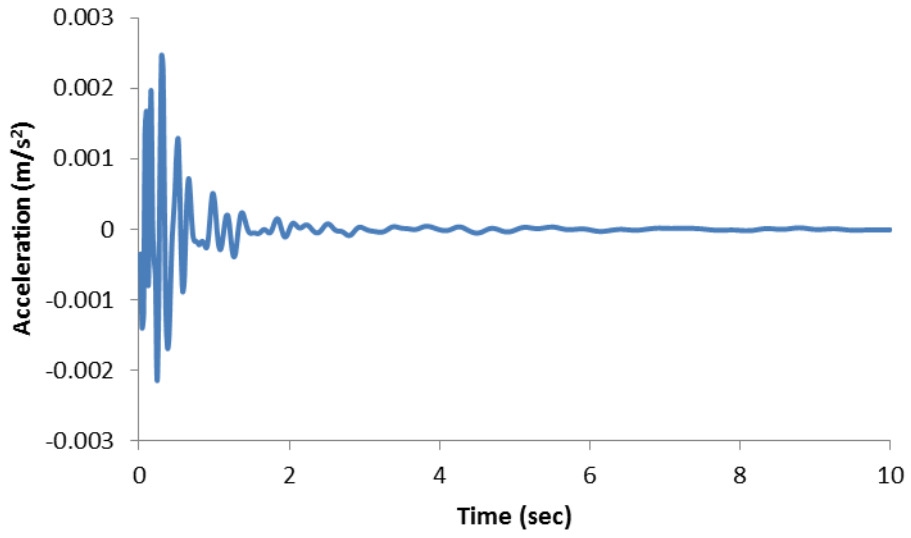


Figure E-3: Impact 1 Channel 88 - Longitudinal Acceleration

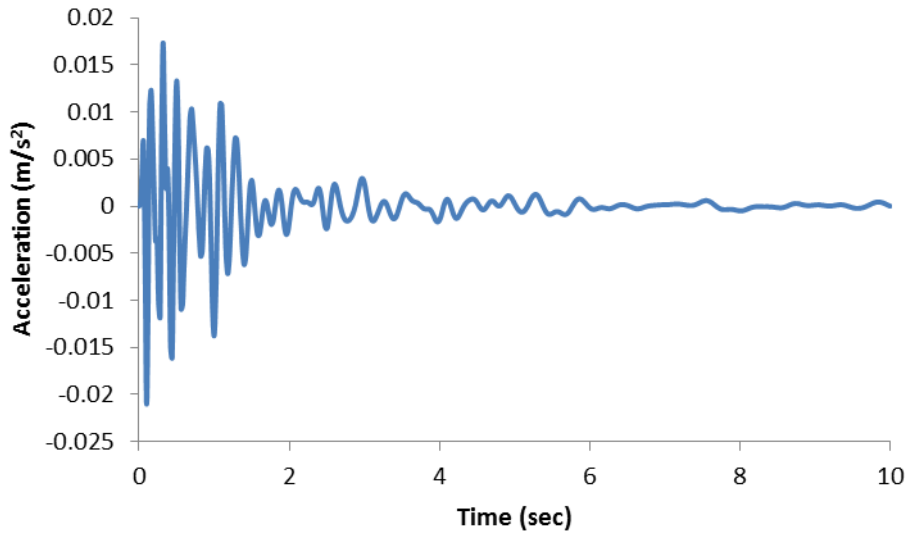


Figure E-4: Impact 2 Channel 28 - Vertical Acceleration

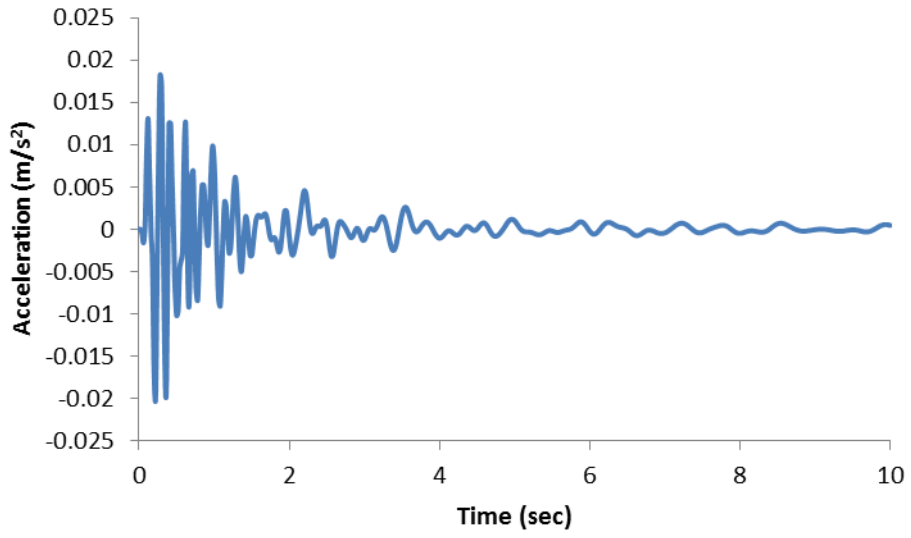


Figure E-5: Impact 3 Channel 20 - Vertical Acceleration

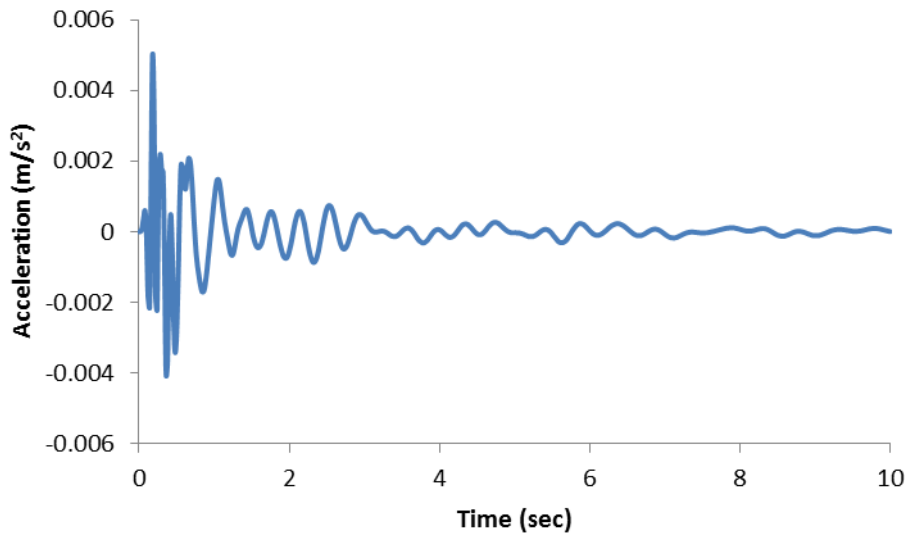


Figure E-6: Impact 4 Channel 65 - Horizontal Acceleration